2013

Satellite-derived potential evapotranspiration for distributed hydrologic runoff modeling in Midwestern basins

Ryan Randall Spies
Iowa State University

Satellite-derived potential evapotranspiration for distributed hydrologic runoff modeling in Midwestern basins

by

Ryan Randall Spies

A thesis submitted to the graduate faculty

in partial fulfillment of the requirements for the degree of

MASTER OF SCIENCE

Major: Geology

Program of Study Committee:
Kristie J. Franz, Major Professor
Brian K. Hornbuckle
William W. Simpkins

Iowa State University
Ames, Iowa
2013

TABLE OF CONTENTS

LIST OF FIGURES

LIST OF TABLES

ABSTRACT

The historical lack of distributed input data has been a key factor in hindering the use of distributed hydrologic models for operational streamflow prediction by the National Weather Service (NWS), which currently relies primarily on lumped models. Satellite remote sensing has held the promise of providing the needed spatial variables for hydrologic applications for some time, and currently sufficient data from sensors such as the Moderate Resolution Imaging Spectro-radiometer (MODIS) have amassed such that robust modeling applications testing is now possible.

The goal of this study is to test the use of satellite-derived potential evapotranspiration (PET) estimates, computed using 13 MODIS observations and the Priestly Taylor formula (MODIS-PET), as input in the NWS Hydrology Laboratory Research Distributed Hydrologic Model (HL-RDHM). Daily PET grids at 4km resolution are generated for 13 watersheds in the upper Mississippi River basin. Precipitation data are obtained from the Climate Prediction Center's (CPC) Climatology-Calibrated Precipitation Analysis (CCPA). Application of the MODIS-PET is compared to model results using the PET grids that are provided as a default in the HL-RDHM. The default PET grids are based on historical ground-based evaporation measurements and are spatially and temporally less variable than the MODIS-PET. Model results are evaluated for the May 1 through September 30 period for eight years using observed evapotranspiration (ET) adjacent to two watersheds and daily discharge observations for all watersheds.

Results indicate that even with the more physically realistic MODIS-PET input, simulated basin discharge at the outlet shows little to no improvement compared to the default PET

simulations. The simulated basin mean ET results exhibit mixed results when analyzing the MODIS-PET simulations against the default PET simulations. Calibrating several model parameters substantially improves simulated discharge for both MODIS-PET and default PET simulations; however, the range of improvement for simulated streamflow among individual basins varies between the two different PET data sources, and simulated discharge errors can often be directly related to simulated ET errors.

CHAPTER 1. GENERAL INTRODUCTION

1.1 Background

Potential evapotranspiration (PET) is defined as the rate at which ET would occur given a uniform growing vegetation cover with an unlimited supply of soil water and without advection or heat-storage effects. PET is used in hydrologic modeling as an estimate of the "drying power" of the meteorological or climate conditions controlling the transport of water vapor from the ground surface to the surrounding atmosphere via evaporation and transpiration (Dingman 2002). Traditional PET estimates require several meteorological measurements from ground-based stations, but the sporadic coverage of meteorological stations has forced many scientists to use regionalized climatological records in place of daily observations (Farnsworth and Thompson 1982).

To improve stream discharge simulations, streamflow forecasters have turned to the application of physically based parameters and forcing data by incorporating next generation radar (NEXRAD) data, soil records, digital elevation models (DEM), and land-use data to more accurately reflect the physical conditions of a given basin (K. Ajami et al. 2004). Operational forecasts from the NWS have primarily focused on using lumped models which represent a watershed as one large system in which sub-basin processes are not resolved. Distributed models differ by disaggregating the watershed into multiple units (generally grid-based or sub-watershed based). Water balance simulations are performed for each grid cell or subbasin individually, and channel routing routines move water from one unit to the next allowing discharge simulations within a basin. Distributed models have shown the potential to perform

up to lumped model standards (Koren et al. 2004; Smith et al. 2012a), but additional research is warranted to generate more reliable spatially distributed parameters and forcing inputs (Reed et al. 2004; Koren et al. 2004; Smith et al. 2004; Koren et al. 1999; Smith et al. 2012a).

Satellite data has long held the potential to provide observations for hydrologic modeling, particularly for distributed modeling needs. Andréassian et al. (2004) noted that most watershed models can cope with flawed PET estimates compared to rainfall estimates; however, model simulations are clearly sensitive to PET input. For this reason researchers have looked to satellite data as a means to better estimate the spatial and temporal PET variability within a watershed (e.g. Kim and Hogue 2008; Jacobs et al. 2009). Kim and Hogue (2008) examined a new method of estimating PET using satellite based observations and the radiation based Priestley-Taylor equation. The Kim & Hogue method uses only satellite based data, eliminating the need for spatially limited ground-based meteorological observations. After accumulating over a decade of reliable data, studies like this one can begin to test the full potential of spatially distributed satellite products.

The Hydrology Laboratory Research Distributed Hydrologic Model (HL-RDHM) was developed as a stand-alone tool for investigating the potential improvement of several operational forecast needs such as providing stream discharge forecasts at interior points within basins (lumped models only provide discharge data at the outlet), improving flash flood guidance, and providing an infrastructure capable of testing the applicability of new gridded input products such as model parameters, precipitation, soil moisture, and evapotranspiration (Koren et al. 2004; NWS 2011). The HL-RDHM uses a rectangular grid structure based on the

NEXRAD Hydrologic Rainfall Analysis Project (HRAP) grid coordinate system. Within each grid cell the Sacramento Soil Moisture Accounting Model (SAC-SMA) component performs the water balance functions and a hillslope and channel routing component drains water into a conceptual channel within each cell. The SAC-SMA uses a two layer structure to simulate soil moisture conditions controlling surface runoff, groundwater runoff (interflow and baseflow), and the available moisture to meet PET demands (NWS 2011).

A major obstacle associated with physically based distributed models is the application of estimated parameter values used to represent the vertical and horizontal heterogeneous properties within a watershed. Simulations using the physically based a priori parameters are often unsatisfactory due to basin specific conditions, and it is common to calibrate 'effective' parameters unique to each basin to improve stream discharge accuracy (e.g. Reed et al. 2004; Smith et al. 2012b). Calibrated parameters typically result in substantially improved discharge simulations, but the need for adjusted parameters questions the true nature of the application of physically based parameters (Koren et al. 2004). In this study parameters are carefully calibrated to observed discharge at the outlet using a predetermined range of parameter variability reasonable for the study region.

This study is designed to test the MODIS-PET product within the SAC-SMA component of the HL-RDHM. Working in conjunction with the North Central River Forecast Center (NCRFC) in Chanhassen, MN, several Midwestern study basins are chosen to test the new satellite derived potential evapotranspiration within the HL-RDHM. These study basins include several

watersheds noted for forecast difficulties within the NCRFC and include a wide distribution of land use, annual precipitation, and geological conditions.

1.2 Thesis Organization

This thesis follows the journal paper format. Chapter 1 includes the general introduction to the thesis. Chapter 2 contains the paper that will be submitted to a peer reviewed journal yet to be determined. Chapter 3 comprises the general conclusions from the journal paper, and the final appendix section contains additional useful tables and figures pertaining to the paper.

Throughout this paper the term "default simulations" refers to model simulations using the default PET input, and the term "MODIS simulations" refers to model simulations using the MODIS-PET input.

My role as the student author on this paper included gathering the data, running the model simulations, analyzing the results, and writing the paper. Dr. Kristie Franz oversaw the project, provided support, and helped with corrections to the journal paper draft.

References

Andréassian, V., Perrin, C., & Michel, C. (2004). Impact of imperfect potential evapotranspiration knowledge on the efficiency and parameters of watershed models. *Journal of Hydrology*, *286*(1-4), 19–35. doi:10.1016/j.jhydrol.2003.09.030

Burnash, R. J. C. (1995). *Computer Models of Watershed Hydrology*. (V. Singh, Ed.) (pp. 311–366). Littleton, CO: Water Resources Publications.

Dingman, L. (2002). *Physical Hydrology* (Second Edi.). Long Grove, IL: Waveland Press, Inc.

Douglas, E. M., Jacobs, J. M., Sumner, D. M., & Ray, R. L. (2009). A comparison of models for estimating potential evapotranspiration for Florida land cover types. *Journal of Hydrology*, *373*(3-4), 366–376. doi:10.1016/j.jhydrol.2009.04.029

Farnsworth, R., & Thompson, E. (1982). *NOAA Technical Report NWS 34*. Silver Spring, MD.

Gupta, H. V., Sorooshian, S., & Yapo, P. O. (1998). Toward improved calibration of hydrologic models : Multiple and noncommensurable measures of information, *34*(4), 751–763.

Hogue, T., Sorooshian, S., Gupta, H., Holz, A., & Braatz, D. (2000). A Multistep Automatic Calibration Scheme for River Forecasting Models. *Journal of Hydrometeorology*, *1*, 524–542.

Irmak, S., Kabenge, I., Skaggs, K. E., & Mutiibwa, D. (2012). Trend and magnitude of changes in climate variables and reference evapotranspiration over 116-yr period in the Platte River Basin, central Nebraska–USA. *Journal of Hydrology*, *420-421*, 228–244. doi:10.1016/j.jhydrol.2011.12.006

Jacobs, J. M., Lowry, B., Choi, M., & Bolster, C. H. (2009). GOES Solar Radiation for Evapotranspiration Estimation and Streamflow Prediction. *Journal of Hydrologic Engineering*, (March).

K. Ajami, N., Gupta, H., Wagener, T., & Sorooshian, S. (2004). Calibration of a semi-distributed hydrologic model for streamflow estimation along a river system. *Journal of Hydrology*, *298*(1-4), 112–135. doi:10.1016/j.jhydrol.2004.03.033

Kim, J., & Hogue, T. S. (2008). Evaluation of a MODIS-Based Potential Evapotranspiration Product at the Point Scale. *Journal of Hydrometeorology*, *9*(3), 444–460. doi:10.1175/2007JHM902.1

Koren, V., Reed, S., Smith, M., Zhang, Z., & Seo, D.-J. (2004). Hydrology laboratory research modeling system (HL-RMS) of the US national weather service. *Journal of Hydrology*, *291*(3-4), 297–318. doi:10.1016/j.jhydrol.2003.12.039

NWS (2008), The National Weather Service Hydrology Laboratory-Research Distributed Hydrologic Model (HL-RDHM), available online at http://www.mdl.nws.noaa.gov/~applications/LAD/, referenced version was downloaded on February 13th, 2012.

Oudin, L., Hervieu, F., Michel, C., Perrin, C., Andréassian, V., Anctil, F., & Loumagne, C. (2005). Which potential evapotranspiration input for a lumped rainfall–runoff model? *Journal of Hydrology*, *303*(1-4), 290–306. doi:10.1016/j.jhydrol.2004.08.026

Priestley, C. H. B., & Taylor, R. J. (1972). On the Assessment of Surface Heat Flux and Evaporation Using Large-Scale Parameters. *Monthly Weather Review*, *100*(February), 81–92.

Reed, S., Koren, V., Smith, M., Zhang, Z., Moreda, F., Seo, D.-J., & DMIP Participants, and. (2004). Overall distributed model intercomparison project results. *Journal of Hydrology*, *298*(1-4), 27–60. doi:10.1016/j.jhydrol.2004.03.031

Smith, M. B., Koren, V. I., Zhang, Z., Reed, S. M., Pan, J.-J., & Moreda, F. (2004). Runoff response to spatial variability in precipitation: an analysis of observed data. *Journal of Hydrology*, *298*(1-4), 267–286. doi:10.1016/j.jhydrol.2004.03.039

Smith, M. B., Koren, V., Reed, S., Zhang, Z., Zhang, Y., Moreda, F., Cui, Z., et al. (2012). The distributed model intercomparison project – Phase 2: Motivation and design of the Oklahoma experiments. *Journal of Hydrology*, *418-419*, 3–16. doi:10.1016/j.jhydrol.2011.08.055

Smith, M. B., Koren, V., Zhang, Z., Zhang, Y., Reed, S. M., Cui, Z., Moreda, F., et al. (2012). Results of the DMIP 2 Oklahoma experiments. *Journal of Hydrology*, *418-419*, 17–48. doi:10.1016/j.jhydrol.2011.08.056

Sumner, D. M., & Jacobs, J. M. (2005). Utility of Penman–Monteith, Priestley–Taylor, reference evapotranspiration, and pan evaporation methods to estimate pasture evapotranspiration. *Journal of Hydrology*, *308*(1-4), 81–104. doi:10.1016/j.jhydrol.2004.10.023

CHAPTER 2. SATELLITE-DERIVED POTENTIAL EVAPOTRANSPIRATION FOR DISTRIBUTED HYDROLOGIC MODELING IN MIDWESTERN BASINS

A paper to be submitted to a *Journal TBD*

Ryan R. Spies and Kristie J. Franz

2.1 Abstract

The historical lack of distributed input data has been a key factor in hindering the use of distributed hydrologic models for operational streamflow prediction by the National Weather Service (NWS), which currently relies primarily on lumped models. Satellite remote sensing has held the promise of providing the needed spatial variables for hydrologic applications for some time, and currently sufficient data from sensors such as the Moderate Resolution Imaging Spectro-radiometer (MODIS) have amassed such that robust modeling applications testing is now possible. The goal of this study is to test the use of satellite-derived potential evapotranspiration (PET) estimates, computed using 13 MODIS observations and the Priestly Taylor formula (MODIS-PET), as input in the NWS Hydrology Laboratory Research Distributed Hydrologic Model (HL-RDHM). Daily PET grids at 4km resolution are generated for 13 watersheds in the upper Mississippi River basin. Precipitation data are obtained from the Climate Prediction Center's (CPC) Climatology-Calibrated Precipitation Analysis (CCPA). Application of the MODIS-PET is compared to model results using the PET grids that are provided as a default in the HL-RDHM. The default PET grids are based on historical ground-based evaporation measurements and are spatially and temporally less variable than the MODIS-PET. Model results are evaluated for the May 1 through September 30 period for eight

years using observed evapotranspiration (ET) adjacent to two watersheds and daily discharge observations for all watersheds. Results indicate that even with the more physically realistic MODIS-PET input, simulated basin discharge at the outlet shows little to no improvement compared to the default PET simulations. The simulated basin mean ET results exhibit mixed results when analyzing the MODIS-PET simulations against the default PET simulations. Calibrating several model parameters substantially improves simulated discharge for both MODIS-PET and default PET simulations; however, the range of improvement for simulated streamflow among individual basins varies between the two different PET data sources, and simulated discharge errors can often be directly related to simulated ET errors.

2.2 Introduction

Hydrologic forecasters are currently looking to improve streamflow simulations with up-to-date physically based data, and distributed models have shown a promising future implementing new spatially variable input data (Koren et al. 2004; Jacobs et al. 2009; Smith et al. 2012a). Projects like the distributed modeling intercomparison project (DMIP) have examined numerous distributed and semi-distributed models (including the National Weather Service model used in this study) and found comparable results to current lumped model skill (Reed et al. 2004).

Due to the lack of an extensive network of ground based measurements necessary to estimate potential evapotranspiration (PET) and actual evapotranspiration (ET) over a watershed, hydrologic forecasters have typically relied on climatology-based values as input into hydrologic models used to simulate stream discharge (Farnsworth and Thompson 1982).

Current default long-term PET estimates are unable to account for the spatial or temporal variations within a watershed which can lead to added uncertainty within hydrologic models. Andréassian et al. (2004) found watershed models are sensitive to PET inputs, yet the models are able to adapt to biases in the input data through the calibration process. The expanding use of spatially-distributed models has brought forth the need for a reliable spatially and temporally robust input data such as PET to advance current hydrologic models (Smith et al. 2012b).

Kim and Hogue (2008) proposed a new method of estimating daily PET through the use of satellite-based measurements and the Priestley-Taylor method (Priestley and Taylor 1972). This new method has several benefits ideal for application in distributed models such as not requiring any ground-based point observations, estimating PET for both clear and cloudy days, spatially variable PET data potentially available anywhere on earth, and data is available daily.

The radiation-based Priestley-Taylor method is ideal for modeling at the watershed scale due to the limited meteorological inputs required. Despite the simplifications applied to the equation, the Priestley-Taylor method has been shown to provide accurate estimates of PET for a variety of land cover types (Oudin et al. 2005; Sumner and Jacobs 2005; Douglas et al. 2009). A physically based PET data source also has the potential to capture future changes in the hydrologic cycle associated with climate change (Pechlivanidis et al. 2011; Irmak et al. 2012).

The Hydrology Laboratory Research Distributed Hydrologic Model (HL-RDHM) was developed to investigate the potential improvement of several operational forecast needs. These needs include providing river discharge forecasts at interior points within basins,

improving flash flood guidance, and creating an infrastructure capable of testing the applicability of new gridded input products such as model parameters, precipitation, soil moisture, and evapotranspiration (NWS, 2011). Distributed models have shown the potential to perform up to lumped model standards, but additional research is warranted to generate more reliable spatially distributed parameters and forcing inputs (Koren et al. 1999; Reed et al. 2004; Koren et al. 2004; Smith et al. 2004; Smith et al. 2012b). Previous studies have also shown significantly improved discharge simulations after calibrating a priori parameters to each basin (e.g. Reed et al. 2004; K. Ajami et al. 2004), and this study follows current practices for calibrating selected parameters to observed discharge.

This study seeks to determine if an innovative satellite-based PET product can represent the actual daily PET variability within a watershed while replicating or improving the stream discharge accuracy from current default PET model simulations. We analyze the simulated discharge and ET components from the model simulations using two PET inputs.

2.3 Methodology

2.3.1 Study Area

The study area includes 13 headwater basins (Table 1) located throughout the states of Iowa, Minnesota, and Wisconsin, in the north-central United States (Figure 1). All basins are within the Upper Mississippi River Basin and are official forecast points of the NWS North Central River Forecast Center (NCRFC). Daily discharge data for each basin is available from the United States Geological Survey (USGS). Study basins were selected to provide a range of watershed size, mean annual precipitation, and land use. The catchment area of individual

study basins range from 572 km^2 to 6242 km^2. The Midwestern plain states are characterized by minimal topographic relief, and all study basins have less than 200 meters of elevation change.

Basin Name	USGS Station	Location	River	Size (km^2)
AMEI4	05470000	Ames, IA	South Skunk River	816
AMWI4	05470500	Ames, IA	Squaw Creek	530
BCHW3	05433000	Blanchardville, WI	East Branch, Pecatonica River	572
BERW3	04073500	Berlin, WI	Fox River	3471
DARW3	05432500	Darlington, WI	Pecatonica River	707
HICM5	05327000	Henderson, MN	High Island Creek	617
MILW3	05426000	Milford, WI	Crawfish River	1974
MMLM5	05315000	Marshall, MN	Redwood River	671
NHRI4	05463000	New Hartford, IA	Beaver Creek	899
PLUM5	05078000	Plummer, MN	Clearwater River	2847
RAPM5	05320000	Rapidan, MN	Blue Earth River	6242
SANM5	05336700	Sandstone, MN	Kettle River	2248
SCRI4	05482300	Sac City, IA	North Raccoon River	1813

Table 1. Location and characteristics of the 13 study sites.

The climate of the north central United States varies significantly by season and is susceptible to both flood and drought conditions. Summers are characterized by warm and humid conditions and winters are cool and dry. A pronounced wet season occurs from early spring into late summer, with convective thunderstorm systems enhanced by moisture transport from the Gulf of Mexico producing a large percentage of the annual precipitation. Heavy winter snowpack can also be an important factor in replenishing soil moisture and streamflow during spring melting, which can prime the region for early season flooding.

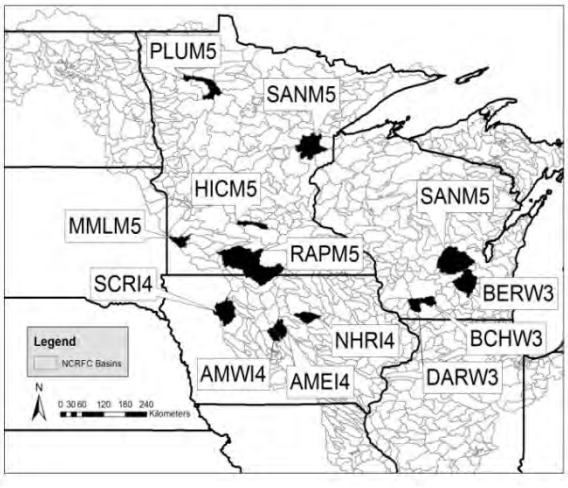

Figure 1. Map of all NCRFC forecast basins with study basin highlighted in black and identified by RFC basin name.

Land use in this region is characterized as largely agricultural with extensive areas cultivated for corn, soybeans, and pasture land (Figure 2a). The abundant precipitation during the growing season negates the need for extensive irrigation in this region. Several basins in Iowa and southern Minnesota have artificial drainage networks intended to lower the water table and promote increased agricultural productivity. Shilling and Libra (2004) and Shilling and Helmers (2008) noted increasing groundwater discharge to stream channels in the second half of the 20th century corresponding to the baseflow increases from tile-drained row crop landscapes. This finding highlights a potential source of uncertainty within the model simulations, which do not directly account for the effects of tile drainage. Basins in Northern Minnesota and Wisconsin also contain large forested and wetland regions (Figure 2a) (Fry et al. 2011).

Soil characteristics in this region can often be correlated to the type of vegetation grown. The vast area of land used for cultivated crops is typically made up of the nutrient-enriched Mollisol soil order defined by the United States Department of Agriculture soil

taxonomy (Figure 2b). A clay-enriched subsoil region (alfisols) encompasses much of Wisconsin and the eastern half of Minnesota, and this area marks the transition to a more forested region. Northern sections of Minnesota and Wisconsin contain a wide distribution of soil types with areas of saturated soils (histosols), poorly developed horizons (entisols), and moderately developed soil horizons (inceptiosls) (Figure 2b).

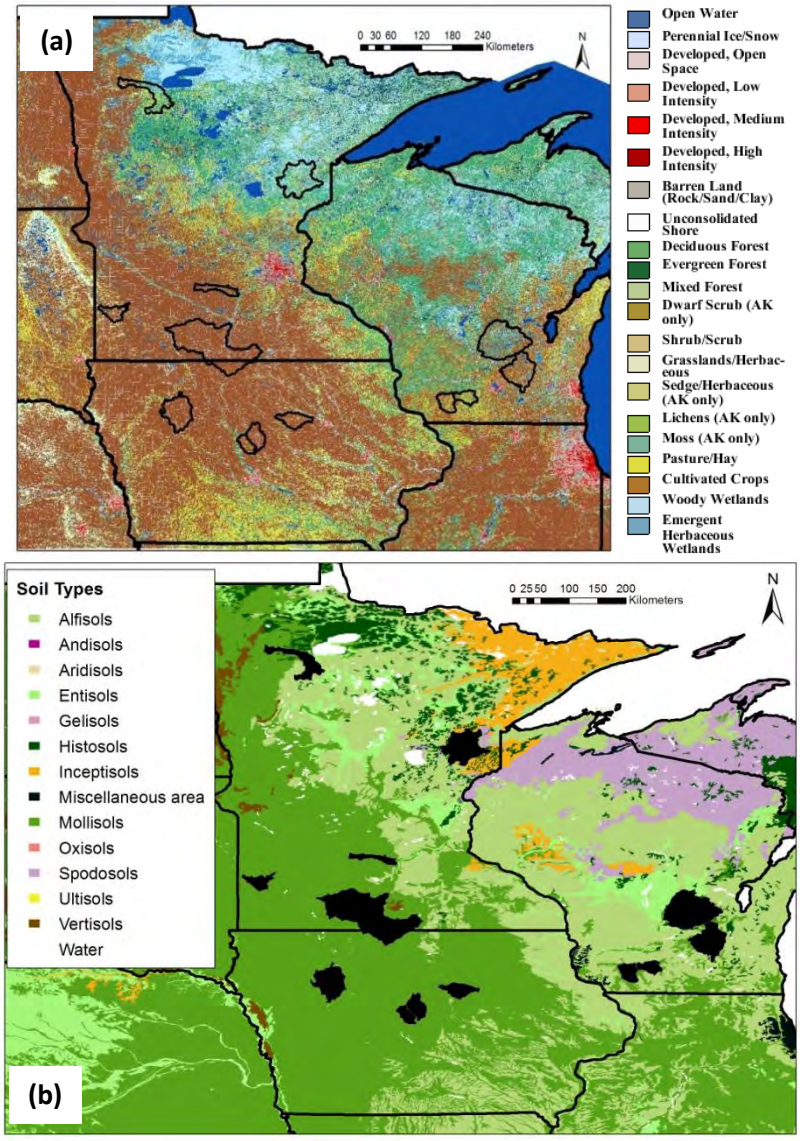

Figure 2. (a) Map of major land cover types of the Upper Midwest from the 2006 National Land Cover Database (Fry et al. 2011). (b) Map of soil taxonomy from Soil Survey Geographic (SSURGO) by the United States Department of Agriculture's Natural Resources Conservation Service.

2.3.2 Evaluation Statistics

To evaluate both ET and discharge simulations, four summary statistics are computed: bias, percent bias (P Bias), correlation coefficient (R^2), and mean absolute error (MAE):

$$Bias = \frac{1}{n}\left[\sum_{i=1}^{n}\left(x_{model,i} - x_{obs,i}\right)\right] \quad (1)$$

$$PBias = \left[\frac{\sum_{i=1}^{n}\left(x_{model,i} - x_{obs,i}\right)}{\sum_{1=1}^{n}\left(x_{obs}\right)}\right] \times 100 \quad (2)$$

$$R^2 = \left[\frac{\sum_{i=1}^{n}\left(x_{model,i} - \overline{x_{model}}\right)\left(x_{obs,i} - \overline{x_{obs}}\right)}{\sqrt{\sum_{i=1}^{n}\left(x_{model,i} - \overline{x_{model}}\right)^2}\sqrt{\sum_{i=1}^{n}\left(x_{obs,i} - \overline{x_{obs}}\right)^2}}\right]^2 \quad (3)$$

$$MAE = \frac{1}{n}\sum_{i=1}^{n}\left|x_{model,i} - x_{obs,i}\right| \quad (4)$$

where n is the number of days analyzed; $x_{obs,i}$ and $x_{model,i}$ are the observed and modeled data at day i; and $\overline{x_{obs}}$ and $\overline{x_{model}}$ are the mean of the observed and modeled data. All error statistics discussed in this paper are calculated for the warm season months only (May-September) unless otherwise noted.

The Nash-Sutcliffe (Nash and Sutcliffe 1970) model efficiency coefficient is used to evaluate the model skill in predicting discharge values via the following equation:

$$NSE = 1 - \frac{\sum_{1=1}^{n}\left(x_{obs,i} - x_{model,i}\right)^2}{\sum_{1=1}^{n}\left(x_{obs,i} - \overline{x_{obs}}\right)^2} \quad (5)$$

where NSE is the Nash-Sutcliffe efficiency coefficient; n is the number of days analyzed; $x_{obs,i}$ and $x_{model,i}$ are the observed and modeled discharge at time i; and $\overline{x_{obs}}$ is the mean of the observed discharge data. NSE values range can range from -∞ to 1. A value of 1 indicates a

perfect match of simulated to observed, a value of 0 indicates the model simulation is as accurate as the mean of the observed data, and negative values indicate the observed mean is a better predictor than the model.

2.3.3 Default Evapotranspiration

The NWS Office of Hydrologic Development (OHD) has developed CONUS monthly grids of climatological potential evaporation (PE) and potential evaporation adjustment factors for use with the HL-RDHM (Figure 3). The climatological PE data is based primarily on the unpublished work by V. Koren, J. Schaake, Q. Duan, M. Smith, and S. Cong which combines data from seasonal and annual free water surface maps in the National Oceanic and Atmospheric Administration (NOAA) Technical Report 33 and mean monthly station data from NOAA Technical Report 34 (NWS, 2008). The NOAA data is used to derive an equation to predict long-term mean daily PE variability which is used to compute the monthly PE grids. PE adjustment factors are used in an attempt to account for the effects of seasonal vegetation transpiration changes throughout the year. The PE adjustment grids are also developed by the same individuals using an empirical function linking calibrated PE adjustment factors to green vegetation fraction data derived from satellite observations (NWS, 2008). The HL-RDHM applies the product of the PE and PE adjustment grids and then interpolates daily grids of potential evaporation demand (PED) from the monthly values. Throughout this study the PED input is referred to as default PET. The default PET input is used as a baseline simulation to compare the new remotely-sensed PET product simulations. In this study “default simulations” refer to model simulations with the default PET input.

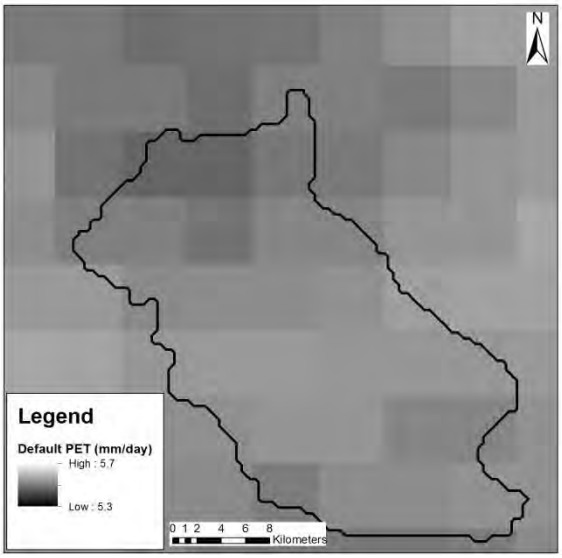

Figure 3. Example of interpolated total daily default PET for AMWI4 basin on July 5th, 2007. Note the small range of PET variability across the watershed.

All input data used in this study are projected in the Hydrologic Rainfall Analysis Project (HRAP) grid coordinate system developed for the Next Generation Weather Radar (NEXRAD) products used within the NWS (Fulton 1998). The grid cell resolution of 1 HRAP pixel is approximately 4km x 4km and grid data are mapped by a polar stereographic projection. All model simulations are run in the default resolution of 1 HRAP, and all input parameters and inputs are either provided or manually developed in this format.

2.3.4 Satellite-based Potential Evapotranspiration

The MODIS (Moderate Resolution Imaging Spectroradiometer) instrument aboard the Aqua and Terra satellites collects data in 36 spectral bands (http://modis.gsfc.nasa.gov/about/). Kim and Hogue (2008) present an algorithm that applies 13 variables from the MODIS dataset (Table 2) and the Priestly-Taylor equation to estimate a daily time series of PET. This data is

hereafter referred to as MODIS-PET. MODIS-PET is unique in that it uses only MODIS derived data and does not require ground-based information.

The Priestly-Taylor Equation (equation 6) is used to compute instantaneous PET at each grid cell using estimates of net radiation (Rn), air temperature (Ta), and soil heat flux (G). Longwave radiation is estimated using Normalized Difference Vegetation Index (NDVI), air temperature (Ta), dew point temperature, geopotential height, surface temperature (Ts), and emissivity. Shortwave radiation is estimated by two methods depending on the amount of cloud cover at the time of the satellite overpass. For clear days (cloud fractional coverage < 0.2) the solar zenith angle, precipitable water, ozone, and albedo are used to estimate shortwave radiation at the surface. On cloudy days (cloud fraction coverage > 0.2) the algorithm derives a theoretical clear-day shortwave radiation by interpolating between adjacent clear days. The daily mean cloud fraction and daily cloud optical depth products are incorporated into an empirical formula to estimate the theoretical clear-sky shortwave radiation product. The shortwave radiation is then used to estimate net radiation by applying a simple linear regression, and finally a cloudy-day PET can be determined. Soil heat flux (G) is estimated using a relationship with the NDVI, albedo, and land surface temperature values.

The Priestley-Taylor equation (Priestley and Taylor 1972):

$$\lambda PET = \alpha \frac{\Delta}{\Delta+\gamma}(R_n - G) \quad (6)$$

where PET is the daily PET (mm/day); λ is the latent heat of vaporization (MJ/kg) and λ=2.501-0.002361 T; T is the daily mean air temperature (°C); α = 1.26 for wet or humid conditions; Δ is

the slope of the saturation vapor pressure temperature curve (kPa/°C) and Δ = 0.2(0.00738 T + 0.8072)^{7} -1.16e^{-4}; and ϒ is the modified psychrometric constant (kPa/°C)

$$\gamma = \frac{c_p P}{0.622\lambda} \quad (7)$$

where c_p is the specific heat of moist air (kJ/kg/°C) and c_p = 1.013 kJ/kg/°C; p is the estimated atmospheric pressure (kPa) and where p = 101.3 exp(-A/8200); A is the altitude above sea level for each location (m); Rn is the net radiation (MJ/m^2/day); and G is the heat flux density to the ground (MJ/m^2/day).

A sinusoidal model is applied to the instantaneous net radiation and PET using the day length (difference between sunrise and sunset time) to estimate the daily mean net radiation and daily total PET. By applying the sinusoidal model to the day length period the algorithm ignores negative net radiation values thus assuming a situation with no ground-surface condensation (dew) within the system.

Satellite	Product	Variable	Resolution
Terra	MOD03	Geolocation Data	1km
		geodetic coordinates	
		ground elevation	
		solar and satellite zenith	
		azimuth angle	
Terra	MOD05	Total Precipitable Water	1km & 5km
Terra	MOD06	Cloud Product	1km & 5km
Terra	MOD07	Atmospheric Profiles	5x5 1km
		total ozone burden	
		atmospheric stability	
		temperature and wind profile	
		atmospheric water vapor	
Terra	MOD11L2	Land Surface Temperature and Emissivity 5-minute L2 Swath	1km
Aqua	MYD11A2	Land Surface Temperature and Emissivity 8-Day L3 Global	1km
Terra	MOD13Q1	Vegetation Indices 16-Day L3 Global	250m

Aqua	MYD13Q1	Vegetation Indices 16-Day L3 Global	250m
Combined	MCD43A3	Albedo 16-Day L3 Global	500m

Table 2. MODIS satellite products applied to Kim and Hogue (2008) PET algorithm.

MODIS-PET is generated for May through September when ET rates have the largest impact on the water balance in the study region. Daily MODIS-PET data are produced for each basin individually for the time period 2003-2010. Days with missing MODIS-PET data along with the cool season months (October-April) are replaced with the default PET grids within the model simulations. The MODIS-PET data is originally computed at the native 500m resolution of the MODIS data (Figure 4a). Geographic coordinates of each 500m pixel are converted to the HRAP coordinate system and grid cells are aggregated to 4km resolution (Figure 4b), which is the default spatial resolution of the HL-RDHM (1-HRAP). During the model simulation, the PET is uniformly interpolated into 6-hour timesteps where the daily PET is simply divided by four and the same value is applied to each timestep within a specific day. Maintaining the 4km spatial and 6-hr temporal resolution of the HL-RDHM allowed comparison to the default-PET and use of the default parameters, which are potentially sensitive to the spatial and temporal resolution. In this study MODIS simulations refer to model simulations with the MODIS-PET input.

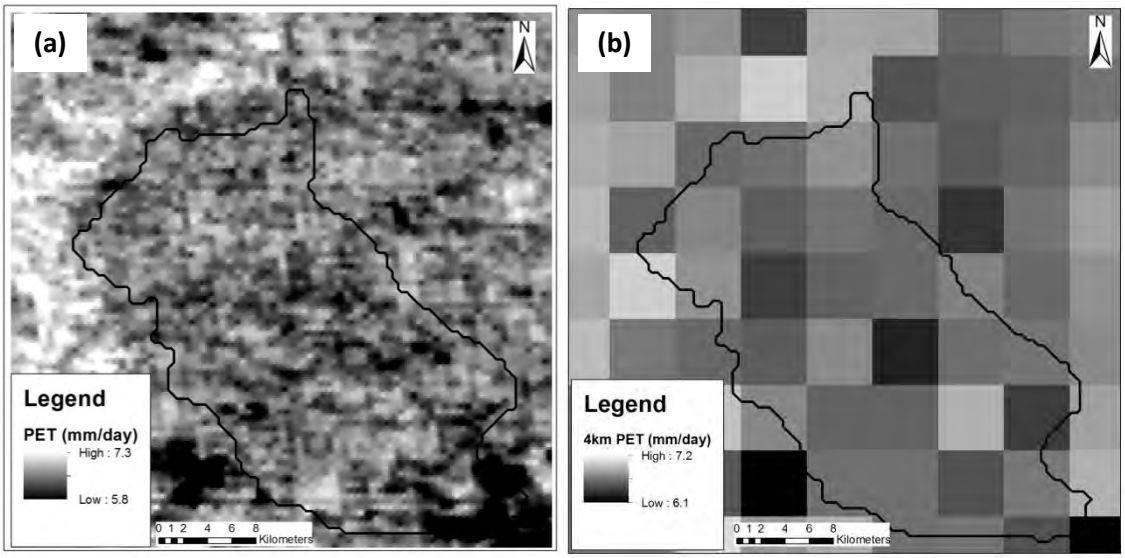

Figure 4. Total daily PET for AMWI4 basin on July 5th, 2007 at (a) 500m resolution and (b) 4km resolution.

2.3.5 Flux-tower Observations

Latent heat flux (LHF), net radiation, ground heat flux, and air temperature data are collected from two Ameriflux flux-tower sites located within 5km of study basin AMWI4 and within 20km of study basin MMLM5 (Table 3).

Site	Longitude	Latitude	Elevation (m)	Vegetation	ET/PET (mm/day)	Data Period
Ames, IA	-93.6936	41.9747	313	corn, soybean	3.00/5.02	2005-2010
Brookings, SD	-96.8362	44.3453	510	pasture, grassland	3.86/5.16	2004-2009

Table 3. Location and characteristics of the two flux towers used in this study. Note: mean annual ET and PET values are calculated for the warm season only.

Both sites use a sonic anemometer and an open path CO_2/H_2O gas analyzer instruments to calculate LHF values with the Webb et al. (1980) and coordinate rotation corrections applied. Daily mean values are calculated for the warm season months (May-September) by averaging the available 30 minute interval flux station data.

Positive LHF values are converted to an equivalent depth of liquid water evapotranspiration by applying the latent heat of vaporization. The daily ET data are used to

evaluate the simulated ET for the two nearby basins. Net radiation and air temperature measurements are also converted to daily mean values and used to compute PET using the Priestly–Taylor equation (Eq 1). Ground heat flux measurements are available at both flux-tower locations. This data is used to provide an initial evaluation of the MODIS-PET data in the next section (Section 2.3.6). To be consistent with the MODIS-PET techniques, only positive values of net radiation are applied in the daily net radiation calculation used in the Priestly-Taylor equation.

2.3.6 Evaluation of MODIS-PET and default-PET

To aid in drawing conclusions about the applicability of a satellite-based product in the HL-RDHM, the accuracy of the MODIS-PET data is first evaluated against PET values computed using ground-based observations at the two flux tower sites (Table 4). In addition, the default-PET is examined for comparison.

The basin average MODIS-PET demonstrates fair correlation to flux-tower PET values (average R^2 = 0.66) (Figure 5c, 5d). This is similar to the findings of Kim and Hogue (2008) who noted a good correlation (R^2 = 0.89) and low bias (-0.34 mm day^{-1}) when assessing a point-scale daily comparison between the MODIS-PET and flux-tower PET for humid sites. Note that the analysis here includes only May-September while the Kim and Hogue (2008) study includes the entire year, which may also explain the slightly lower correlation and larger bias found here. The basin average default-PET has poorer correlation to the flux-tower PET (average R^2 = 0.13). The range of the default-PET is also smaller than the MODIS-PET. Although MODIS-PET has

better correlation, the default-PET has lower bias on average, and both PET products have similar MAE values (Table 4).

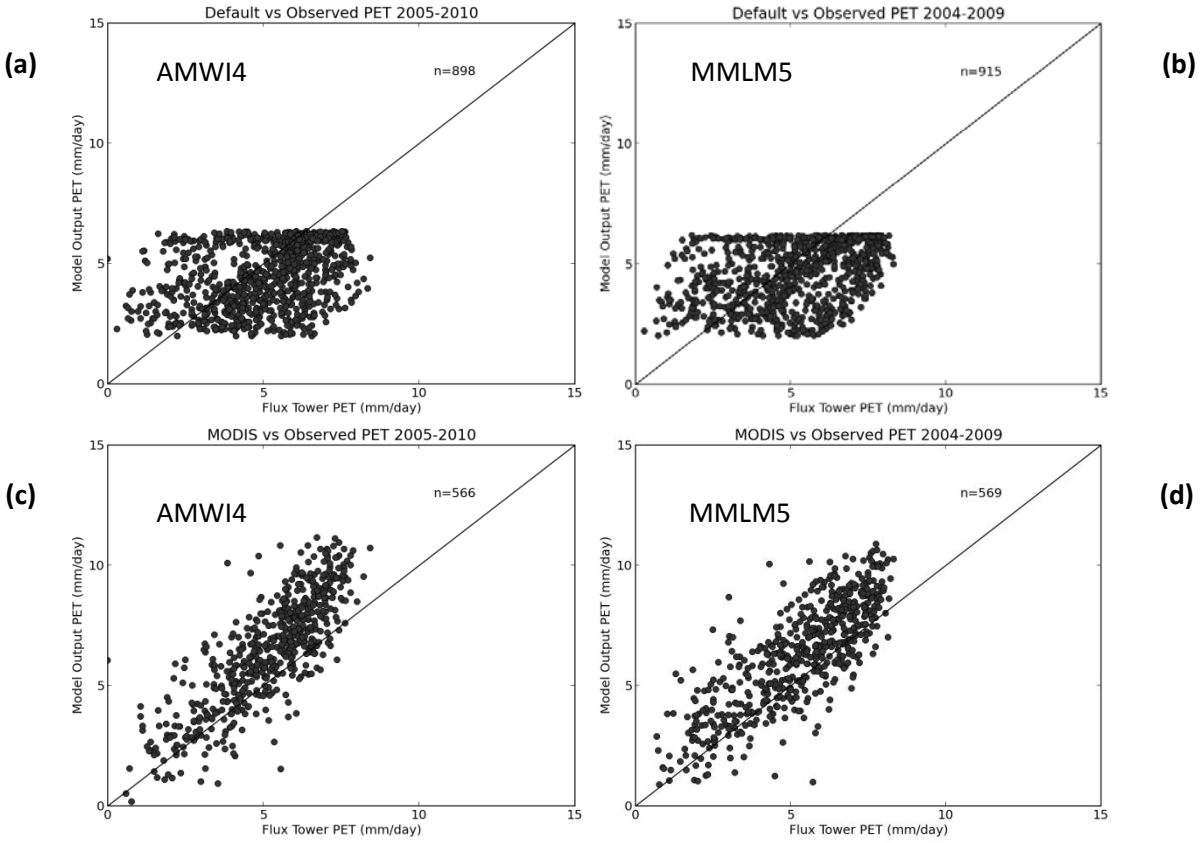

Figure 5. Comparison of mean daily Flux-Tower PET and (a,b) basin mean default PET and (c,d) basin mean MODIS-PET for AMWI4 and MMLM5. Black line illustrates the one to one correlation.

Even with the limiting climatological range, the default PET seems to represent a slightly better overall warm season average PET value where the MODIS-PET has a prominent high bias during the same period. These results would indicate that while the more physically realistic MODIS-PET has the potential to better represent the day-to-day PET variability, the default PET

is likely a better representation of the long-term average PET conditions under expected climate situations.

	Bias (mm/day)			R^2			MAE (mm/day)		
	AMWI4	MMLM5	Mean	AMWI4	MMLM5	Mean	AMWI4	MMLM5	Mean
PET									
Default	-0.6	-0.5	-0.5	0.13	0.13	0.13	1.5	1.6	1.5
MODIS	1.3	1.0	1.2	0.67	0.64	0.66	1.5	1.3	1.4

Table 4. Analysis of PET bias (mm/day) and correlation for the basin mean MODIS-PET and default PET at AMWI4 and MMLM5.

2.3.7 Temperature

Ground-based station data are used to develop temperature grids for model input. The Automated Surface Observing System (ASOS) and Automated Weather Observing System (AWOS) networks record atmospheric variables, including temperature, approximately every 20 minutes. All ASOS and AWOS quality controlled data within the watershed boundaries and within close proximity of each basin are downloaded from the Iowa Environmental Mesonet (http://mesonet.agron.iastate.edu/). Station data are converted to a 6-hour mean value and a 4 km resolution grid is interpolated for each region through the Inverse Distance Weighting (IDW) method for the years 2002-2010.

Air temperature data is needed to run the HL-RDHM throughout the winter months, allowing for continuous simulations. Air temperature is used only during winter months to determine precipitation type (rain or snow), and to simulate the snowpack using the SNOW17 modeling component. Because the focus of this study is on warm season evaporation, extensive review of the accuracy of the temperature data is not a priority. However, it should

be noted that snow influences soil moisture conditions leading into the spring, and as a result, may impact simulations in the early part of the warm season.

2.3.8 Precipitation

Precipitation data are from the National Centers for Environmental Prediction (NCEP) Environmental Modeling Center Climatology-Calibrated Precipitation Analysis (CCPA). CPPA combines the CPC Unified Global Daily Gauge Analysis (24 hour accumulation at one-eighth degree spatial resolution) and the NCEP Stage IV analysis (6-hourly estimates at 4-km resolution) precipitation data sets to "take advantage of the higher climatological reliability of the CPC dataset and the higher temporal and spatial resolution of the Stage IV dataset" (Hou et al. 2012). The resulting data is a 6-hourly precipitation product for the CONUS at the HRAP resolution from 2002 to present.

Basin Name	CCPA Annual Precip (mm)	Precipitation Adj (%)	Adjusted CCPA (mm)	RFC Annual MAP
AMEI4	908	11%	1008	991
AMWI4	839	23%	1032	1011
BCHW3	870	7%	937	935
BERW3	809	0%	809	824
DARW3	732	22%	939	981
HICM5	519	31%	680	718
MILW3	901	1%	939	925
MMLM5	587	19%	725	706
NHRI4	942	3%	970	966
PLUM5	436	25%	545	602
RAPM5	654	18%	798	814
SANM5	560	24%	694	725
SCRI4	736	9%	809	818

Table 5. Annual precipitation values and precipitation adjustment factors for all study basins. Adjusted CCPA precipitation data represents the actual data used for simulations. Note RFC MAP does not include 2010 calendar year.

Initial analysis of stream discharge simulations for six basins revealed that the simulated discharge is biased low when compared to observed basin discharge; this occurred for a priori and calibrated simulations. Hou et al. (2012) noted improvement in precipitation estimates with the CCPA is more significant with lower and medium daily precipitation amounts, but this product is "subject to limitations due to the validity of the linear regression model and the relative scarcity of heavy precipitation events". To explore this possible bias in the CPPA data further, the mean precipitation is computed for each basin from the CCPA and compared to the Mean Areal Precipitation (MAP) obtained from the NCRFC. MAPs, which are used to calibrate the operational forecast models, are developed using a combination of ground-based and radar measurements and are quality controlled by the NCRFC. The annual accumulation of the CPPA is consistently lower than the MAP (Table 5).

The HL-RDHM allows a basin specific adjustment factor to be applied to every grid cell corresponding to a study basin. Therefore, a precipitation adjustment factor is developed for each basin by calculating the average difference between total March-September precipitation from the CCPA and MAP data for the 2003-2008 period. The March-September period is analyzed to capture the more abundant liquid precipitation event differences and ignore snowfall differences. Table 5 shows the adjustment factors for each basin and adjusted mean CPPA. The final annual mean CCPA values are in better agreement with the annual MAP values.

2.3.9 HL-RDHM

The HL-RDHM was developed by the NWS Office of Hydrologic Development (OHD) Hydrology Laboratory (HL) to promote research into the potential use of an operational

distributed hydrologic forecasting model. In this study, the SNOW-17, the Sacramento Soil Moisture Accounting (SAC-SMA), and the physically-based kinematic hillslope and channel routing modeling options from HL-RDHM version 3.2.0 are used to simulate the watersheds' hydrologic processes

Figure 6). The SNOW-17 is an empirically-based snow accumulation model that uses air temperature as an index to the energy balance of the snowpack (Anderson 2006). The SAC-SMA is conceptual rainfall-runoff model that simulates the processes producing interflow, runoff, percolation, and evapotranspiration. The hillslope and channel routing component uses surface and subsurface runoff output from the SAC-SMA simulations to route water over a conceptual hillslope into a conceptual channel using drainage density, hillslope slope, and hillslope roughness data (Koren et al. 2004). To move water from upstream to downstream a topographically defined cell-to-cell connectivity sequence was developed by the OHD using Digital Elevation Model (DEM) data (Reed 2003; NWS 2008).

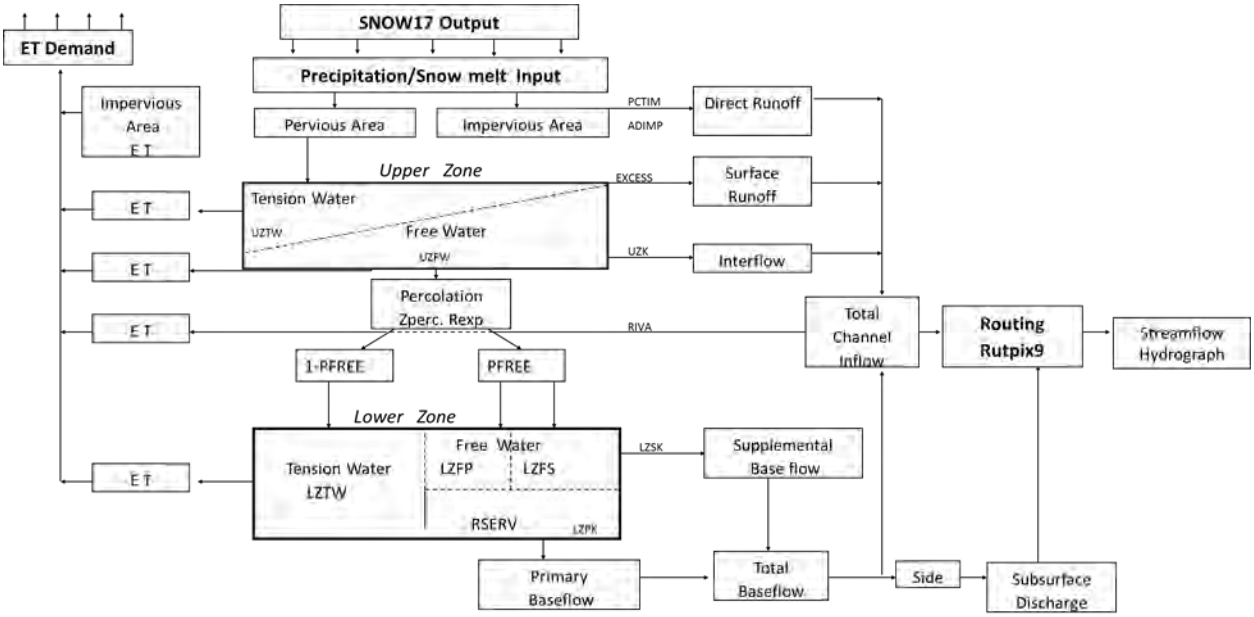

Figure 6. Flow chart of the HL-RDHM illustrating the SAC-SMA model parameters controlling surface runoff, interflow, baseflow, and ET.

Default parameter grids (4km resolution) are available from the OHD for nearly all of the parameters implemented in the SAC-SMA, Snow-17, and Overland and Channel Routing components. SAC-SMA parameter grids are derived using methods presented by Koren et al. (2000) and Koren et al. (2003), which utilize the State Soil Geographic Database (STATSGO) soil characteristics products. Where gridded data were not available from the OHD, a single value was used for the entire basin. In such cases, the basin specific value used by the NCRFC in their lumped operational modeling system is applied. All model simulations are run continuously at a 6-hr timestep and calendar year 2002 is included as a spin-up period to allow states to equilibrate and stabilize.

ET values are simulated by the model as a function of the moisture available and the PET input. Five separate ET components are calculated within the SAC-SMA: ET output from the upper zone tension water component, ET output from the upper zone free water component, ET output from the lower zone tension water component, ET output from the impervious area component, and ET output from the total channel inflow

Figure 6). The ET output variables are calculated as a function of the available moisture within each component and the total PET value at each timestep. Total simulated ET must not exceed the PET at any time step.

2.3.10 Calibration

The HL-RDHM was calibrated to stream discharge at the basin outlet using an Automated Stepwise Line Search (SLS) procedure (NWS 2008). The SLS technique steps through

each parameter one at a time, minimizing the objective function with respect to each parameter. If the parameter value remains the same for three consecutive loops, it is eliminated in subsequent optimization loops. The HL-RDHM uses a multi-scale objective function which optimizes parameters at 24, 240, and 720 hour time scales (NWS 2008).

Rather than calibrating the value of the parameter itself, the HL-RDHM requires the user to calibrate multipliers for each parameter that then are applied to the a priori values. For a given basin and parameter, a single multiplier value is identified. The same multiplier value is applied to each grid cell associated with that basin.

Multiplier values for ten SAC-SMA and two SNOW-17 parameters were calibrated (Table 6). Parameter selection and the allowable range of the multipliers were based on previous studies and NWS documentation (Hogue et al. 2000; Anderson 2002; Ajami et al. 2004; NWS 2004; Tang et al. 2007; Wagener et al. 2009; Franz et al. 2010; He et al. 2011; Steffens and Franz 2012). First, feasible parameter ranges are established using previously published values. Second, the basin mean value of each a prior parameter is computed. Finally, basin-specific maximum and minimum multipliers are computed for each parameter according to the following equations:

$$x_{min} = \alpha / p_{min} \tag{8}$$

$$x_{max} = \alpha / p_{max} \tag{9}$$

Where x_{min} and x_{max} are the minimum and maximum multipliers; α is the basin mean a priori parameter value; and p_{min} and p_{max} are the maximum and minimum bounds for a specific parameter (Table 6).

Not all basin mean a priori parameter values fall within the established calibration range (Table 6). For these instances the minimum or maximum parameter value is set to the a priori mean value $\pm$10%.

		Calibration Range	
Variable	**Description**	**Min**	**Max**
snow_MFMAX	Maximum non-rain melt factor, occurs on June 21 (mm/°C/6hr)	0.8	1.5
snow_PLWHC	Percent liquid water holding capacity (decimal fraction)	0.05	0.4
sac_UZTWM	Upper-zone tension water maximum storage (mm)	20	120
sac_UZFWM	Upper-zone free water maximum storage (mm)	10	100
sac_UZK	Upper-zone free water lateral depletion rate (day^{-1})	0.1	0.8
sac_ZPERC	Maximum percolation rate (dimensionless)	10	200
sac_REXP	Exponent of the percolation rate (dimensionless)	1.5	3.5
sac_LZTWM	Lower-zone tension water maximum storage (mm)	100	200
sac_LZFSM	Lower-zone free water supplementary maximum storage (mm)	5	200
sac_LZFPM	Lower-zone free water primary maximum storage (mm)	5	150
sac_LZSK	Lower-zone free water depletion rate (fraction/day)	0.01	0.5
sac_LZPK	Lower-zone primary free water depletion rate (fraction/day)	0	0.2

Table 6. Parameters selected for calibration and designated range of parameter variability for calibration.

Initial hydrograph analysis indicated that the timing of the peak discharge events was quite accurate relative to the magnitude, therefore, for calibration efficiency purposes, routing parameters were not included in the calibrations. Sample tests revealed that calibration of the routing parameters resulted in only small changes to the simulated hydrograph while adding substantial computing time to the calibration process.

Tang et al. (2007) found significant parameter sensitivity when comparing calibrations to dry versus wet conditions. Therefore we attempt to capture a combination of both wet and dry

conditions by choosing a four year calibration period of January 1, 2007 through December 31, 2010. Both above average and below average annual precipitation conditions occur during this time for most study basins (Table A.13); among all basins the range of precipitation is 947mm for the calibration period and 697mm for the verification period. The verification period is then set to January 1, 2003 to December 31, 2006.

2.4 Results

2.4.1 Calibration Results

The calibration results are summarized as the percent change in the parameter value (equation 11) relative to the range of the parameter multipliers (recall that the allowable range of multipliers varied by parameter and basin):

$$x_{calib} = a \times x_{a\ priori} \tag{10}$$

$$\Delta = \left[x_{calib} - x_{a\ priori}\right] / (x_{max} - x_{min}) \times 100\% \tag{11}$$

where Δ is the percent change, x_{calib} is the calibrated parameter; $x_{a\ priori}$ is the a priori basin mean parameter value, x_{max} and x_{min} are the specified maximum and minimum parameter range, respectively, and a is the calibrated parameter multiplier (Table 6).

The range, variance, and mean percent change for each of the calibrated parameters for two PET inputs are shown in Table 7. SAC-SMA parameters UZTWM (upper-zone tension water maximum storage) and LZTWM (lower-zone tension water maximum storage) have the largest mean change of all parameters. These two parameters define the amount of moisture available to meet PET demands. Prior to calibration the discharge was under-simulated. The

decrease in both these parameters is a result of the calibration algorithm attempting to distribute more water towards discharge to better match the observed.

Movement of moisture into the tension water storages is unidirectional and the tension water storages tend to be a sink for excess water in the model (Steffens and Franz 2012). Tang et al. (2007) found that upper zone storage and percolation parameters are very important during dry conditions, while during wet conditions the lower zone storages become the dominant controlling factors. Because tension water storages were decreased, free water and supplemental water storages are increased to allow for the water to be held as soil moisture thus promoting runoff during precipitation events to be routed to streamflow. Due to the negative streamflow bias evident in nearly every basin, UZFWM also has a considerable increase on average in order for the peak discharge events to be improved (e.g. Figure 7a and Figure 7b).

Lower zone storage and depletion parameters do not exhibit a prominent pattern across all basins; however, individual basins typically show a significant improvement in baseflow simulations after calibration. Calibration results from BCHW3, for example, produce a substantial increase in the LZFSM and LZFMP parameters and a substantial decrease in the UZTWM parameter. This change partitions less moisture available for ET while increasing the moisture available to baseflow (Figure 7c and Figure 7d).

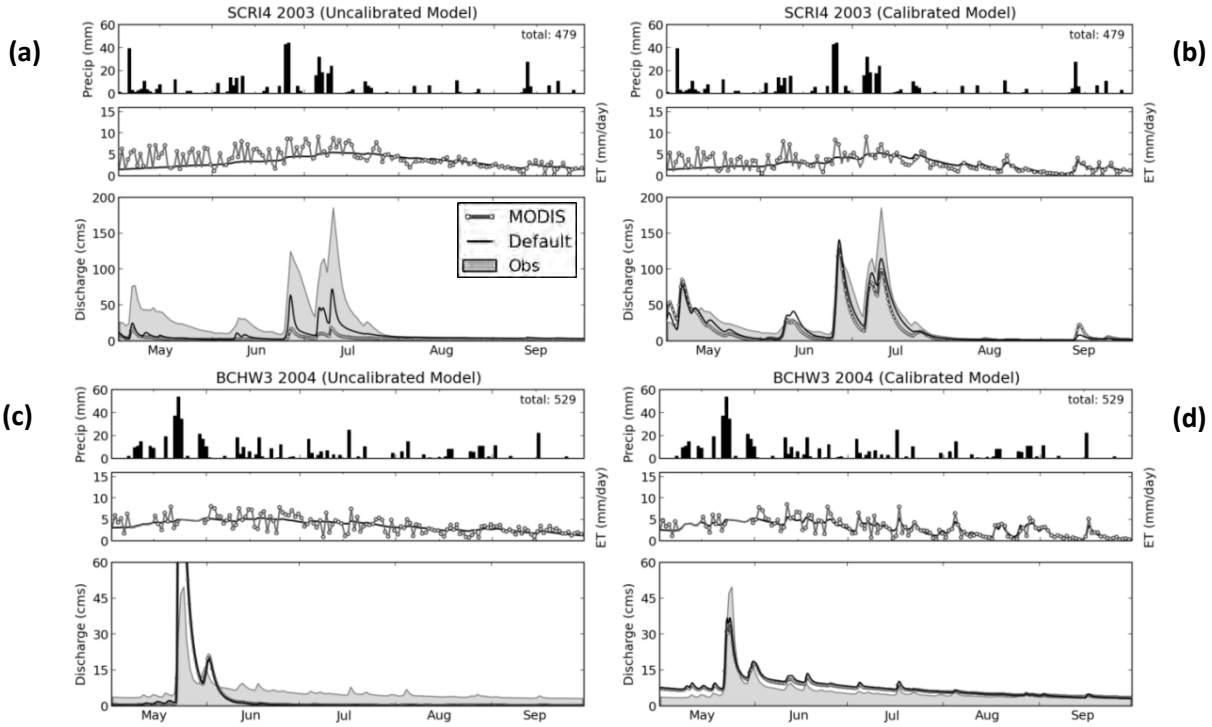

Figure 7. Daily precipitation (top), ET (middle), stream discharge (bottom) for SCRI4 (a,b) and BCHW3 (c,d). Figures on left are a priori parameter simulations and figures on right are calibrated parameter simulations.

ZPERC also has a notable mean decrease (Table 7). ZPERC controls the maximum rate at which water percolates from the upper, faster zone to the lower, slower zone. ZPERC is decreased on average, which again results in larger peak discharge events by slowing the movement of moisture from the upper zone to the lower zone. Calibration results as a whole increase the amount of free water storage (moisture available for baseflow, interflow, and runoff) while also slowing the percolation of water from the upper zone to the lower zone (more upper zone moisture available for interflow and storm runoff). These changes cause substantial changes to the water balance components as evident in the ET and discharge results with a priori and calibrated parameters.

Table 7. Range (min and max), variance, and mean of the percent change of the model parameters for all study basins. Values greater than 100% or less than -100% indicate a change larger than the predetermined range of parameter variability (see section 2.3.10). This occurs when the a priori value is outside the default parameter range and the calibration range was adjusted.

	Default PET				MODIS PET			
Parameter	**Range**		**Variance**	**Mean**	**Range**		**Variance**	**Mean**
sac_UZTWM	-114.1%	-21.6%	7.1%	-59.2%	-100.2%	-21.6%	4.8%	-57.9%
sac_UZFWM	-15.1%	68.7%	6.3%	33.3%	0.0%	71.8%	6.2%	35.6%
sac_ZPERC	-129.6%	51.1%	31.4%	-42.5%	-155.1%	41.7%	32.9%	-28.2%
sac_REXP	-69.2%	86.4%	18.8%	3.5%	-69.2%	93.1%	26.5%	16.7%
sac_LZFSM	-12.4%	83.4%	9.9%	30.0%	-14.5%	57.6%	5.9%	14.4%
sac_LZFPM	-73.4%	87.0%	15.9%	-5.9%	-113.2%	70.3%	25.3%	-22.2%
snow_MFMAX	-113.9%	102.4%	40.0%	3.7%	-184.8%	102.4%	56.9%	-12.3%
sac_LZPK	-9.8%	53.2%	3.6%	15.0%	-9.8%	61.8%	5.5%	16.1%
sac_LZSK	-32.8%	25.0%	3.6%	-6.7%	-27.4%	37.7%	4.0%	-1.7%
sac_UZK	-64.3%	55.3%	14.9%	-0.1%	-64.3%	55.3%	11.1%	-11.7%
snow_PLWHC	-57.1%	85.7%	23.1%	8.8%	-57.1%	85.7%	22.3%	10.0%
sac_LZTWM	-218.0%	14.8%	55.4%	-133.7%	-235.6%	14.8%	50.1%	-148.2%

Comparison of basin averaged simulated ET (a priori parameters) to local flux tower observations show mixed results. For AMWI4, the default simulation had better correlation, bias, and MAE values compared to the MODIS simulation; however, for MMLM5 the MODIS simulation had marginally better correlation and bias and similar MAE values (Table 8).

In both default and MODIS simulations we find a decrease in the ET bias (improved at AMWI4 and degraded at MMLM5) after calibration (Table 8). The bias decrease evident at both basins after calibration is also a direct consequence of the calibration processes proportioning less water available to meet PET demands. Compared to flux-tower observations, the calibration improves the simulated daily ET bias and MAE at the AMWI4 site, but not at MMLM5 where the average daily ET prior to calibration is closer to flux-tower observations.

Consequently, the resulting simulated ET R^2 values following calibration are degraded slightly or remain constant at both basins (Table 8).

	Bias (mm/day)		**R^2**		**MAE (mm/day)**	
	Default	MODIS	Default	MODIS	Default	MODIS
a priori						
AMWI4	0.9	2.2	0.35	0.20	1.3	2.4
MMLM5	-0.4	0.0	0.13	0.24	1.4	1.5
Mean	0.2	1.1	0.24	0.22	1.3	1.9
calibrated						
AMWI4	0.3	1.3	0.22	0.18	1.2	1.9
MMLM5	-0.7	-0.4	0.13	0.18	1.5	1.7
Mean	-0.2	0.5	0.18	0.18	1.3	1.8

Table 8. Analysis of daily bias (mm/day), correlation (R^2), and MAE (mm/day) for MODIS and default simulated ET (a priori parameters) when validated against flux-tower PET/ET observations.

After calibration, simulated hydrographs were improved for all the watersheds based on visual inspection and basic summary statistics of percent bias, NSE, and correlation coefficient (R^2) (Table 9, Table 10, and Table 11). The average bias in simulated basin discharge prior to calibration is negative among all study basins for both the default PET (average bias: -38%) and MODIS-PET (average bias: -62%). The bias is larger for the MODIS-PET application because MODIS-PET values are larger than the default-PET as discussed in section 2.3.6. The negative bias improves substantially after calibration. Mean bias values amongst all basins still show a negative bias with the MODIS-PET input versus the slightly positive bias values with the default PET input.

	Default (a priori)		MODIS (a priori)		Default (Calibrated)		MODIS (Calibrated)		
Basin	Ver	Cal	Ver	Cal	Ver	Cal	Ver	Cal	Annual Precip
BCHW3	-43.73	-44.05	-48.90	-51.20	30.78	26.15	22.25	16.35	937
BERW3	-48.83	-44.40	-64.18	-63.90	-23.00	-20.00	-38.88	-36.80	809
DARW3	-44.23	-46.25	-48.83	-53.55	-4.05	-12.23	-16.93	-24.05	939
MILW3	-14.10	-2.25	-30.05	-28.10	12.65	15.50	-2.43	-1.78	939
AMEI4	-19.13	-8.57	-64.90	-51.38	36.13	19.03	-6.48	-20.08	1008
AMWI4	-49.30	-29.90	-75.45	-58.50	1.35	0.03	-41.10	-38.08	1032
NHRI4	-12.78	-22.83	-56.00	-57.83	53.08	15.33	14.45	-20.42	970
SCRI4	-40.05	-23.15	-74.40	-65.58	6.68	15.43	-7.68	1.20	809
HICM5	-49.80	-41.65	-69.05	-64.80	33.35	25.67	-19.70	-17.88	680
MMLM5	-47.05	-54.83	-61.20	-69.47	58.63	17.13	43.18	4.65	725
PLUM5	-83.90	-77.32	-87.95	-84.23	-52.78	-49.45	-60.08	-61.13	545
RAPM5	-18.15	-9.25	-59.55	-52.95	46.73	38.23	-4.45	-2.45	798
SANM5	-53.08	-59.95	-81.63	-86.08	-44.25	-48.93	-69.45	-71.30	694
Mean	-40.32	-35.72	-63.24	-60.58	11.95	3.22	-14.41	-20.91	837

Table 9. Stream discharge percent bias (%) based on measured values at basin outlet and mean of all basins. Dark shaded bars indicate negative percent bias values (poor performance). Light shaded bars indicate positive percent bias values (poor performance). Basins are divided into sets by state where rows 1-4 contain basins in Wisconsin, rows 5-8 contain basins in Iowa, and rows 9-13 contain basins in Minnesota.

NSE values also improve after calibration, and values for MODIS and default simulations are similar. This finding demonstrates that even with considerably different PET inputs, simulations are heavily influenced by the model parameters and the calibration processes applied. While many basins appear to have very similar error statistics between the two PET simulations, the calibrated default PET simulations result in slightly better mean NSE values than the MODIS-PET simulations (Table 10). Interestingly, both default and MODIS simulations with the a priori parameters show considerably better NSE values during the 2007-2010 period compared to 2003-2006.

	Default (a priori)		MODIS (a priori)		Default (Calibrated)		MODIS (Calibrated)		
Basin	Ver	Cal	Ver	Cal	Ver	Cal	Ver	Cal	Annual Precip
BCHW3	-3.55	-0.57	-2.69	-0.28	0.5	0.29	0.63	0.41	937
BERW3	-0.02	0.1	-0.16	0.12	0.78	0.82	0.61	0.72	809
DARW3	0.06	0.31	0.15	0.4	0.65	0.79	0.76	0.68	939
MILW3	0.44	0.07	0.51	0.49	0.86	0.9	0.87	0.92	939
AMEI4	0.7	0.8	0.23	0.51	0.57	0.8	0.4	0.68	1008
AMWI4	0.3	0.7	-0.02	0.46	0.69	0.84	0.48	0.72	1032
NHRI4	0.72	0.66	0.46	0.45	0.23	0.64	0.1	0.56	970
SCRI4	0.43	0.66	-0.04	0.19	0.66	0.73	0.57	0.63	809
HICM5	0.25	0.32	-0.03	0.04	0.58	0.65	0.57	0.52	680
MMLM5	0.22	0.22	0.07	0.04	-0.34	0.53	-0.15	0.54	725
PLUM5	-0.58	-0.16	-0.69	-0.27	0.19	0.35	0.03	0.17	545
RAPM5	0.26	0.42	0.06	0.21	0.12	0.34	0.57	0.46	798
SANM5	0.17	0.19	-0.34	-0.27	0.44	0.45	0.06	0.11	694
Mean	-0.05	0.29	-0.19	0.16	0.46	0.63	0.42	0.55	837

Table 10. Stream discharge NSE values for each basin and mean of all basins. Values are displayed for both PET inputs and before/after calibration. Verification period is 2003-2006 and calibration period is 2007-2010. Dark shaded bars indicate negative NSE values (poor performance). Light shaded bars indicate positive NSE values (good performance). Basins are divided into sets by state where rows 1-4 contain basins in Wisconsin, rows 5-8 contain basins in Iowa, and rows 9-13 contain basins in Minnesota.

	Default (a priori)		MODIS (a priori)		Default (Calibrated)		MODIS (Calibrated)		
Basin	Ver	Cal	Ver	Cal	Ver	Cal	Ver	Cal	Annual Precip
BCHW3	0.80	0.71	0.82	0.71	0.75	0.50	0.73	0.51	937
BERW3	0.75	0.62	0.75	0.65	0.92	0.89	0.92	0.89	809
DARW3	0.77	0.71	0.76	0.71	0.80	0.82	0.85	0.77	939
MILW3	0.70	0.49	0.70	0.56	0.91	0.94	0.89	0.92	939
AMEI4	0.78	0.83	0.75	0.78	0.82	0.84	0.69	0.75	1008
AMWI4	0.60	0.76	0.55	0.69	0.73	0.86	0.59	0.78	1032
NHRI4	0.79	0.69	0.77	0.69	0.77	0.73	0.76	0.70	970
SCRI4	0.63	0.70	0.52	0.63	0.74	0.78	0.64	0.66	809
HICM5	0.77	0.61	0.64	0.45	0.76	0.72	0.61	0.54	680
MMLM5	0.54	0.48	0.44	0.37	0.64	0.64	0.54	0.56	725
PLUM5	0.44	0.43	0.41	0.43	0.54	0.54	0.47	0.49	545
RAPM5	0.36	0.46	0.41	0.42	0.69	0.70	0.72	0.61	798
SANM5	0.48	0.51	0.35	0.37	0.60	0.59	0.52	0.48	694
Mean	0.65	0.62	0.61	0.57	0.74	0.73	0.69	0.67	837

Table 11. Stream discharge correlation coefficient (R^2) values for each basin and mean of all basins. Light shaded bars indicate positive R^2 values near 1 (good performance). Basins are divided into sets by state where rows 1-4 contain basins in Wisconsin, rows 5-8 contain basins in Iowa, and rows 9-13 contain basins in Minnesota.

There is a prominent pattern of model skill based on the basin location. The basins in southern Wisconsin (Tables 9-11, rows 1-4) typically performed the best, followed by the central Iowa basins (Tables 9-11, rows 5-8), with Minnesota (Tables 9-11, rows 9-13) basins performing the worst. Values of percent bias, NSE, and correlation coefficient (R^2) all show this

trend (Table 9, Table 10, and Table 11). The wetter basins tend to have the best calibrated discharge simulations regardless of the PET data used. Coincidently, the drier Minnesota basins also have the largest mean precipitation correction factors of the three study states (Table 5), suggesting that the application of the precipitation data and precipitation adjustment factors may not be as reliable for drier sites.

2.4.2 Simulation analysis

Correlation between simulated daily ET and observed ET was slightly better for the MODIS simulation ($R^2 = 0.18$) compared to the default simulation ($R^2 = 0.13$) for MMLM5 (Table 3). However, the MODIS simulation ($R^2 = 0.19$) produced a slightly lower correlation than the default simulation ($R^2 = 0.22$) for AMWI4. The default simulation produces a higher correlation in part because the range of observed ET at AMWI4 is smaller relative to MMLM5 which has higher observed ET values. Because the default PET inputs are smaller than the MODIS-PET, less ET is simulated in the case of the former, resulting in less over-estimation as occurs in the MODIS-PET simulation (Figure 8). The observed mean daily ET is larger at MMLM5, and the larger values of the MODIS-PET appear to allow the model to simulate the ET more accurately. At both sites, there are instances where the default PET underestimates the observed ET, and as can be seen in both Figure 8a and Figure 8b, the upper bound of possible simulated ET is obvious. Despite the large variance of daily ET, the small mean bias values indicate long term ET estimates are well represented in both simulations at AMWI4 and MMLM5.

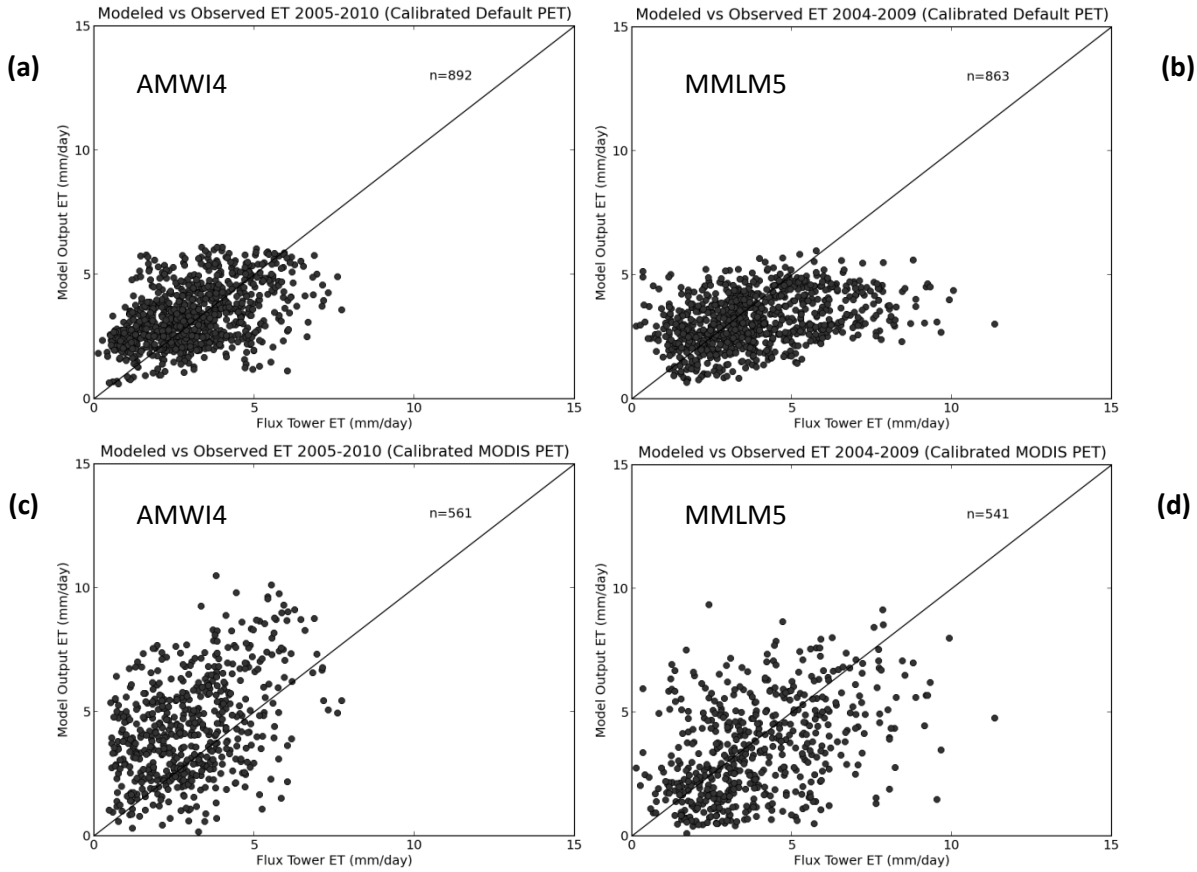

Figure 8. Comparison of mean daily Flux-Tower ET and basin mean default simulated ET (a)(b) and basin mean MODIS simulated ET (c)(d) for AMWI4 and MMLM5 using the calibrated parameters. Smaller number of MODIS simulated ET values due to missing MODIS-PET time periods

To better understand the impact of the simulated ET errors on the long-term water balance, an analysis on the warm season ET accumulation is shown in Figure 9 for two verification years at AMWI4 and MMLM5 and similar accumulation differences are observed in the other six years of the study period. For the two years examined, the MODIS-PET simulation results in approximately 100mm more accumulated ET at the AMWI4 site (Figure 9a and Figure 9b); however, MODIS and default simulations accumulate nearly identical ET totals by the end of the warm season at MMLM5 (Figure 9c and Figure 9d).

At both basins we see a fairly uniform rate of change in the accumulation of simulated ET until late August or early September when the rate decreases as seen by the change in slope (Figure 9) for all years. This matches the observed trend at the AMWI4 site fairly well (Figure 9a and Figure 9b). The drier MMLM5 basin shows a more linear observed ET accumulation trend through September in all years (Figure 9c and Figure 9d) which is poorly captured by the model simulations. The over-estimation of ET from the MODIS simulations during the first month of the warm period results in an overestimation of the total ET at the AMWI4 site in all years (Figure 9a and Figure 9b). In contrast, MODIS simulation typically produces a better match during May and June at MMLM5 due to the larger PET values, but a significant deficit in accumulated ET develops by the end of the warm season (Figure 9c and Figure 9d). This deficit also occurs with the default simulation, indicating both simulations have a similar available moisture limitation during this period.

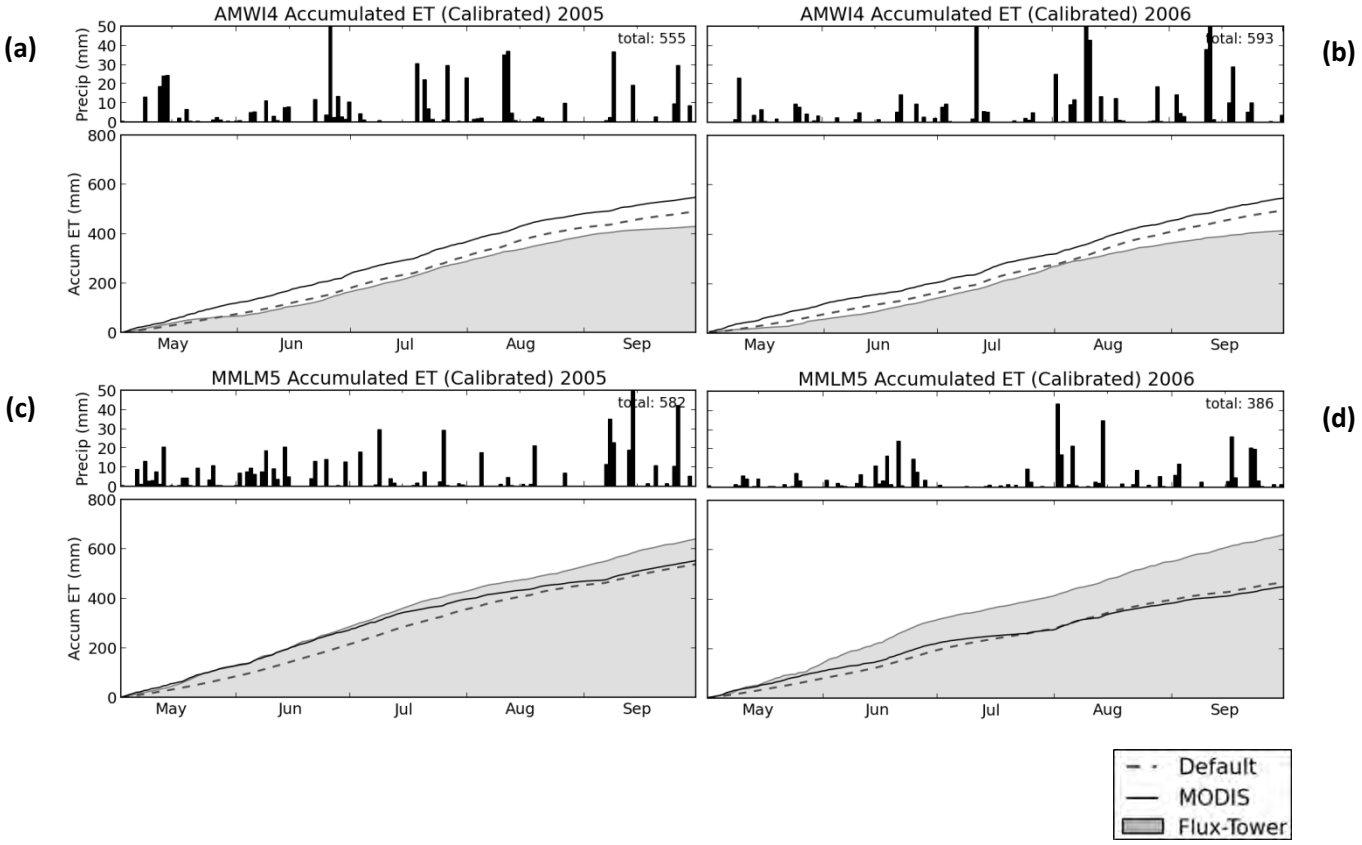

Figure 9. Seasonal ET accumulation for AMWI4 and MMLM5 simulations with corresponding flux-tower record. Plots show a representative wet (column 1) and dry (column 2) warm season period at each location.

At both sites we find the MODIS simulation typically results in larger simulated daily ET values than the default simulation (Figure 10), particularly during the spring (May and June). In contrast, simulated daily ET values from both PET inputs are similar during the last two months of the study period (August and September). This is likely the result of drier conditions typical of this time period resulting in relatively drier soil moisture conditions within the model. As soil moisture depletes in the upper soil zones, available ET moisture is controlled by the less transient lower soil zone moisture resulting in more consistent ET withdraw between the two simulations.

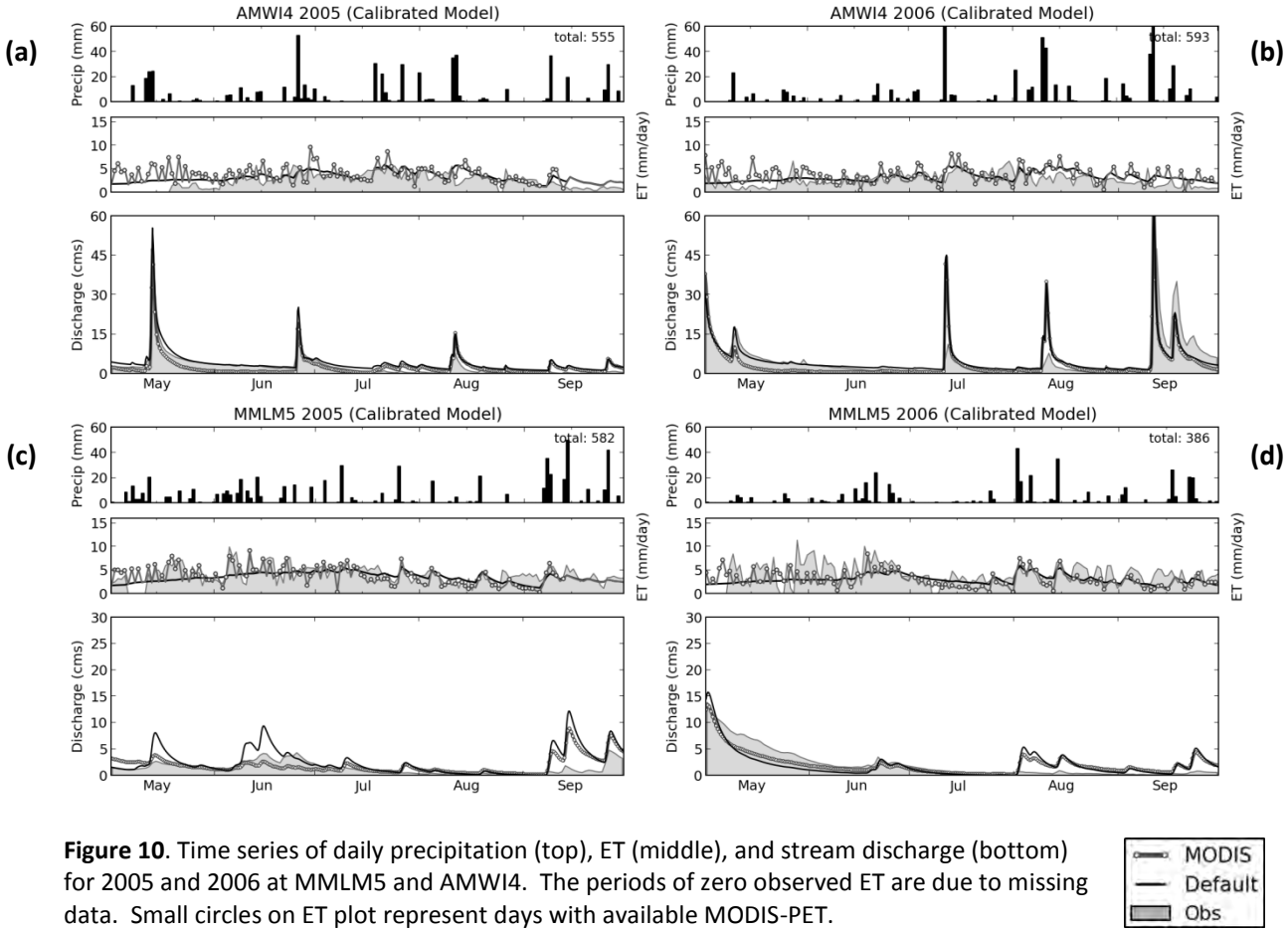

Figure 10. Time series of daily precipitation (top), ET (middle), and stream discharge (bottom) for 2005 and 2006 at MMLM5 and AMWI4. The periods of zero observed ET are due to missing data. Small circles on ET plot represent days with available MODIS-PET.

The over-estimate of ET produced by the MODIS simulation results in under-estimated May and June discharge values at AMWI4 (Figure 10a and Figure 10b). MODIS ET accumulation shows a positive displacement early in the season and then remains somewhat constant until the August September period when the positive displacement is increased again. The default ET accumulation shows a better match to observed data for most of the warm season (Figure 9a and Figure 9b). As expected the default PET, which also resulted in a closer match to the observed PET, produces slightly better discharge simulations in this case.

The simulated hydrograph results with both PET inputs at MMLM5 show a substantial over-estimation of discharge in the second half of the warm season for all years (Figure 10c and Figure 10d). This can also be directly related to the under-estimated simulated ET accumulation in Figure 9c and Figure 9d. The large negative ET displacement is indication that the model is not allowing for enough moisture to exit the soil thus resulting in lower ET values and higher stream discharge values. A simple test increasing the MODIS PET by 50% during July, August, and September results in little to no change in the over-estimated discharge during this time period. This finding indicates the model struggles to reproduce the soil moisture available to ET possibly due to vegetation water use not captured by the model parameters or PET input. Simulated discharge during May and June appear to be slightly improved with the MODIS-PET (Figure 10c and Figure 10d), as ET accumulations from the MODIS simulation are also slightly better than default ET accumulations (Figure 9c and Figure 9d).

Accumulated flux-tower PET for the same time period appears to be fairly well represented by the MODIS-PET albeit with a small positive bias for both basins and all years

(Figure 11). The accumulated default PET has a small negative bias for all years examined with the largest deficits peaking in the middle of the warm season and then slightly recovering by the end of September. MODIS-PET appears to show a slightly better accumulation trend for all years until the accumulated surplus in August and September. In some cases simulated ET accumulation trends deviate considerably from the PET trends with respect to the flux-tower data, therefore we must consider the possible errors from the assumptions made in the Priestley-Taylor equation, errors in the input precipitation, and the SAC-SMA model components' limitations under a wide range of conditions.

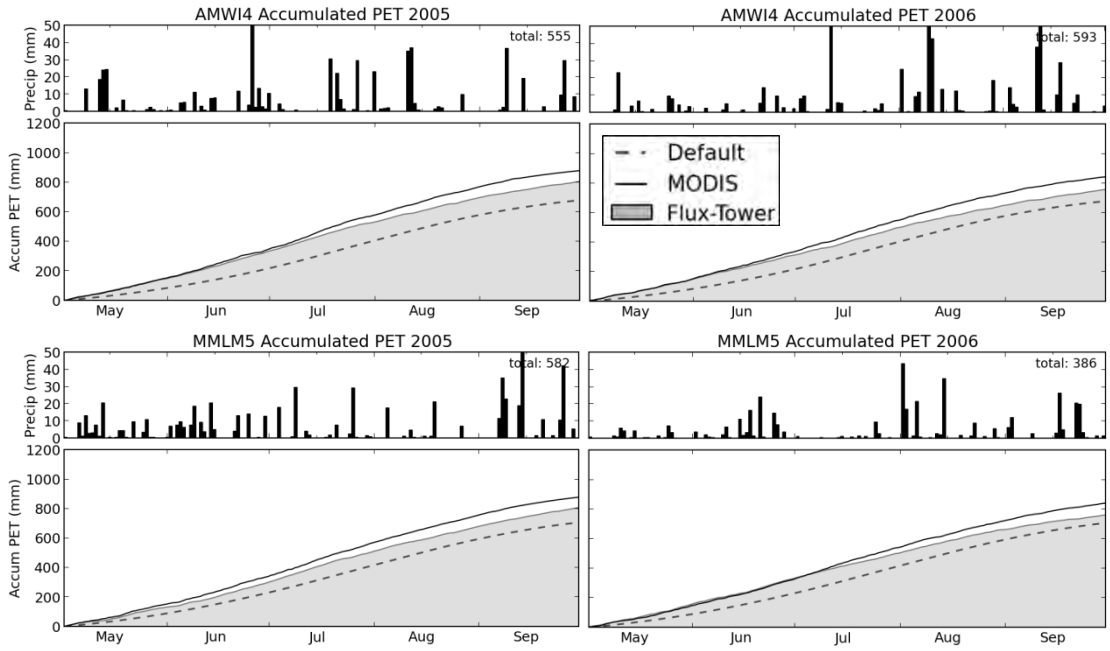

Figure 11. Seasonal PET accumulation for AMWI4 and MMLM5 simulations with corresponding flux-tower record. Plots show a representative wet (column 1) and dry (column 2) warm season period at each location.

2.4.3 Simulated Water Balance

The water balance from the model simulations during the 8-year study period at MMLM5 partition a much larger percentage of the input precipitation for evapotranspiration

output compared to the AMWI4 site (Figure 12a,b,c,d). The large differences in the ET and discharge component magnitude among all 13 basins also emphasize the role climate conditions play in determining the magnitude of each output component. Basins with higher annual precipitation amounts correspond to decreased percent ET output and increased percent discharge output, thus we see the Minnesota basins have the highest ET output percentages.

The default simulations at the AMWI4 basin result in a relatively larger quantity of water output as river discharge (36.3%) compared to the MODIS simulation (27.9%), but the MMLM5 basin discharge simulations demonstrate limited difference between the two PET inputs (16.0% for default and 16.9% for MODIS). This analysis also emphasizes the importance ET plays on the overall water balance of the watershed model with the majority of water exiting the watershed through ET (>50% ET output for all study basins). Interestingly, all 13 basins show less than 8% difference between the MODIS and default ET simulations after calibration, despite the previously noted larger MODIS-PET values. The MMLM5 basin even shows slightly less ET output with the MODIS simulation (81.4%) compared to the default simulation (81.6%). This is an example of the calibration procedure finding different parameter solutions based on the input. These results also suggest that significant changes are made to the simulated ET component after calibration to allow both PET inputs to simulate similar discharge values (appendix A.11).

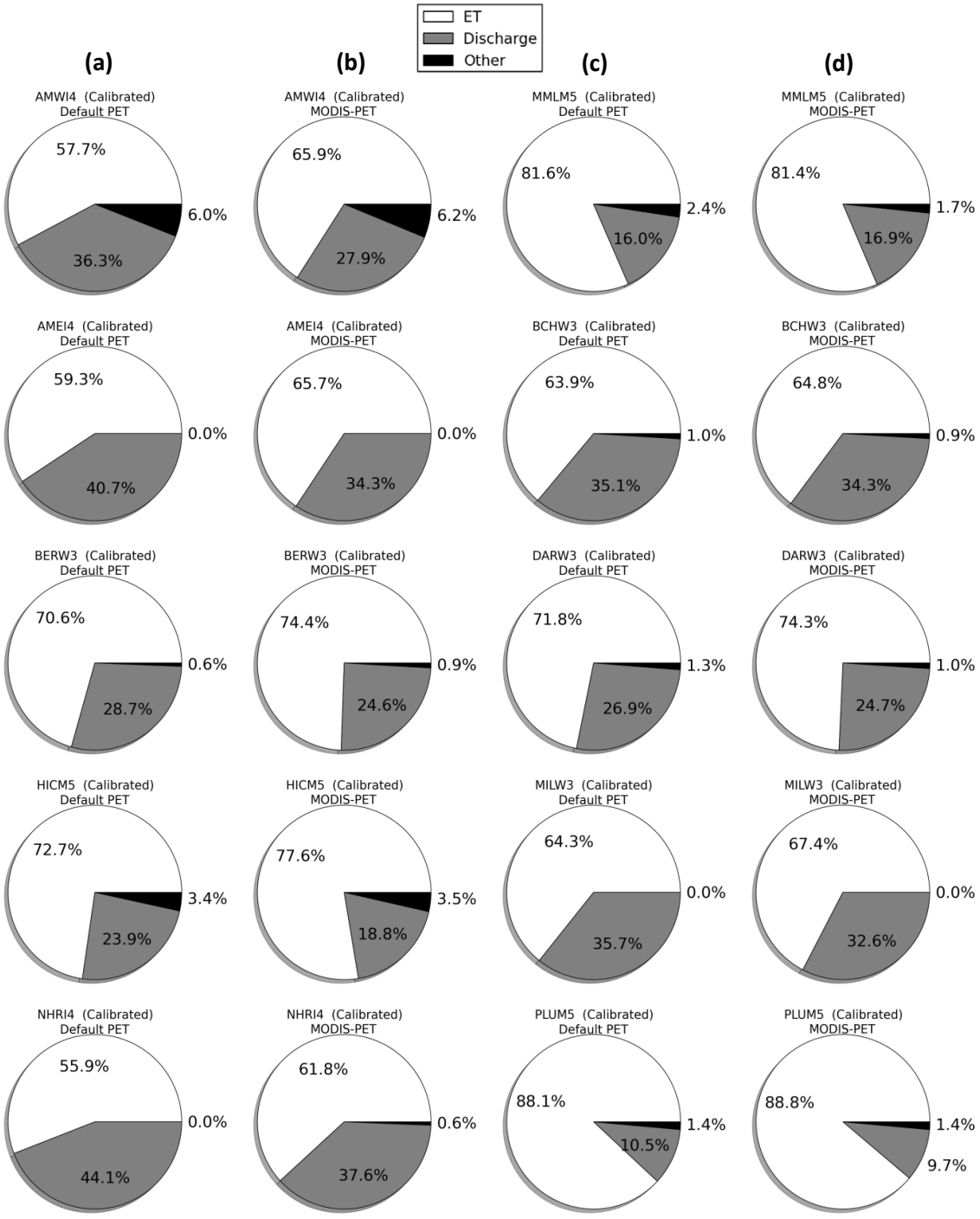
ET
Discharge
Other
(a)
(b)
(c)
(d)
AMWI4 (Calibrated) Default PET
57.7%
6.0%
36.3%
AMWI4 (Calibrated) MODIS-PET
65.9%
6.2%
27.9%
MMLM5 (Calibrated) Default PET
81.6%
2.4%
16.0%
MMLM5 (Calibrated) MODIS-PET
81.4%
1.7%
16.9%
AMEI4 (Calibrated) Default PET
59.3%
0.0%
40.7%
AMEI4 (Calibrated) MODIS-PET
65.7%
0.0%
34.3%
BCHW3 (Calibrated) Default PET
63.9%
1.0%
35.1%
BCHW3 (Calibrated) MODIS-PET
64.8%
0.9%
34.3%
BERW3 (Calibrated) Default PET
70.6%
0.6%
28.7%
BERW3 (Calibrated) MODIS-PET
74.4%
0.9%
24.6%
DARW3 (Calibrated) Default PET
71.8%
1.3%
26.9%
DARW3 (Calibrated) MODIS-PET
74.3%
1.0%
24.7%
HICM5 (Calibrated) Default PET
72.7%
3.4%
23.9%
HICM5 (Calibrated) MODIS-PET
77.6%
3.5%
18.8%
MILW3 (Calibrated) Default PET
64.3%
0.0%
35.7%
MILW3 (Calibrated) MODIS-PET
67.4%
0.0%
32.6%
NHRI4 (Calibrated) Default PET
55.9%
0.0%
44.1%
NHRI4 (Calibrated) MODIS-PET
61.8%
0.6%
37.6%
PLUM5 (Calibrated) Default PET
88.1%
1.4%
10.5%
PLUM5 (Calibrated) MODIS-PET
88.8%
1.4%
9.7%

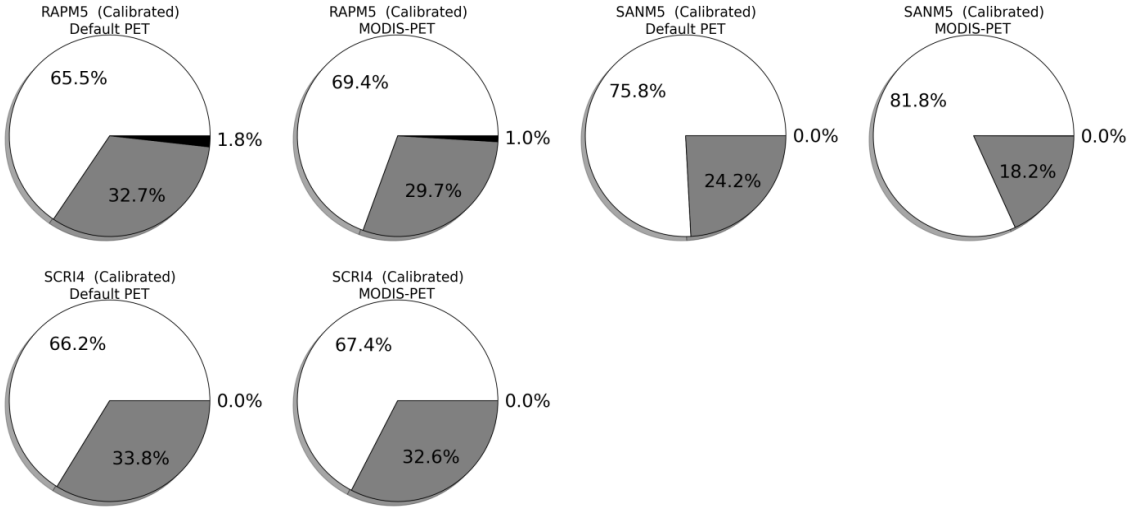

Figure 12. Water balance percentages calculated for all 13 basins for the full study period with calibrated parameters and (a)(c) default PET and (b)(d) MODIS-PET. Deep groundwater percolation and change in soil moisture storage are lumped together in the other category.

2.5 Summary and conclusions

This study examines the potential for the spatially and temporally variable satellite-based PET estimation technique of Kim and Hogue (2008) to be implemented into the distributed HL-RDHM. We analyze the simulated ET and discharge values from the new MODIS-PET simulations as well as the standard default PET simulations and compare the results to discharge observations from the 13 upper Midwestern basins and PET/ET observations at two nearby flux tower locations. Through an analysis of the simulated water balance at the daily, seasonal, and multi-year time scale of several we have examined the role PET estimates play in simulating stream discharge at a basin outlet. Results show we were able to reproduce and in some cases improve upon stream discharge simulations using the new MODIS-PET product; however, there are also several instances where the MODIS-PET results in a slight degradation in the simulated discharge accuracy (MODIS NSE = 0.42, default NSE = 0.46). Model simulated discharge accuracy shows a strong relationship to basin mean annual precipitation, with the

lower latitude and larger annual precipitation basins demonstrating the best model skill. This finding could be the result of multiple conditions including the calibration period chosen, the input precipitation and precipitation correction applied to all events, and the limitations associated with the HL-RDHM model components. Jacobs et al. (2009) also noted difficulties in model prediction using the SAC-SMA during low flows.

An examination of simulated daily ET values against observed ET measurements for the AMWI4 and MMLM5 basins shows both PET inputs result in similar simulated ET accuracy statistics (MODIS and default R^2 = 0.18 after calibration). In many instances simulated discharge errors can be directly related to accumulated errors in simulated ET. It is important to remember the flux-tower PET and ET records are from a single point location and we are evaluating them against basin averages, so a perfect match is not expected. However, these records are currently the best available ground based measurements and were useful to perform a simple validation of the MODIS-PET and simulated ET.

While these results cannot definitively conclude which PET product results in a better simulation of ET, the all-around relatively poor correlation to observed ET results with both PET products (R^2 values range from 0.13 to 0.35) would suggest the model has difficulties reproducing the processes governing ET at the daily time scale. It is also important to keep in mind some of the limitations associated with using a conceptual model such as the use of model parameters without a direct physical interpretation to measurable values, the simplification of hydrological processes, and the essential calibration procedure implemented for each basin. Observed daily PET variability is captured reasonably well by the MODIS-PET,

and the resulting simulated daily ET variability trends show a better match to observed conditions than the default simulations. Unfortunately, the larger MODIS-PET range also leads to larger error possibilities, limiting the benefits of long-term ET simulations over default simulations.

With the advancement of coupled surface-subsurface hydrologic models on the horizon, a spatially and temporally accurate PET data source is essential for improved future hydrologic simulations. The application of the globally available daily MODIS PET product has shown promising potential as an alternative to the current climatological default PET product in hydrologic models while maintaining simulated discharge accuracy.

2.6 Acknowledgements

Financial support for this work was provided by NASA grant #NNX10AQ77G S01. Special thanks to Mike DeWeese at the NCRFC and Mike Smith at the OHD for their assistance with the model logistics and sharing their data. The authors are also grateful to Dave Flory for his assistance installing the model.

2.7 References

AmeriFlux, 2012. AmeriFlux Network http://public.ornl.gov/ameriflux

Anderson, E. (2006). Snow Accumulation and Ablation Model – SNOW-17, (January).

Anderson, E. A. (2002), Calibration of Conceptual Hydrologic Models for Use in River Forecasting, Office of Hydrologic Development, National Weather Service, Silver Spring, MD.

Andréassian, V., Perrin, C., & Michel, C. (2004). Impact of imperfect potential evapotranspiration knowledge on the efficiency and parameters of watershed models. *Journal of Hydrology*, *286*(1-4), 19–35. doi:10.1016/j.jhydrol.2003.09.030

Bisht, G., Venturini, V., Islam, S., & Jiang, L. (2005). Estimation of the net radiation using MODIS (Moderate Resolution Imaging Spectroradiometer) data for clear sky days. *Remote Sensing of Environment*, *97*(1), 52–67. doi:10.1016/j.rse.2005.03.014

Boyle, D. P., Gupta, H. V., Sorooshian, S., Koren, V., Zhang, Z., & Smith, M. (2001). Toward improved streamflow forecasts: value of semidistributed modeling. *Water Resources Research*, *37*(11), 2749. doi:10.1029/2000WR000207

Burnash, R. J. C. (1995). *Computer Models of Watershed Hydrology*. (V. Singh, Ed.) (pp. 311–366). Littleton, CO: Water Resources Publications.

Butts, M. B., Payne, J. T., Kristensen, M., & Madsen, H. (2004). An evaluation of the impact of model structure on hydrological modelling uncertainty for streamflow simulation. *Journal of Hydrology*, *298*(1-4), 242–266. doi:10.1016/j.jhydrol.2004.03.042

Dingman, L. (2002). *Physical Hydrology* (Second Edi.). Long Grove, IL: Waveland Press, Inc.

Douglas, E. M., Jacobs, J. M., Sumner, D. M., & Ray, R. L. (2009). A comparison of models for estimating potential evapotranspiration for Florida land cover types. *Journal of Hydrology*, *373*(3-4), 366–376. doi:10.1016/j.jhydrol.2009.04.029

Franz, K. J., P. Butcher, N. K. Ajami (2010), Addressing snow model uncertainty for hydrologic prediction, Adv. Water Resour., 33, 820-832.

Franz, K. J., & Karsten, L. R. (2013). Calibration of a distributed snow model using MODIS snow covered area data. *Journal of Hydrology*, *494*, 160–175. doi:10.1016/j.jhydrol.2013.04.026

Fry, J., Xian, G., Jin, S., Dewitz, J., Homer, C., Yang, L., Barnes, C., Herold, N., and Wickham, J., 2011. Completion of the 2006 National Land Cover Database for the Conterminous United States, PE&RS, Vol. 77(9):858-864.

Fulton, R. A. (1998). *WSR-88D Polar-to-HRAP Mapping* (pp. 1–33). Silver Spring, MD.

Gourley, J. J., & Vieux, B. E. (2006). A method for identifying sources of model uncertainty in rainfall-runoff simulations. *Journal of Hydrology*, *327*(1-2), 68–80. doi:10.1016/j.jhydrol.2005.11.036

Gupta, H. V., Sorooshian, S., & Yapo, P. O. (1998). Toward improved calibration of hydrologic models : Multiple and noncommensurable measures of information, *34*(4), 751–763.

He, M., Hogue, T. S., Franz, K. J., Margulis, S. a., & Vrugt, J. a. (2011). Characterizing parameter sensitivity and uncertainty for a snow model across hydroclimatic regimes. *Advances in Water Resources*, *34*(1), 114–127. doi:10.1016/j.advwatres.2010.10.002

Hogue, T., Sorooshian, S., Gupta, H., Holz, A., & Braatz, D. (2000). A Multistep Automatic Calibration Scheme for River Forecasting Models. *Journal of Hydrometeorology*, *1*, 524–542.

Hou, D., Charles, M., Luo, Y., Toth, Z., Zhu, Y., Krzysztofowicz, R., Lin, Y., et al. (2012). Climatology-Calibrated Precipitation Analysis at Fine Scales: Statistical Adjustment of STAGE IV towards CPC Gauge-Based Analysis. *Journal of Hydrometeorology*.

Hydrology Laboratory-Research Distributed Hydrologic Model (HL-RDHM) User Manual V. 3.2.0. (2011)., *0*.

Irmak, S., Kabenge, I., Skaggs, K. E., & Mutiibwa, D. (2012). Trend and magnitude of changes in climate variables and reference evapotranspiration over 116-yr period in the Platte River Basin, central Nebraska–USA. *Journal of Hydrology*, *420-421*, 228–244. doi:10.1016/j.jhydrol.2011.12.006

Jacobs, J. M., Lowry, B., Choi, M., & Bolster, C. H. (2009). GOES Solar Radiation for Evapotranspiration Estimation and Streamflow Prediction. *Journal of Hydrologic Engineering*, (March).

K. Ajami, N., Gupta, H., Wagener, T., & Sorooshian, S. (2004). Calibration of a semi-distributed hydrologic model for streamflow estimation along a river system. *Journal of Hydrology*, *298*(1-4), 112–135. doi:10.1016/j.jhydrol.2004.03.033

Kim, J., & Hogue, T. S. (2008). Evaluation of a MODIS-Based Potential Evapotranspiration Product at the Point Scale. *Journal of Hydrometeorology*, *9*(3), 444–460. doi:10.1175/2007JHM902.1

Koren, V., Finnerty, B., Schaake, J., Smith, M., Seo, D.-J., & Duan, Q.-Y. (1999). Scale dependencies of hydrologic models to spatial variability of precipitation. *Journal of Hydrology*, *217*(3-4), 285–302. doi:10.1016/S0022-1694(98)00231-5

Koren, V., Reed, S., Smith, M., Zhang, Z., & Seo, D.-J. (2004). Hydrology laboratory research modeling system (HL-RMS) of the US national weather service. *Journal of Hydrology*, *291*(3-4), 297–318. doi:10.1016/j.jhydrol.2003.12.039

Looper, J. P., Vieux, B. E., & Moreno, M. a. (2012). Assessing the impacts of precipitation bias on distributed hydrologic model calibration and prediction accuracy. *Journal of Hydrology*, *418-419*, 110–122. doi:10.1016/j.jhydrol.2009.09.048

Lu, J., Sun, G., Mcnulty, S. G., & Amatya, D. M. (2005). A Comparison of Six Potential Evapotranspiration Methods for Regional Use in the Southeastern Unites States. *Journal of the American Water Resources Association*, *29414*, 621–633.

Lu, X., & Zhuang, Q. (2010). Evaluating evapotranspiration and water-use efficiency of terrestrial ecosystems in the conterminous United States using MODIS and AmeriFlux data. *Remote Sensing of Environment*, *114*(9), 1924–1939. doi:10.1016/j.rse.2010.04.001

Moreda, F., Koren, V., Zhang, Z., Reed, S., & Smith, M. (2006). Parameterization of distributed hydrological models: learning from the experiences of lumped modeling. *Journal of Hydrology*, *320*(1-2), 218–237. doi:10.1016/j.jhydrol.2005.07.014

Nash, J.E., Sutcliffe, J.V., 1970. River flow forecasting through conceptual models. Part I—a discussion of principles. Journal of Hydrology 10, 282–290.

NWS (2004), The National Weather Service River Forecast System User's Manual, available online at http://www.nws.noaa.gov/ohd/hrl, referenced version was downloaded on September 17th, 2007.

NWS (2008), The National Weather Service Hydrology Laboratory-Research Distributed Hydrologic Model (HL-RDHM), available online at http://www.mdl.nws.noaa.gov/~applications/LAD/, referenced version was downloaded on February 13th, 2012.

Oudin, L., Hervieu, F., Michel, C., Perrin, C., Andréassian, V., Anctil, F., & Loumagne, C. (2005). Which potential evapotranspiration input for a lumped rainfall–runoff model? *Journal of Hydrology*, *303*(1-4), 290–306. doi:10.1016/j.jhydrol.2004.08.026

Pechlivanidis, I. G., Jackson, B. M., Mcintyre, N. R., & Wheater, H. S. (2011). Catchment scale hydrological modelling: a review of model types, calibration approaches and uncertainty analysis methods in the context of recent developments in technology and applications, *13*(3), 193–214.

Pereira, A. R. (2004). The Priestley–Taylor parameter and the decoupling factor for estimating reference evapotranspiration. *Agricultural and Forest Meteorology*, *125*(3-4), 305–313. doi:10.1016/j.agrformet.2004.04.002

Priestley, C. H. B., & Taylor, R. J. (1972). On the Assessment of Surface Heat Flux and Evaporation Using Large-Scale Parameters. *Monthly Weather Review*, *100*(February), 81–92.

Rana, G., & Katerji, N. (2000). Measurement and estimation of actual evapotranspiration in the field under Mediterranean climate: a review. *European Journal of Agronomy*, *13*(2-3), 125–153. doi:10.1016/S1161-0301(00)00070-8

Reed, S., Koren, V., Smith, M., Zhang, Z., Moreda, F., Seo, D.-J., & DMIP Participants, and. (2004). Overall distributed model intercomparison project results. *Journal of Hydrology*, *298*(1-4), 27–60. doi:10.1016/j.jhydrol.2004.03.031

Reed, S. M. (2003). Deriving flow directions for coarse-resolution (1-4 km) gridded hydrologic modeling. *Water Resources Research*, *39*(9), n/a–n/a. doi:10.1029/2003WR001989

Schilling, K. E., & Helmers, M. (2008). Effects of subsurface drainage tiles on streamflow in Iowa agricultural watersheds : Exploratory hydrograph analysis. *Hydrological Processes*, *4506*(May), 4497–4506. doi:10.1002/hyp

Schilling, K. E., & Libra, R. D. (2004). Increased baseflow in Iowa over the second half of the20th century. *Journal of the American Water Resources Association*, *1319*, 851–860.

Shah, S. M. S., Connellbp, P. E. O., & Hoskingc, J. R. M. (1996). Modelling the effects of spatial variability in rainfall on catchment response . 2 . Experiments with distributed and lumped models, *175*, 89–111.

Smith, M. B., Koren, V. I., Zhang, Z., Reed, S. M., Pan, J.-J., & Moreda, F. (2004). Runoff response to spatial variability in precipitation: an analysis of observed data. *Journal of Hydrology*, *298*(1-4), 267–286. doi:10.1016/j.jhydrol.2004.03.039

Smith, M. B., Koren, V., Reed, S., Zhang, Z., Zhang, Y., Moreda, F., Cui, Z., et al. (2012). The distributed model intercomparison project – Phase 2: Motivation and design of the Oklahoma experiments. *Journal of Hydrology*, *418-419*, 3–16. doi:10.1016/j.jhydrol.2011.08.055

Smith, M. B., Koren, V., Zhang, Z., Zhang, Y., Reed, S. M., Cui, Z., Moreda, F., et al. (2012). Results of the DMIP 2 Oklahoma experiments. *Journal of Hydrology*, *418-419*, 17–48. doi:10.1016/j.jhydrol.2011.08.056

Steffens, K. J., & Franz, K. J. (2012). Late 20th-century trends in Iowa watersheds: an investigation of observed and modelled hydrologic storages and fluxes in heavily managed landscapes. *International Journal of Climatology*, *32*(9), 1373–1391. doi:10.1002/joc.2361

Sumner, D. M., & Jacobs, J. M. (2005). Utility of Penman–Monteith, Priestley–Taylor, reference evapotranspiration, and pan evaporation methods to estimate pasture evapotranspiration. *Journal of Hydrology*, *308*(1-4), 81–104. doi:10.1016/j.jhydrol.2004.10.023

Tang, Y., Reed, P., Van Werkhoven, K., & Wagener, T. (2007). Advancing the identification and evaluation of distributed rainfall-runoff models using global sensitivity analysis. *Water Resources Research*, *43*(6), W06415. doi:10.1029/2006WR005813

Vieux, B. E., Cui, Z., & Gaur, A. (2004). Evaluation of a physics-based distributed hydrologic model for flood forecasting. *Journal of Hydrology*, *298*(1-4), 155–177. doi:10.1016/j.jhydrol.2004.03.035

Wagener, T., Van Werkhoven, K., Reed, P., & Tang, Y. (2009). Multiobjective sensitivity analysis to understand the information content in streamflow observations for distributed

watershed modeling. *Water Resources Research*, *45*(2), n/a–n/a. doi:10.1029/2008WR007347

Yilmaz, K. K., Gupta, H. V., & Wagener, T. (2008). A process-based diagnostic approach to model evaluation: Application to the NWS distributed hydrologic model. *Water Resources Research*, *44*(9), W09417. doi:10.1029/2007WR006716

Zhang, Y., Zhang, Z., Reed, S., Koren, V., Service, N. W., & Spring, S. (2007). *An Enhanced and Automated Approach for Deriving a priori SAC-SMA Parameters from the Soil Survey Geographic Database*. Silver Spring, MD.

CHAPTER 3. GENERAL CONCLUSIONS

3.1 Major Findings

This study was designed to examine the potential benefits of using a satellite-derived daily PET product in place of the current default climatology-based monthly PET estimates. Stream discharge and ET simulations are tested at 13 Midwestern basins using an eight-year study period. The major findings of this study are:

1) Stream discharge simulations show similar model skill using both MODIS-PET and the default PET after calibration (MODIS NSE = 0.42, default NSE = 0.46). Five basins show improved discharge NSE values using the MODIS-PET (BCHW3, DARW3, MILW3, MMLM5, and RAPM5).
2) MODIS-PET exhibits a much improved daily correlation to observed flux-tower PET estimates (MODIS mean R^2 = 0.66, default mean R^2 = 0.13); however, MODIS-PET also shows a higher daily bias (1.2 mm/day) compared to default PET (-0.5 mm/day).
3) ET simulations demonstrate mixed results between the two PET inputs with MODIS simulations showing better accuracy for MMLM5 (after calibration: bias = -0.4 mm/day, R^2 = 0.18, MAE = 1.7 mm/day) and default simulations showing better accuracy for AMWI4 (after calibration: bias = 0.3 mm/day, R^2 = 0.22, MAE = 1.2 mm/day).
4) Calibrating several important model parameters substantially improves discharge simulations for all study basins while slightly degrading the simulated daily ET correlation.

5) Stream discharge simulations show a prominent model skill trend with the more southern latitude and higher annual precipitation basins showing the best results.

3.2 Future Work

There are several aspects of this project that would likely benefit from more testing. The following recommendations may lead to a better understanding of how to improve distributed model simulations using the MODIS-PET:

- Expand calibration procedure to include routing parameters (e.g. several basins exhibit a more prolonged hydrograph storm event than simulations produced, possibly indicating the roughness parameter may need to be calibrated for some basins)
- Expand calibration period to test more dry years
- Examine other precipitation inputs (CCPA precipitation required adjustment factors)
- Test observed PET data as input into the model
- Test new Soil Survey Geographic Database (SSURGO) a priori parameters
- Examine watersheds with different range of climates
- Compare results to a lumped model

ACKNOWLEDGEMENTS

This thesis was made possible by the support and assistance from numerous people to whom I owe sincere thanks. I would like to thank my advisor, Dr. Kristie Franz for allowing me the opportunity to work on this research project. Her advice and patience have kept me on track during the last two years. The skills and connections I have developed under her guidance have helped prepare me for a future career in the hydrology field, and I am eternally grateful to have found a scientific field I can enjoy for the rest of my life.

I would also like to thank Dr. Bill Simpkins and Dr. Brian Hornbuckle for their advice and feedback while serving on my committee as well as their passionate instruction throughout my coursework at ISU.

Thanks to my fellow ISU colleagues Angela Bowman and David Dziubanski for all of their assistance and general entertainment over the last two years. You both made coming into the office everyday an enjoyable experience.

Also thanks to Dave Flory, Chris Karstens, Mike DeWeese, and Mike Smith for their assistance with the model logistics, programming questions, and general advice.

A special thanks goes to my parents and siblings for always supporting me in all of my life goals. I couldn't ask for a more loving and supportive family. I also want to thank Ms. Erin Lower for all of her help and encouragement throughout the last year.

Financial support for this work was provided by NASA grant #NNX10AQ77G S01

APPENDIX

A.1 Study Sites

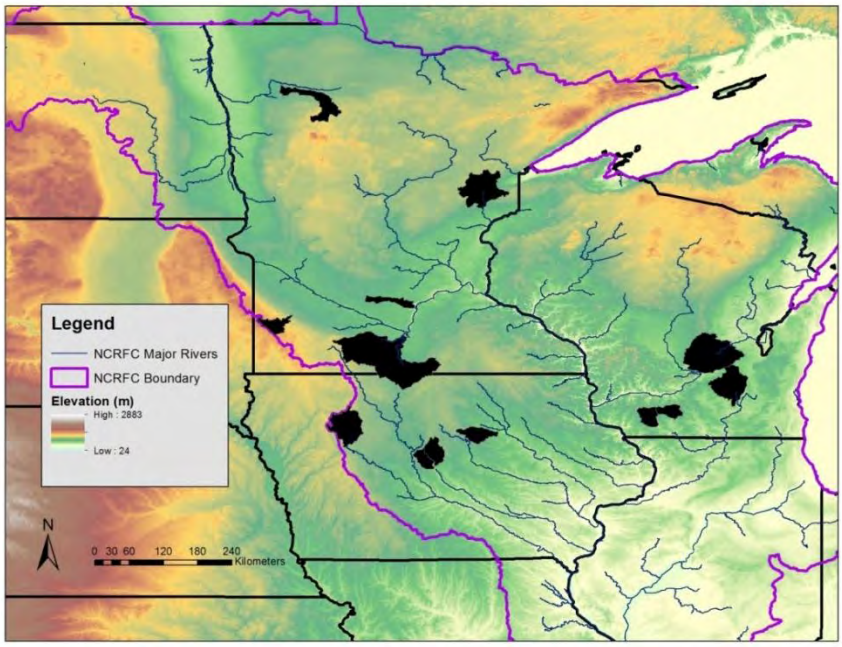

Figure A.13. Map of study basins with major NCRFC rivers and 1km Digital Elevation Model

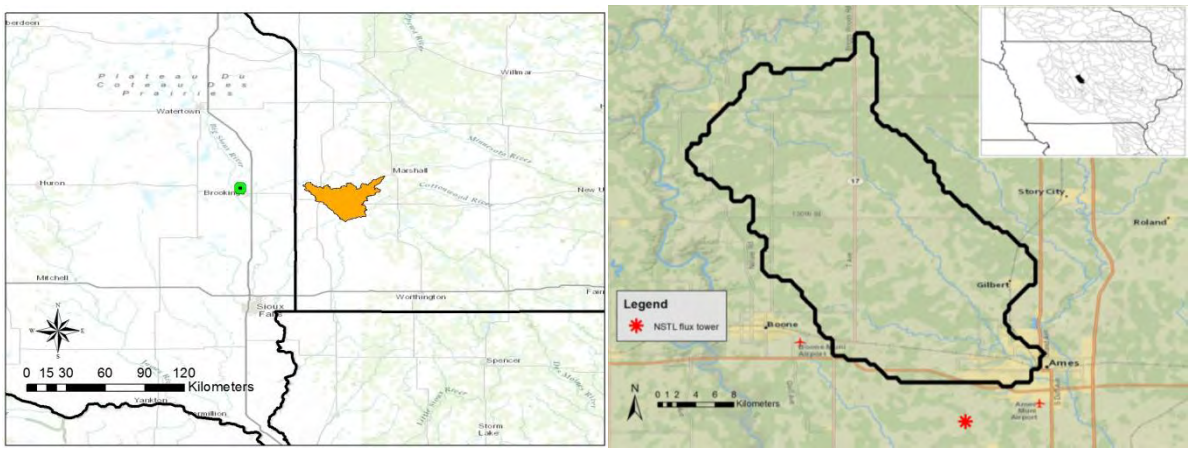

Figure A.14. Flux tower locations for MMLM5 (left) and AMWI4 (right)

A.2 Model Parameters

Parameter	Description	Source
snow_ALAT	Latitude	OHD Grid
snow_SCF	Snow correction factor (dimensionless)	NCRFC mean value
snow_MFMAX	Maximum melt factor [mm $^{o}C^{-1}$ (6 h)$^{-1}$]	OHD Grid
snow_MFMIN	Minimum melt factor [mm $^{o}C^{-1}$ (6 h)$^{-1}$]	OHD Grid
snow_NMF	Maximum negative melt factor [mm $^{o}C^{-1}$ (6 h)$^{-1}$]	NCRFC mean value
snow_UADJ	Average wind function during rain-on-snow periods (mm/mb)	OHD Grid
snow_SI	Mean areal water-equivalent above which 100 percent areal snow cover (mm)	NCRFC mean value
snow_MBASE	Base air temperature for non-rain melt computations (°C)	NCRFC mean value
snow_PXTMP	Air temperature threshold determining precipitation as rain or snow (°C)	NCRFC mean value
snow_PLWHC	Maximum liquid water holding capacity of the snowpack (decimal fraction)	NCRFC mean value
snow_TIPM	Antecedent temperature index (dimensionless)	NCRFC mean value
snow_PGM	Daily ground melt (mm day-1)	NCRFC mean value
snow_ELEV	Mean elevation (m)	OHD Grid
snow_LAEC	Snow-rain split temperature (°C)	NCRFC mean value
snow_ADC	Areal depletion curve (11 values)	NCRFC mean value
sac_UZTWM	Upper-zone tension water maximum storage (mm)	OHD Grid
sac_UZFWM	Upper-zone free water maximum storage (mm)	OHD Grid
sac_UZK	Upper-zone free water lateral depletion rate (day-1)	OHD Grid
sac_PCTIM	Impervious fraction of the watershed (decimal fraction)	OHD Grid
sac_ADIMP	Additional impervious area (decimal fraction)	NCRFC mean value
sac_RIVA	Riparian vegetation (decimal fraction)	NCRFC mean value
sac_ZPERC	Maximum percolation rate (dimensionless)	OHD Grid
sac_REXP	Exponent of the percolation equation (dimensionless)	OHD Grid
sac_LZTWM	Lower-zone tension water maximum storage (mm)	OHD Grid
sac_LZFSM	Lower-zone free water supplementary maximum storage (mm)	OHD Grid
sac_LZFPM	Lower-zone free water primary maximum storage (mm)	OHD Grid
sac_LZSK	Lower-zone supplementary free water depletion rate (day-1)	OHD Grid
sac_LZPK	Lower-zone primary free water depletion rate (day-1)	OHD Grid
sac_PFREE	Fraction of water percolating from upper zone directly to lower-zone free water storage (decimal fraction)	OHD Grid
sac_SIDE	Ratio of deep recharge to channel base flow (decimal fraction)	NCRFC mean value
sac_RSERV	Fraction of lower-zone free water not transferable to lower-zone tension water (decimal fraction)	NCRFC mean value
sac_EFC	Effective forest fraction	OHD Grid
rutpix_SLOPH	Hillslope slope	OHD Grid
rutpix_DS	Drainage density	OHD Grid
rutpix_ROUGH	Hillslope roughness	OHD Grid
rutpix_Q0CHN	Rating curve-based routing parameter	OHD Grid
rutpix_QMCHN	Rating curve-based routing parameter	OHD Grid

Table A.12. Model component parameters and data source for model simulations.

A.3 PET figures

Figure A.15 Breakdown of PET calculation components. Data from July 5th, 2007 for AMWI4 basin (a) land use map (b) total daily PET (c) daily net radiation (d) surface albedo (e) incoming shortwave radiation (f) outgoing longwave radiation (g) ground heat flux and (h) incoming longwave radiation.

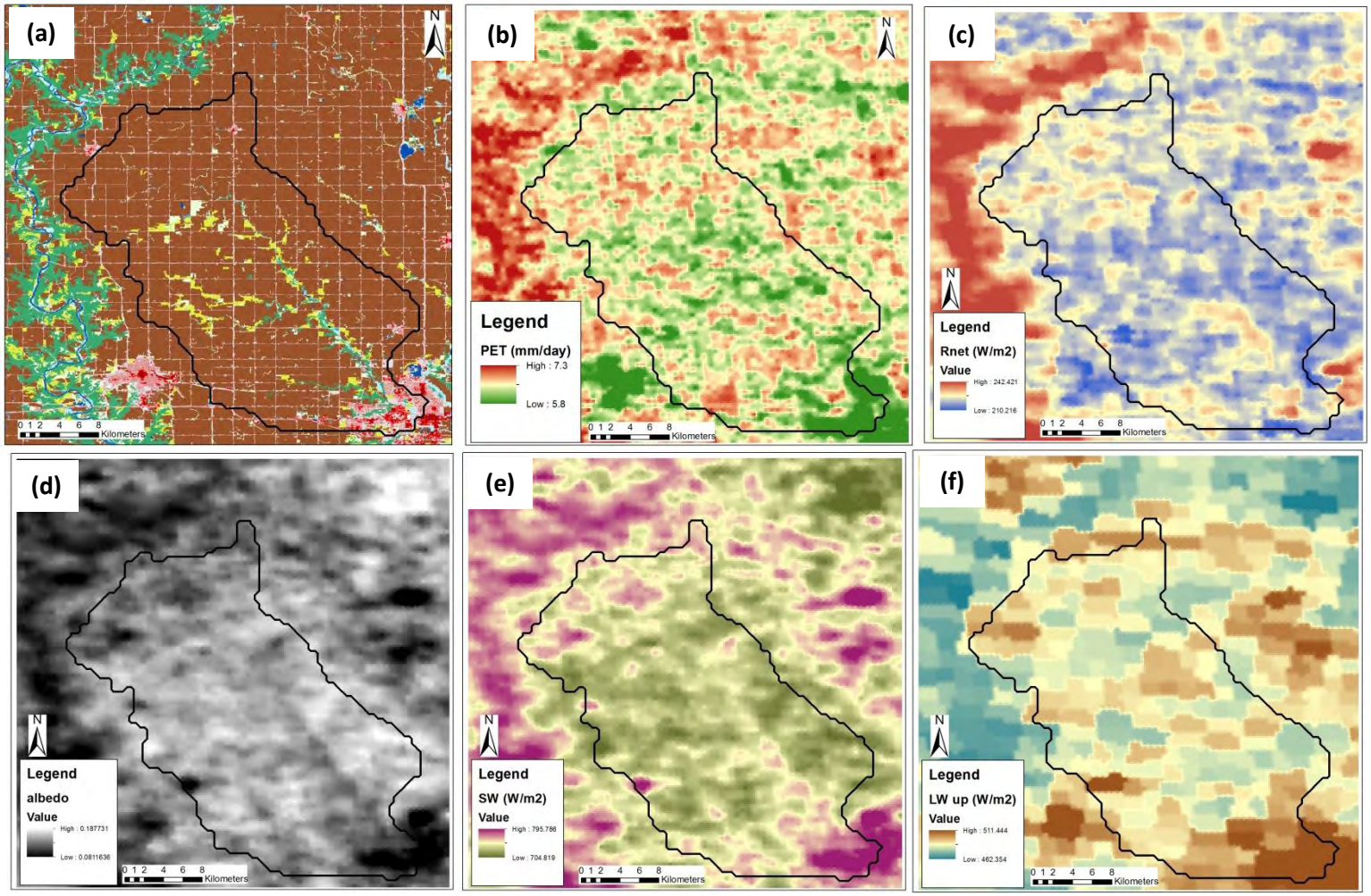

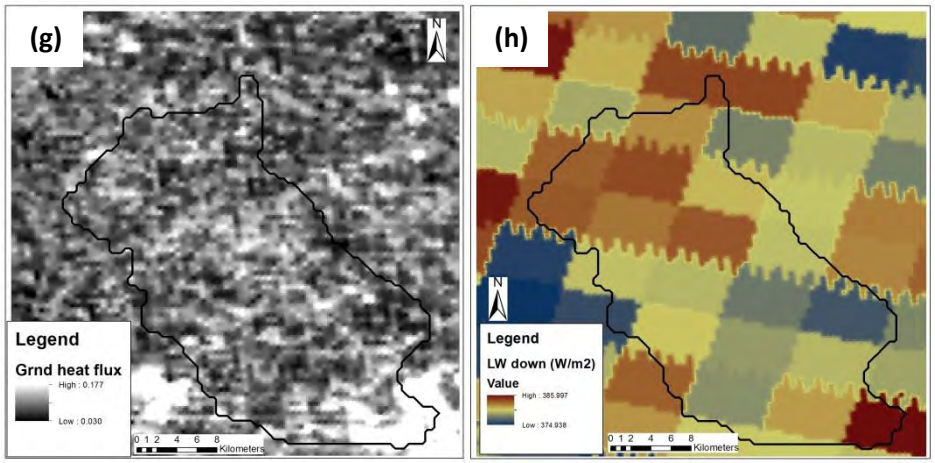

A.4 Annual Precipitation (all basins)

										(2003-2006)		(2007-2010)	
Basin	**2003**	**2004**	**2005**	**2006**	**2007**	**2008**	**2009**	**2010**	**Avg**	Min	Max	Min	Max
AMEI4	753	918	887	967	1078	1228	992	1238	1008	753	967	992	1238
AMWI4	759	924	863	963	1040	1238	1021	1445	1032	759	963	1021	1445
BCHW3	812	894	700	1005	1035	1071	946	1033	937	700	1005	946	1071
BERW3	760	923	638	838	738	938	687	953	809	638	923	687	953
DARW3	823	874	701	957	1107	1075	989	984	939	701	957	984	1107
HICM5	500	795	787	604	637	575	677	861	680	500	795	575	861
MILW3	771	948	681	1054	958	1078	912	1110	939	681	1054	912	1110
MMLM5	615	697	867	572	712	588	703	1049	725	572	867	588	1049
NHRI4	816	925	881	948	1051	1137	949	1054	970	816	948	949	1137
PLUM5	408	579	560	357	648	668	498	638	545	357	579	498	668
RAPM5	569	961	960	779	785	682	712	932	798	569	961	682	932
SANM5	699	774	689	514	575	770	661	871	694	514	774	575	871
SCRI4	639	851	852	697	891	843	686	1015	809	639	852	686	1015

Table A.13. Annual Precipitation (mm) for all 13 study basins

A.5 Calibration Results

Default PET parameter multipliers

Parameter	AMEI4	AMWI4	BCHW3	BERW3	DARW3	HICM5	MILW3	MMLM5	NHRI4	PLUM5	RAPM5	SANM5	SCRI4
sac_UZTWM	0.28	0.26	0.1	0.27	0.2	0.48	0.52	0.28	0.15	0.34	0.28	0.37	0.32
sac_UZFWM	1.74	2.66	1.14	1.37	2.18	3.53	1.16	1.4	1.43	2.03	0.62	2.16	1.56
sac_ZPERC	0.4	0.44	0.65	1.1	0.89	0.33	1.1	0.83	0.22	0.22	0.67	0.41	1.5
sac_REXP	1.12	1.07	0.9	0.92	0.5	0.8	0.71	1	1.54	0.79	0.7	1.88	1.8
sac_LZFSM	2.81	1.83	10	6.6	5.5	2.83	5.01	3.03	0.19	5.7	0.27	0.54	0.33
sac_LZFPM	0.6	1.09	6.2	1.1	1.5	1.05	1.14	0.76	1.14	0.41	1	0.89	0.3
snow_MFMAX	1.1	1.1	1.5	1.16	1.5	0.56	1.1	1.01	1.1	0.69	0.47	0.67	1.18
sac_LZPK	0.9	2.6	4.63	0.57	3.9	8.71	1.61	8.95	0.9	2.98	11.4	3.87	0.9
sac_LZSK	1.51	1.97	0.12	0.31	0.13	1	0.45	1.72	0.09	0.56	1.43	0.16	0.78
sac_UZK	1.69	2.16	0.53	0.18	0.65	1.39	0.28	0.29	0.69	1.43	1.9	1.48	0.34
snow_PLWHC	0.69	0.44	0.5	0.2	0.4	2.67	0.5	1.6	0.2	2.67	1.6	4	1.2
sac_LZTWM	0.35	0.35	0.9	0.42	1.1	0.33	0.43	0.58	0.79	0.7	0.36	0.35	0.38

Default PET percent of allowable change

Parameter	AMEI4	AMWI4	BCHW3	BERW3	DARW3	HICM5	MILW3	MMLM5	NHRI4	PLUM5	RAPM5	SANM5	SCRI4
sac_UZTWM	-51.0%	-56.7%	-98.0%	-53.7%	-100.2%	-21.6%	-42.9%	-58.2%	-114.1%	-38.7%	-50.6%	-33.9%	-50.2%
sac_UZFWM	30.0%	65.1%	7.7%	27.2%	68.7%	57.4%	7.5%	20.2%	22.6%	56.4%	-15.1%	59.8%	24.9%
sac_ZPERC	-61.9%	-59.6%	-22.8%	26.4%	-9.2%	-57.2%	14.4%	-19.4%	-129.6%	-124.0%	-35.4%	-125.4%	51.1%
sac_REXP	12.9%	7.7%	-14.2%	-6.5%	-69.2%	-22.5%	-30.8%	0.0%	61.6%	-19.9%	-32.1%	71.9%	86.4%
sac_LZFSM	32.6%	15.1%	83.4%	52.5%	46.7%	37.5%	60.0%	32.5%	-11.2%	70.0%	-12.4%	-5.0%	-12.0%
sac_LZFPM	-40.7%	8.6%	87.0%	14.0%	11.7%	4.9%	12.7%	-26.0%	9.9%	-73.4%	0.0%	-15.9%	-69.5%
snow_MFMAX	21.6%	21.4%	102.3%	29.7%	102.4%	-90.3%	20.7%	2.1%	21.7%	-52.8%	-113.9%	-56.1%	38.8%
sac_LZPK	-0.3%	5.0%	5.2%	-9.8%	4.9%	33.6%	6.8%	27.3%	-0.3%	22.4%	53.2%	46.9%	-0.3%
sac_LZSK	14.8%	25.0%	-22.6%	-27.4%	-19.5%	0.0%	-15.1%	22.6%	-19.8%	-17.5%	12.7%	-32.8%	-7.2%
sac_UZK	37.4%	55.3%	-20.7%	-64.3%	-13.7%	17.7%	-36.9%	-42.3%	-12.4%	32.9%	49.6%	36.9%	-40.3%
snow_PLWHC	-22.1%	-40.0%	-14.3%	-57.1%	-17.1%	71.6%	-14.3%	42.9%	-57.1%	71.6%	42.9%	85.7%	21.7%
sac_LZTWM	-192.9%	-186.7%	-11.1%	-136.9%	14.8%	-218.0%	-163.8%	-121.3%	-51.0%	-86.9%	-206.5%	-187.9%	-190.5%

MODIS PET parameter multipliers

Parameter	AMEI4	AMWI4	BCHW3	BERW3	DARW3	HICM5	MILW3	MMLM5	NHRI4	PLUM5	RAPM5	SANM5	SCRI4
sac_UZTWM	0.28	0.26	0.1	0.27	0.2	0.48	0.44	0.25	0.41	0.34	0.28	0.37	0.2
sac_UZFWM	2.17	2.83	1.05	1.51	1	2.98	1.59	1.25	1	2.03	2.8	2.16	1.68
sac_ZPERC	0.61	0.69	1.54	1.1	1.5	0.53	1.1	1.1	0.33	0.46	1	0.27	0.71
sac_REXP	1.6	0.86	0.74	0.92	0.5	1.33	0.71	0.85	1.54	0.79	1.64	2.14	1.8
sac_LZFSM	1.83	2.24	5.41	7.14	2.35	1	4.17	0.69	0.19	3.69	0.15	0.54	0.19
sac_LZFPM	0.25	1.09	5.2	1.1	1.5	0.62	1.14	0.6	0.15	0.09	1	1.1	0.1
snow_MFMAX	1.1	1.1	1.5	0.7	1.5	0.56	0.78	1.01	1.1	0.78	0.14	0.67	1.18
sac_LZPK	0.9	0.2	3.9	0.57	3.18	11.46	1.81	6.78	0.9	2.59	12.94	4.78	0.9
sac_LZSK	2.03	1.68	0.12	0.31	0.2	0.9	0.45	2.2	0.09	0.56	1.26	1.26	0.93
sac_UZK	1.28	2.16	0.47	0.18	0.48	0.73	0.28	0.33	0.94	1.23	0.32	1.48	0.34
snow_PLWHC	0.83	0.3	0.5	0.41	0.1	2.67	0.83	1.6	0.2	2.67	1.6	4	1.2
sac_LZTWM	0.34	0.35	0.9	0.42	1.1	0.31	0.4	0.45	0.41	0.48	0.27	0.35	0.55

MODIS PET percent of allowable change

Parameter	AMEI4	AMWI4	BCHW3	BERW3	DARW3	HICM5	MILW3	MMLM5	NHRI4	PLUM5	RAPM5	SANM5	SCRI4
sac_UZTWM	-51.0%	-56.7%	-98.0%	-53.7%	-100.2%	-21.6%	-50.0%	-60.6%	-79.2%	-38.7%	-50.6%	-33.9%	-59.0%
sac_UZFWM	47.5%	71.8%	2.7%	37.5%	0.0%	44.9%	27.6%	12.6%	0.0%	56.4%	71.5%	59.8%	30.2%
sac_ZPERC	-40.2%	-33.0%	35.2%	26.4%	41.7%	-40.1%	14.4%	11.4%	-111.3%	-85.9%	0.0%	-155.1%	-29.6%
sac_REXP	64.3%	-15.3%	-37.0%	-6.5%	-69.2%	37.1%	-30.8%	-15.4%	61.6%	-19.9%	68.4%	93.1%	86.4%
sac_LZFSM	14.9%	22.5%	40.9%	57.6%	14.0%	0.0%	47.4%	-5.0%	-11.2%	40.1%	-14.5%	-5.0%	-14.5%
sac_LZFPM	-76.3%	8.6%	70.3%	14.0%	11.7%	-37.4%	12.7%	-43.4%	-60.0%	-113.2%	0.0%	14.4%	-89.4%
snow_MFMAX	21.6%	21.4%	102.3%	-55.6%	102.4%	-90.3%	-45.6%	2.1%	21.7%	-37.5%	-184.8%	-56.1%	38.8%
sac_LZPK	-0.3%	-2.5%	4.1%	-9.8%	3.7%	45.6%	9.0%	19.8%	-0.3%	18.0%	61.1%	61.8%	-0.3%
sac_LZSK	29.8%	17.5%	-22.6%	-27.4%	-17.9%	-2.4%	-15.1%	37.7%	-19.8%	-17.5%	7.7%	10.1%	-2.3%
sac_UZK	15.2%	55.3%	-23.4%	-64.3%	-20.3%	-12.2%	-36.9%	-39.9%	-2.4%	17.6%	-37.5%	36.9%	-40.3%
snow_PLWHC	-12.1%	-50.0%	-14.3%	-42.1%	-25.7%	71.6%	-4.9%	42.9%	-57.1%	71.6%	42.9%	85.7%	21.7%
sac_LZTWM	-195.8%	-186.7%	-11.1%	-136.9%	14.8%	-224.5%	-172.4%	-158.8%	-143.2%	-150.6%	-235.6%	-187.9%	-138.2%

A.6 PET Accumulation Plots

The following plots illustrate the accumulated MODIS-PET and default PET data with the flux-tower observations. Periods of missing flux-tower observations are replaced with mean value. Note Accumulated PET y-axis is different than ET figures.

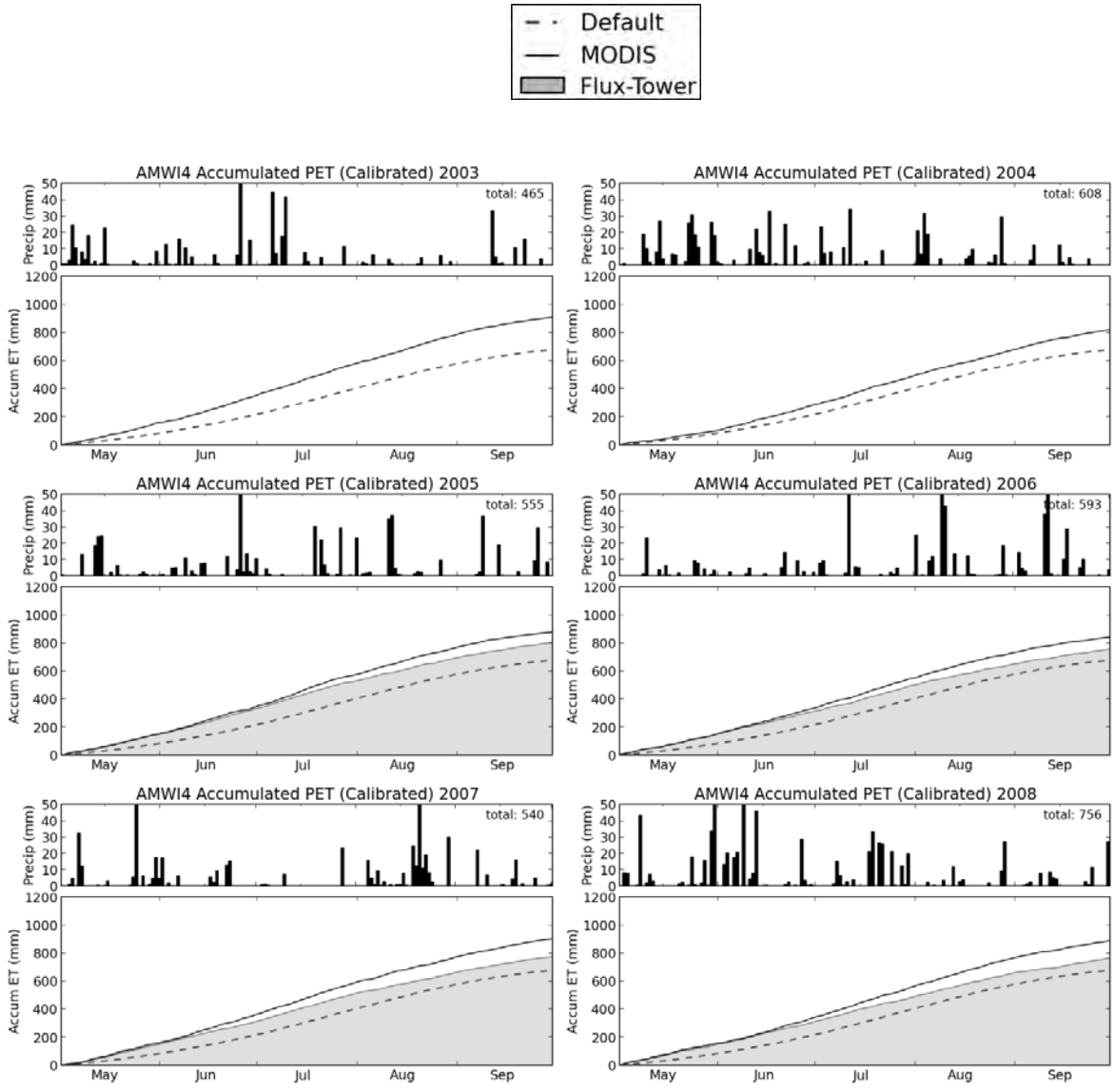

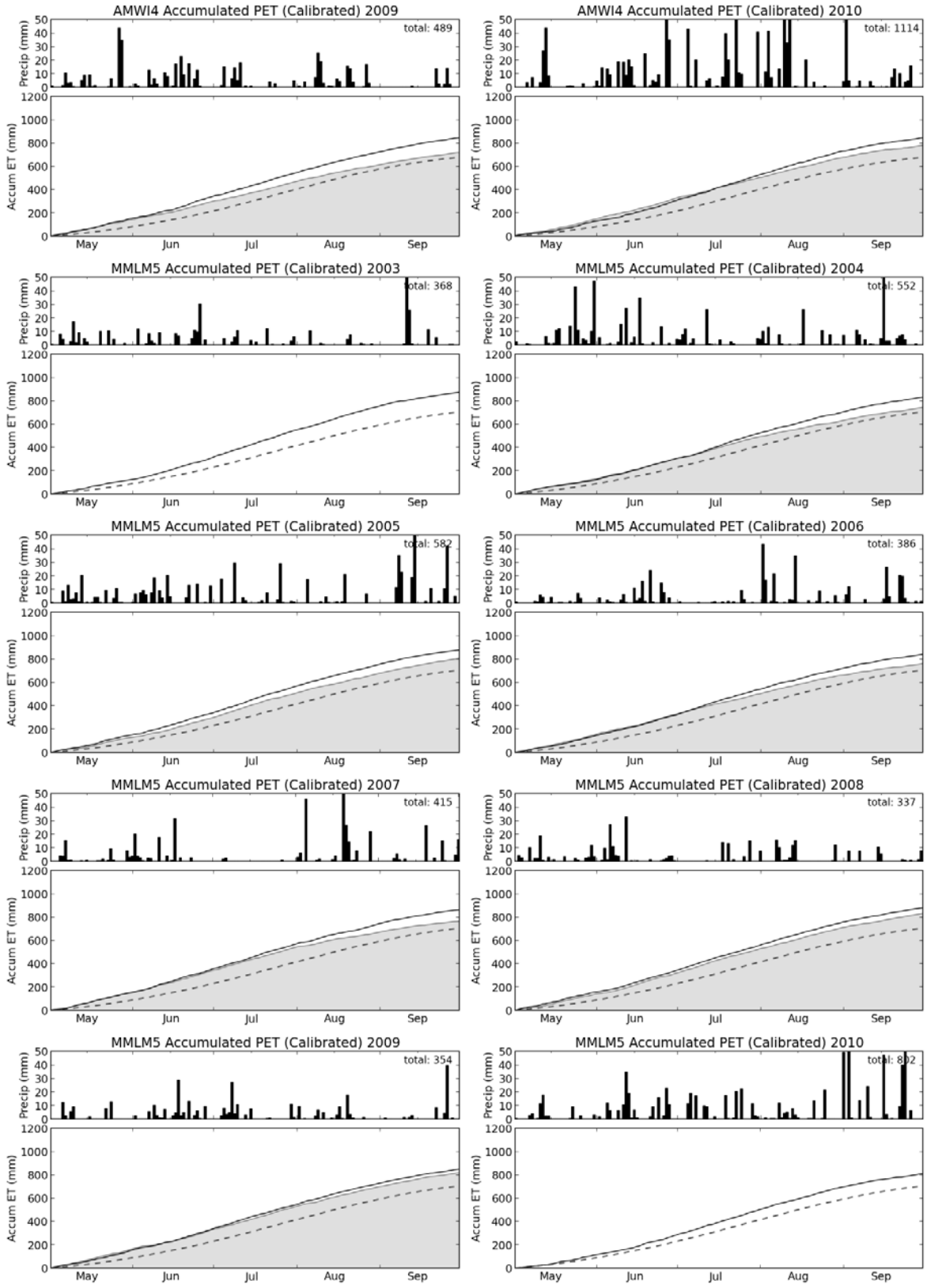
AMWI4 Accumulated PET (Calibrated) 2009
total: 489
AMWI4 Accumulated PET (Calibrated) 2010
total: 1114
MMLM5 Accumulated PET (Calibrated) 2003
total: 368
MMLM5 Accumulated PET (Calibrated) 2004
total: 552
MMLM5 Accumulated PET (Calibrated) 2005
total: 582
MMLM5 Accumulated PET (Calibrated) 2006
total: 386
MMLM5 Accumulated PET (Calibrated) 2007
total: 415
MMLM5 Accumulated PET (Calibrated) 2008
total: 337
MMLM5 Accumulated PET (Calibrated) 2009
total: 354
MMLM5 Accumulated PET (Calibrated) 2010
total: 802
Precip (mm)
Accum ET (mm)
May
Jun
Jul
Aug
Sep

A.7 Simulated ET vs. Observed ET

A priori parameter simulations

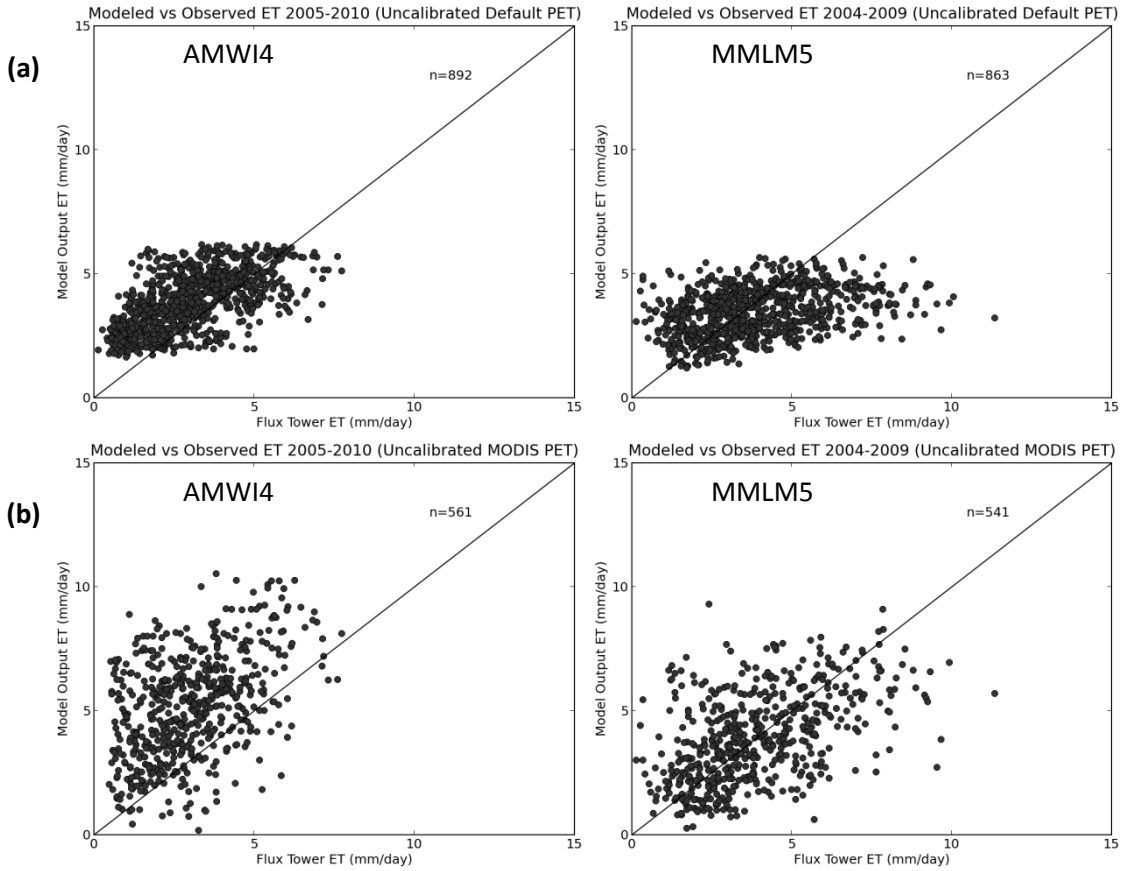

Figure A.16. Comparison of mean daily Flux-Tower ET and (a) basin mean default simulated ET and (b) basin mean MODIS simulated ET for AMWI4 and MMLM5 using the a priori parameters.

Basin	AMWI4	MMLM5
Observed Flux-tower ET	3.00	3.86
Simulated MODIS ET	5.19/4.36	3.91/3.49
Simulated Default ET	3.87/3.29	3.44/3.15

Table A.14. Mean ET depths (mm/day) from flux-tower observations and simulations. All values are calculated for the flux-tower data availability time period. Simulated ET values are displayed with a priori simulation followed by calibrated simulation.

A.8 ET Accumulation Plots

The following plots demonstrate the simulated ET results with MODIS-PET and default PET inputs against the flux-tower observations. Plots also illustrate the effects of calibrating the model parameters and the resulting changes to output ET for each year. Periods of missing flux-tower observations are replaced with mean values.

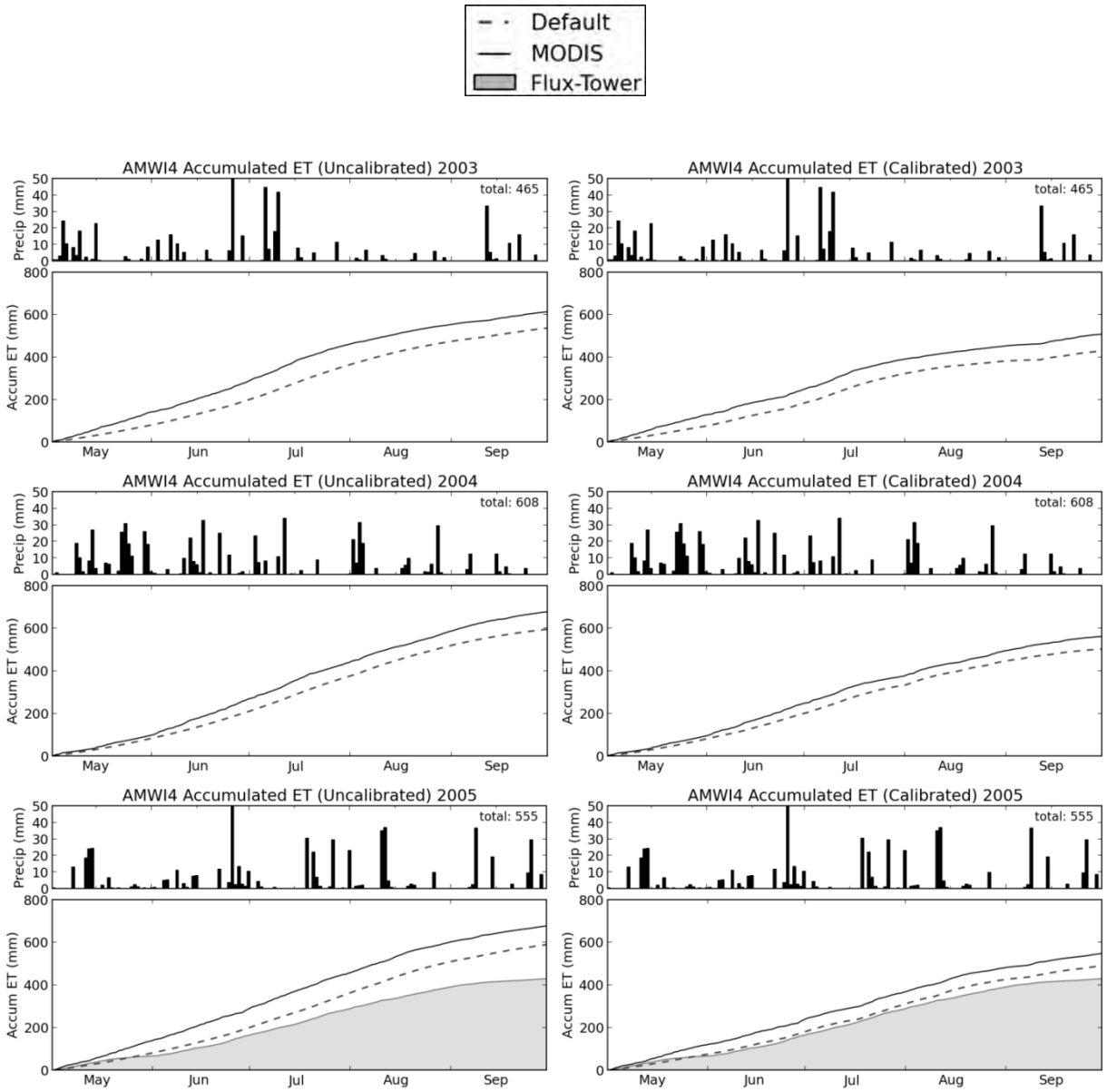

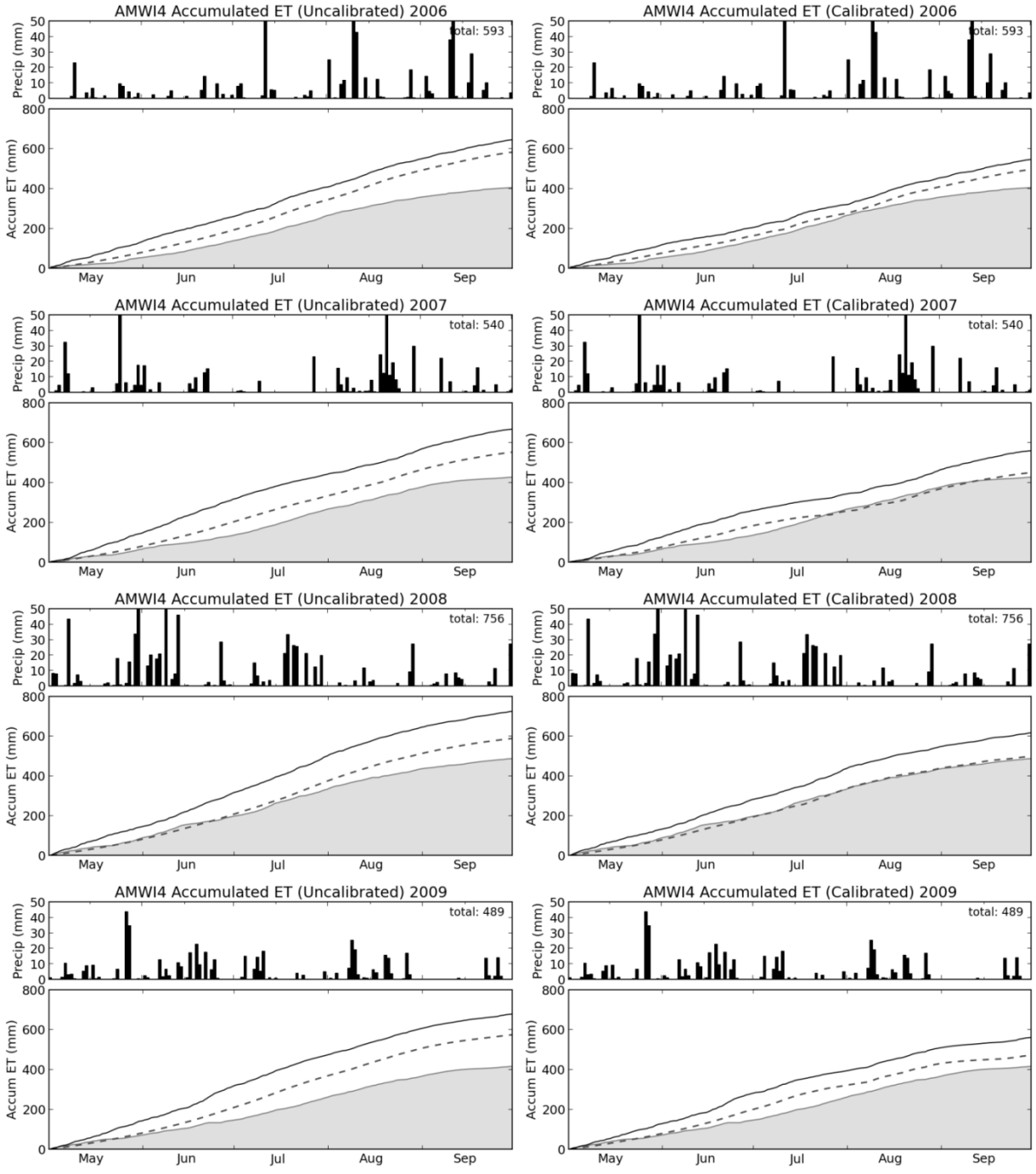
AMWI4 Accumulated ET (Uncalibrated) 2006
AMWI4 Accumulated ET (Calibrated) 2006
AMWI4 Accumulated ET (Uncalibrated) 2007
AMWI4 Accumulated ET (Calibrated) 2007
AMWI4 Accumulated ET (Uncalibrated) 2008
AMWI4 Accumulated ET (Calibrated) 2008
AMWI4 Accumulated ET (Uncalibrated) 2009
AMWI4 Accumulated ET (Calibrated) 2009
Precip (mm)
Accum ET (mm)
total: 593
total: 540
total: 756
total: 489
May
Jun
Jul
Aug
Sep

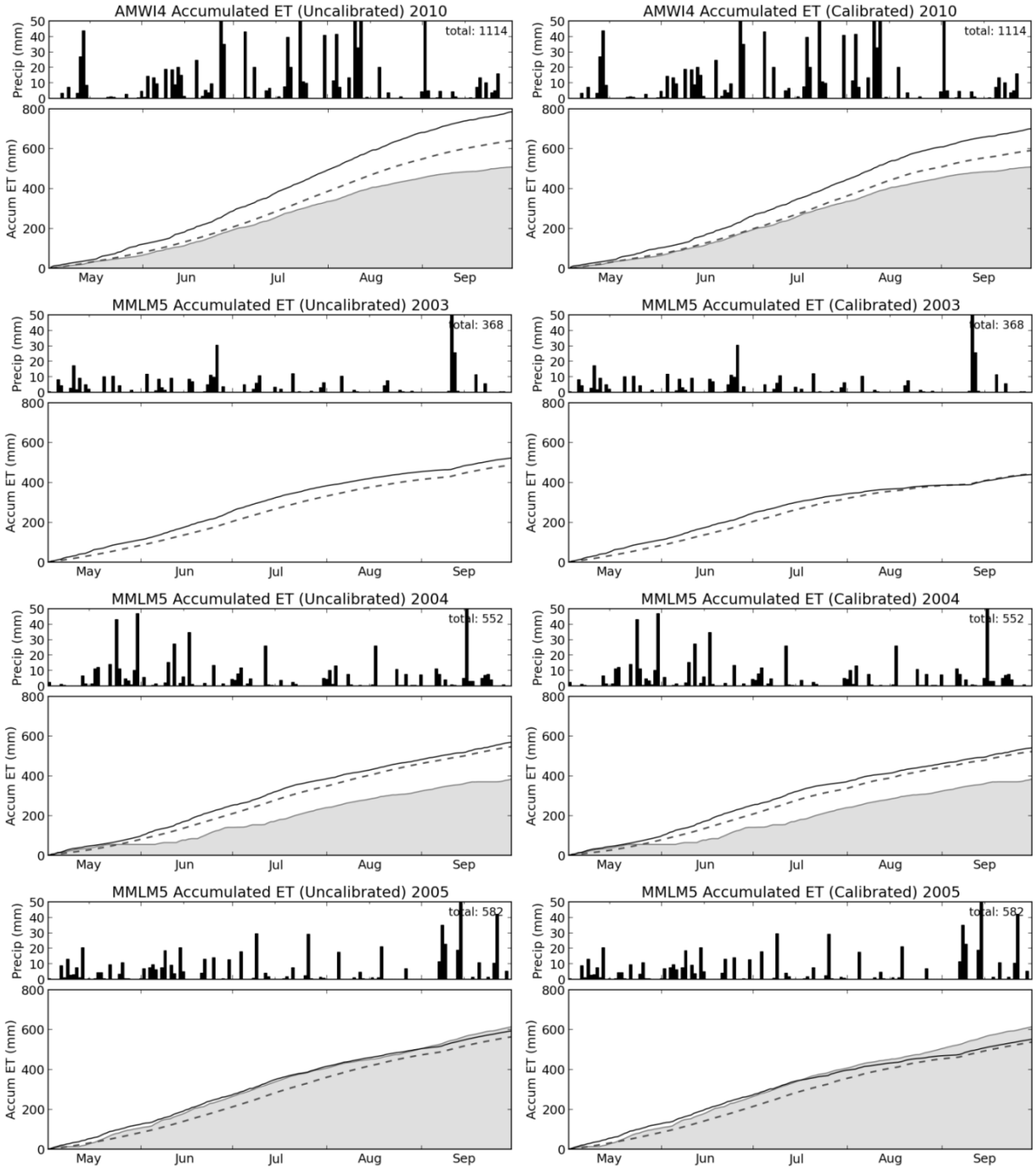
AMWI4 Accumulated ET (Uncalibrated) 2010
AMWI4 Accumulated ET (Calibrated) 2010
MMLM5 Accumulated ET (Uncalibrated) 2003
MMLM5 Accumulated ET (Calibrated) 2003
MMLM5 Accumulated ET (Uncalibrated) 2004
MMLM5 Accumulated ET (Calibrated) 2004
MMLM5 Accumulated ET (Uncalibrated) 2005
MMLM5 Accumulated ET (Calibrated) 2005
Precip (mm)
Accum ET (mm)
total: 1114
total: 368
total: 552
total: 582
May
Jun
Jul
Aug
Sep

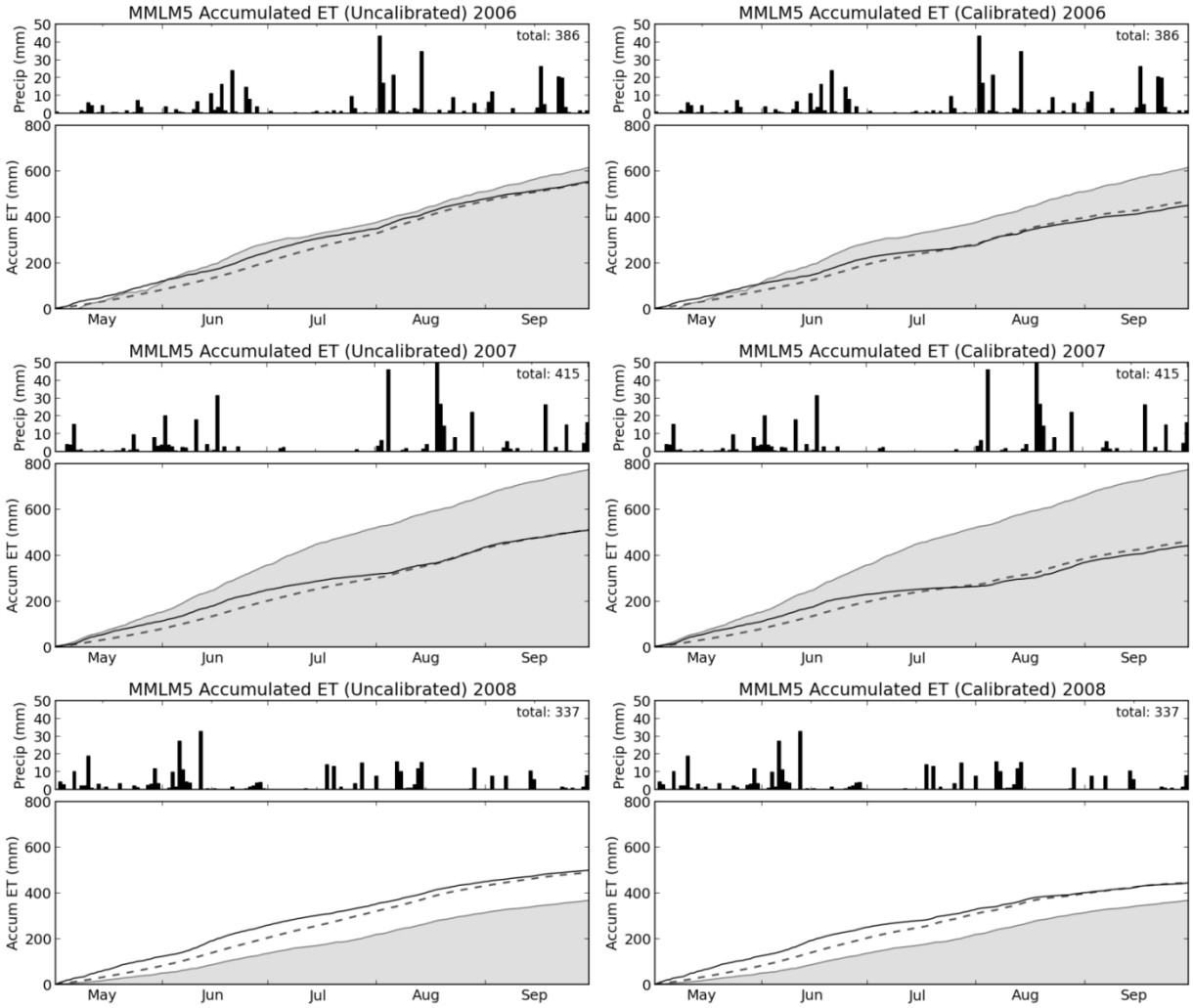
MMLM5 Accumulated ET (Uncalibrated) 2006
MMLM5 Accumulated ET (Calibrated) 2006
MMLM5 Accumulated ET (Uncalibrated) 2007
MMLM5 Accumulated ET (Calibrated) 2007
MMLM5 Accumulated ET (Uncalibrated) 2008
MMLM5 Accumulated ET (Calibrated) 2008
Precip (mm)
Accum ET (mm)
total: 386
total: 415
total: 337
May
Jun
Jul
Aug
Sep

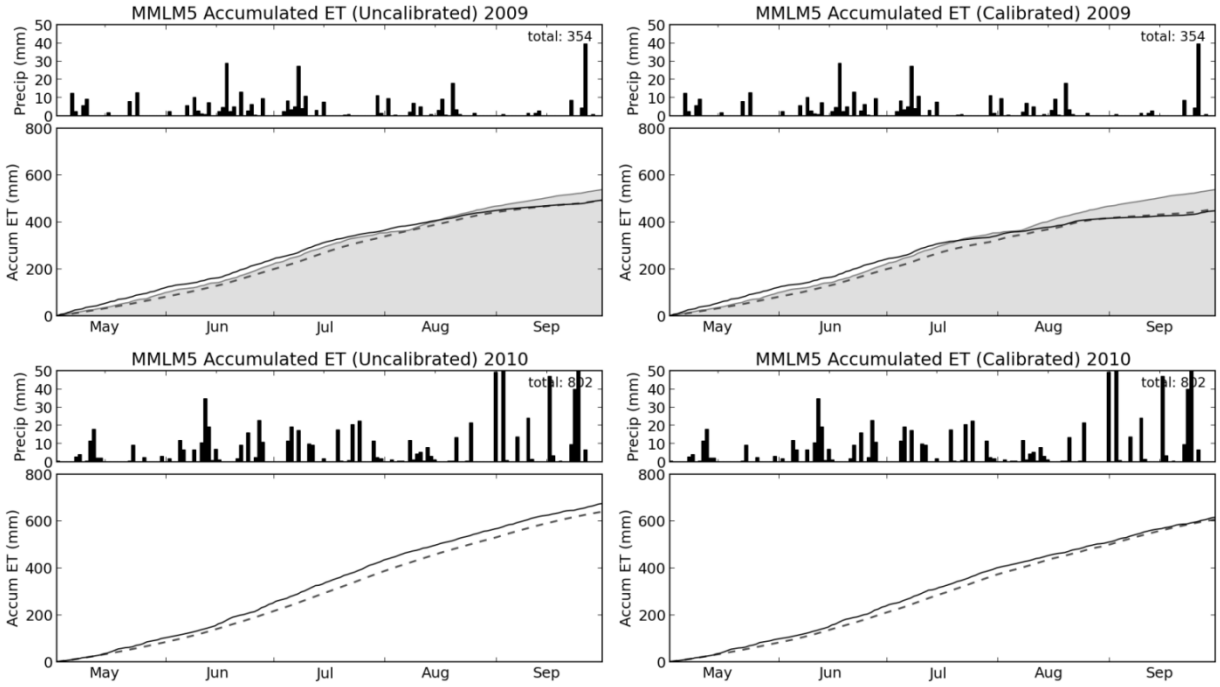

A.9 ET Efficiency

To summarize the difference between PET and ET for the observed measurements and model simulations, we examine a simple calculation of the percentage of the PET met by the actual ET at each basin for the period of interest. This calculation is referred to as the evapotranspiration efficiency (ETE) and it attempts to provide a means to quantify the differing degrees of water-limit or energy-limited systems:

$$ETE = \frac{ET}{PET} \times 100\% \tag{11}$$

In this calculation, values nearing 100% indicate abundant rainfall and thus ET is limited by the available energy. Small ETE values indicate ET is restricted by the amount of precipitation indicating a water-limited system (Dingman 2002). Although only two basins have a record of

observations available, it is apparent that the default simulations result in a slightly better representation of the long-term observed ETE. The mean MODIS ETE is 10% less than the ETE values from the default conditions, further indicating that the MODIS-PET is likely over-estimated in some cases.

Basin	Default	MODIS	Obs
BCHW3	57.1%	52.1%	-
BERW3	65.0%	54.0%	-
DARW3	66.3%	61.9%	-
MILW3	72.1%	61.0%	-
AMEI4	74.2%	65.1%	-
AMWI4	72.5%	66.5%	70.7%
NHRI4	66.4%	57.3%	-
SCRI4	68.9%	54.7%	-
HICM5	63.8%	53.6%	-
MMLM5	69.7%	57.9%	75.3%
PLUM5	68.7%	53.6%	-
RAPM5	69.4%	57.0%	-
SANM5	66.5%	55.5%	-
Mean	67.7%	57.7%	73.0%

Table A.15. Average warm season ET efficiency (ETE) for the entire study period.

A.10 Water Balance Pie Charts

The following pie charts illustrate the overall water balance changes as a result of using the two different PET data sources and a priori and calibrated parameters. The first column (a) represents the default PET with a priori parameters, and the second column (b) represents the default PET with the calibrated parameters. Column three (c) represents the MODIS PET with a priori parameters, and the fourth column (d) represents the MODIS-PET with calibrated parameters. Results are calculated for the entire study period (2003-2010).

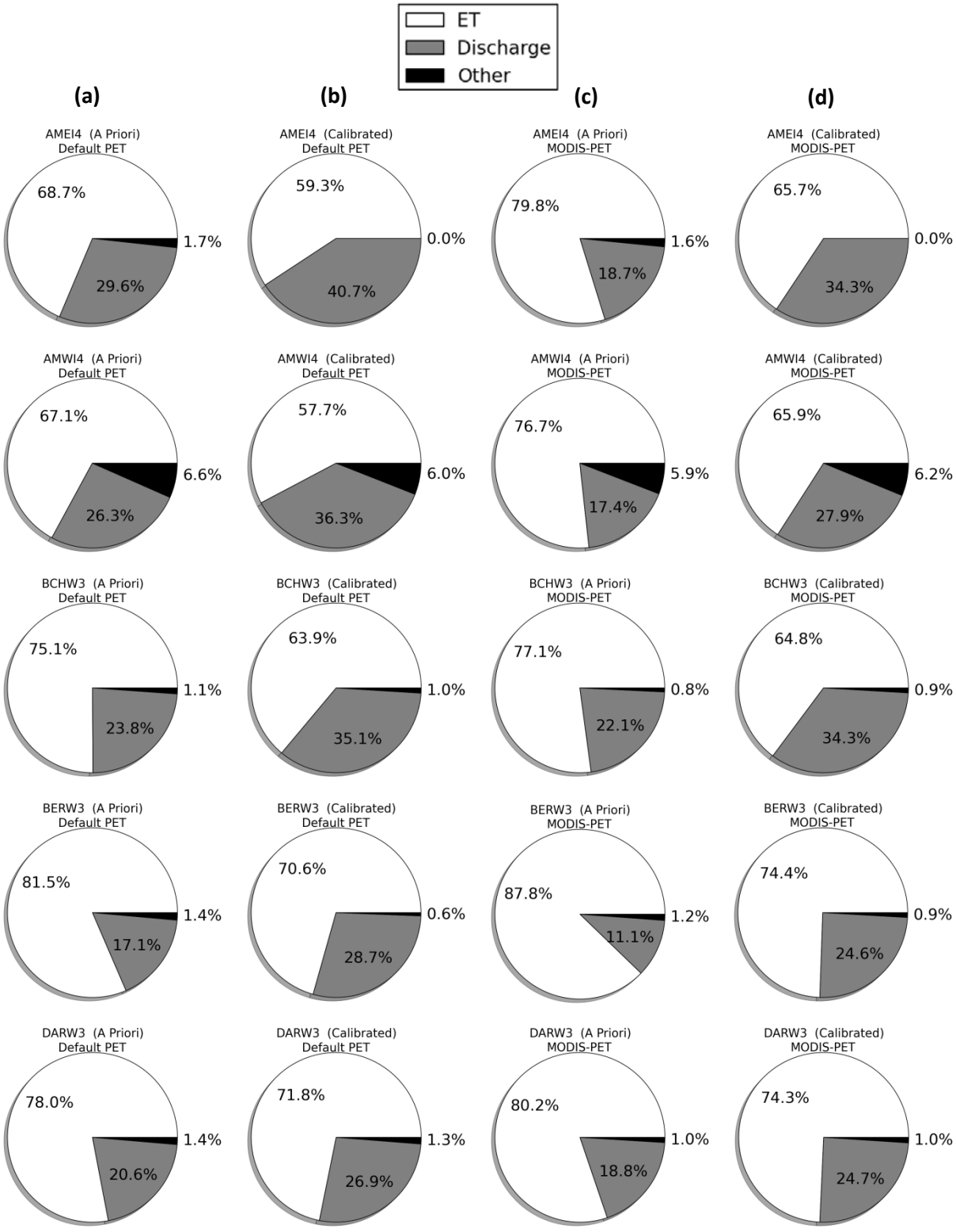
ET
Discharge
Other
(a)
(b)
(c)
(d)
AMEI4 (A Priori) Default PET
68.7%
29.6%
1.7%
AMEI4 (Calibrated) Default PET
59.3%
40.7%
0.0%
AMEI4 (A Priori) MODIS-PET
79.8%
18.7%
1.6%
AMEI4 (Calibrated) MODIS-PET
65.7%
34.3%
0.0%
AMWI4 (A Priori) Default PET
67.1%
26.3%
6.6%
AMWI4 (Calibrated) Default PET
57.7%
36.3%
6.0%
AMWI4 (A Priori) MODIS-PET
76.7%
17.4%
5.9%
AMWI4 (Calibrated) MODIS-PET
65.9%
27.9%
6.2%
BCHW3 (A Priori) Default PET
75.1%
23.8%
1.1%
BCHW3 (Calibrated) Default PET
63.9%
35.1%
1.0%
BCHW3 (A Priori) MODIS-PET
77.1%
22.1%
0.8%
BCHW3 (Calibrated) MODIS-PET
64.8%
34.3%
0.9%
BERW3 (A Priori) Default PET
81.5%
17.1%
1.4%
BERW3 (Calibrated) Default PET
70.6%
28.7%
0.6%
BERW3 (A Priori) MODIS-PET
87.8%
11.1%
1.2%
BERW3 (Calibrated) MODIS-PET
74.4%
24.6%
0.9%
DARW3 (A Priori) Default PET
78.0%
20.6%
1.4%
DARW3 (Calibrated) Default PET
71.8%
26.9%
1.3%
DARW3 (A Priori) MODIS-PET
80.2%
18.8%
1.0%
DARW3 (Calibrated) MODIS-PET
74.3%
24.7%
1.0%

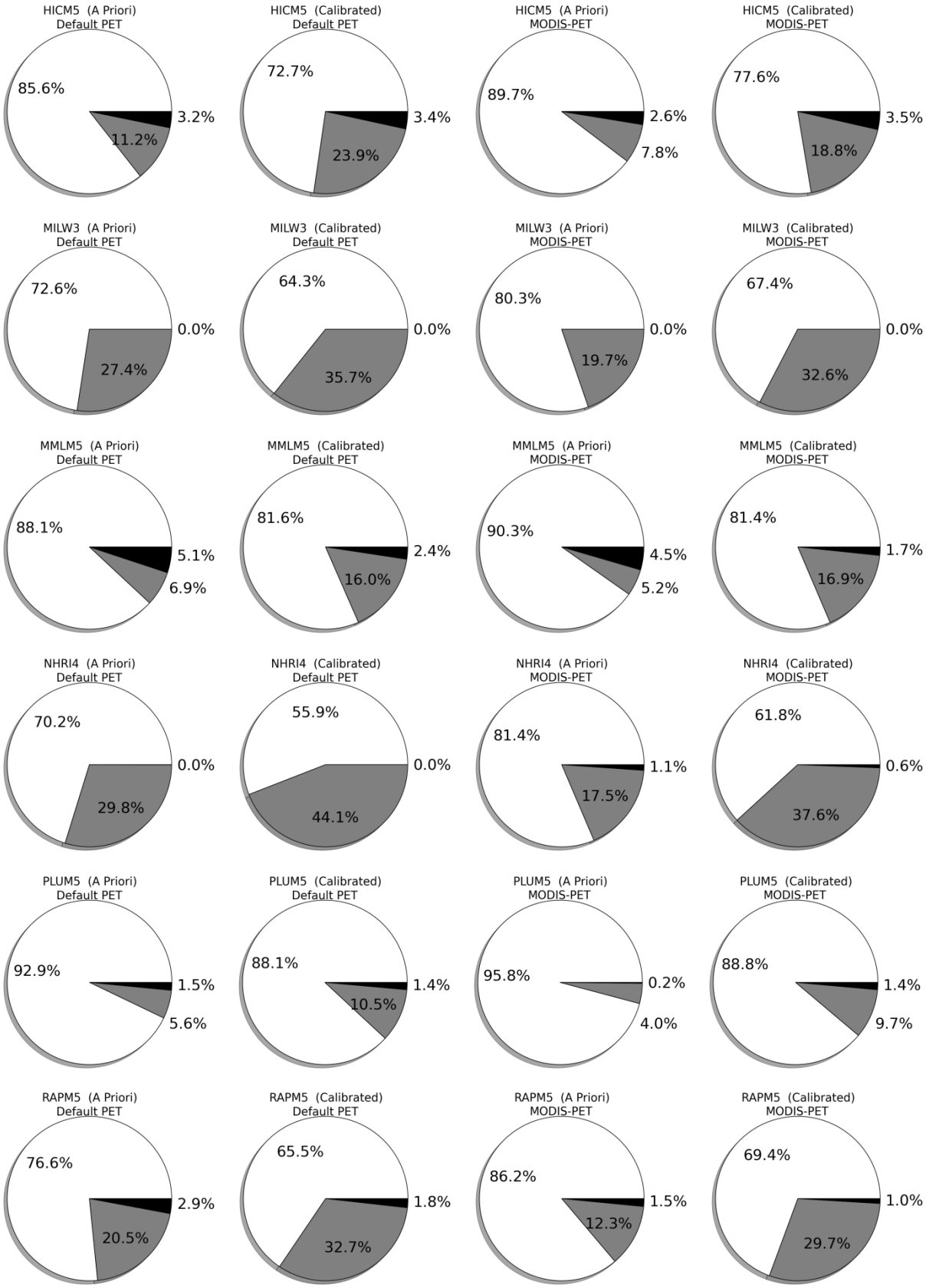
HICM5 (A Priori)
Default PET
85.6%
3.2%
11.2%
HICM5 (Calibrated)
Default PET
72.7%
3.4%
23.9%
HICM5 (A Priori)
MODIS-PET
89.7%
2.6%
7.8%
HICM5 (Calibrated)
MODIS-PET
77.6%
3.5%
18.8%
MILW3 (A Priori)
Default PET
72.6%
0.0%
27.4%
MILW3 (Calibrated)
Default PET
64.3%
0.0%
35.7%
MILW3 (A Priori)
MODIS-PET
80.3%
0.0%
19.7%
MILW3 (Calibrated)
MODIS-PET
67.4%
0.0%
32.6%
MMLM5 (A Priori)
Default PET
88.1%
5.1%
6.9%
MMLM5 (Calibrated)
Default PET
81.6%
2.4%
16.0%
MMLM5 (A Priori)
MODIS-PET
90.3%
4.5%
5.2%
MMLM5 (Calibrated)
MODIS-PET
81.4%
1.7%
16.9%
NHRI4 (A Priori)
Default PET
70.2%
0.0%
29.8%
NHRI4 (Calibrated)
Default PET
55.9%
0.0%
44.1%
NHRI4 (A Priori)
MODIS-PET
81.4%
1.1%
17.5%
NHRI4 (Calibrated)
MODIS-PET
61.8%
0.6%
37.6%
PLUM5 (A Priori)
Default PET
92.9%
1.5%
5.6%
PLUM5 (Calibrated)
Default PET
88.1%
1.4%
10.5%
PLUM5 (A Priori)
MODIS-PET
95.8%
0.2%
4.0%
PLUM5 (Calibrated)
MODIS-PET
88.8%
1.4%
9.7%
RAPM5 (A Priori)
Default PET
76.6%
2.9%
20.5%
RAPM5 (Calibrated)
Default PET
65.5%
1.8%
32.7%
RAPM5 (A Priori)
MODIS-PET
86.2%
1.5%
12.3%
RAPM5 (Calibrated)
MODIS-PET
69.4%
1.0%
29.7%

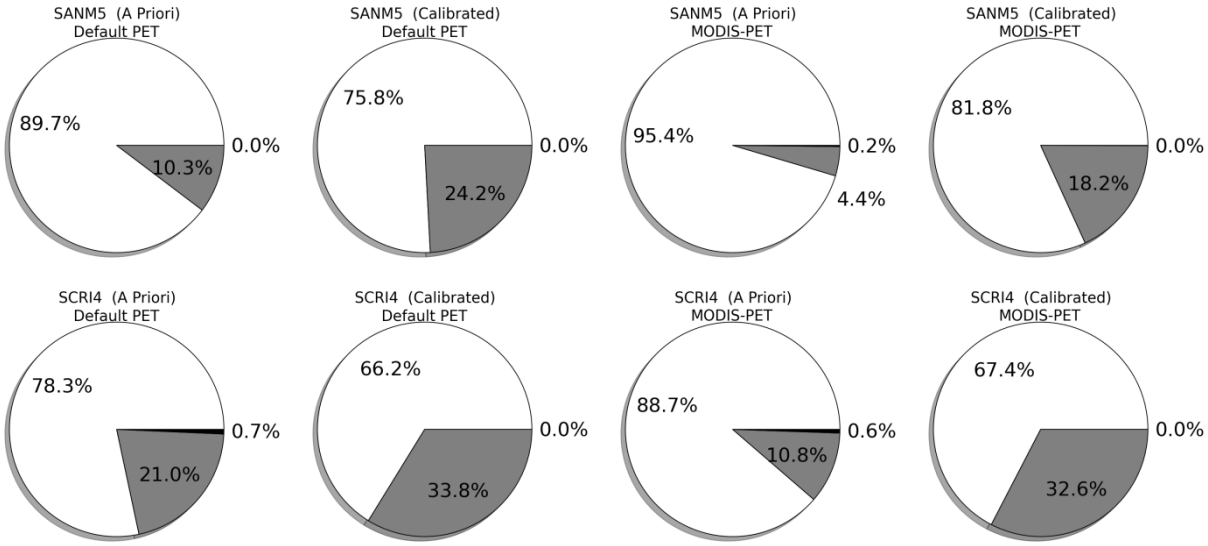

A.11 Hydrograph and ET Plots

Subsequent pages show simulation results for all each study basin. Discharge and ET simulations are shown with daily values for the warm seasons for all eight years of the study period.

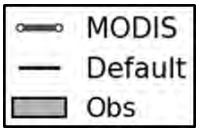

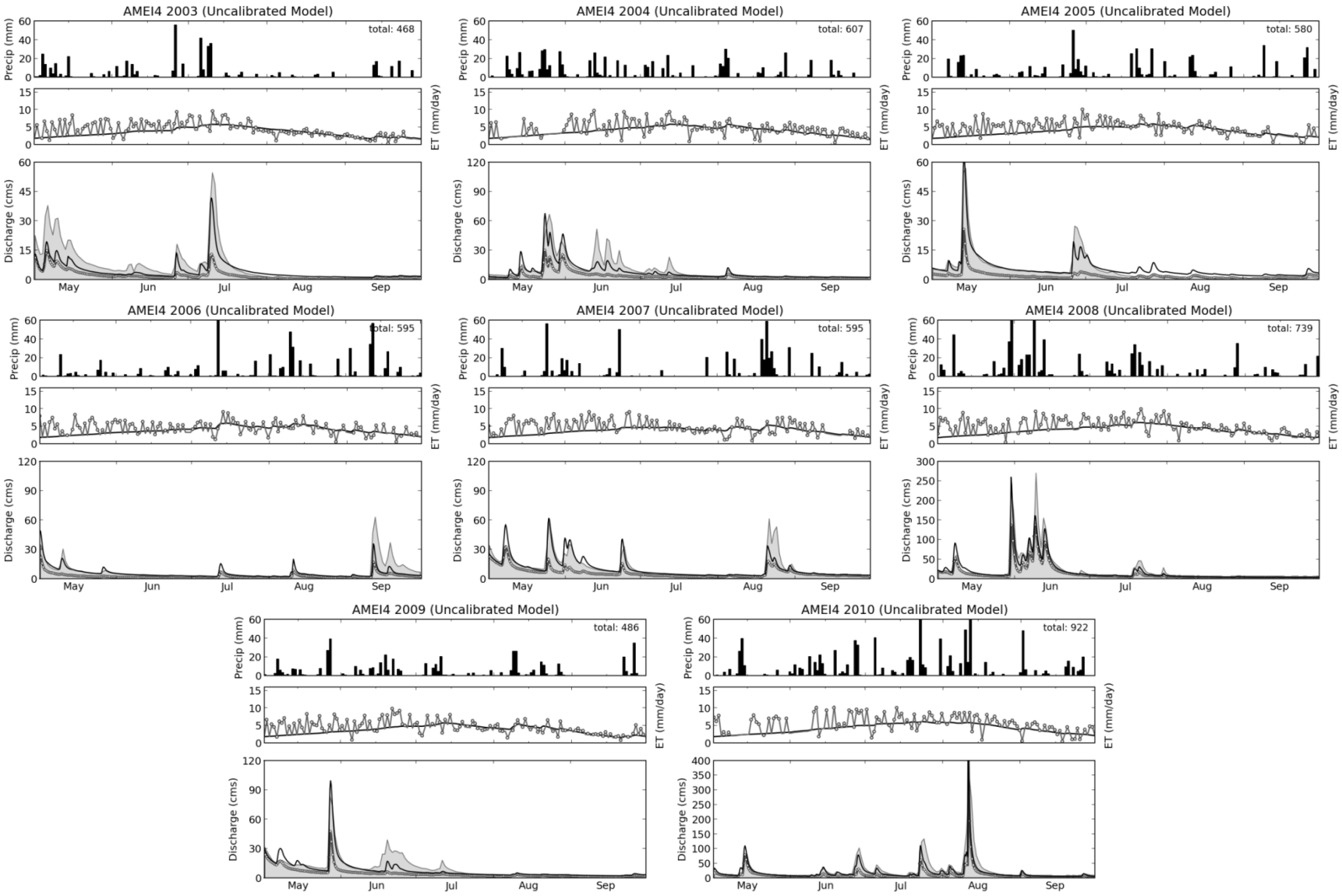
AMEI4 2003 (Uncalibrated Model)
total: 468
AMEI4 2004 (Uncalibrated Model)
total: 607
AMEI4 2005 (Uncalibrated Model)
total: 580
AMEI4 2006 (Uncalibrated Model)
total: 595
AMEI4 2007 (Uncalibrated Model)
total: 595
AMEI4 2008 (Uncalibrated Model)
total: 739
AMEI4 2009 (Uncalibrated Model)
total: 486
AMEI4 2010 (Uncalibrated Model)
total: 922
Precip (mm)
ET (mm/day)
Discharge (cms)
May
Jun
Jul
Aug
Sep

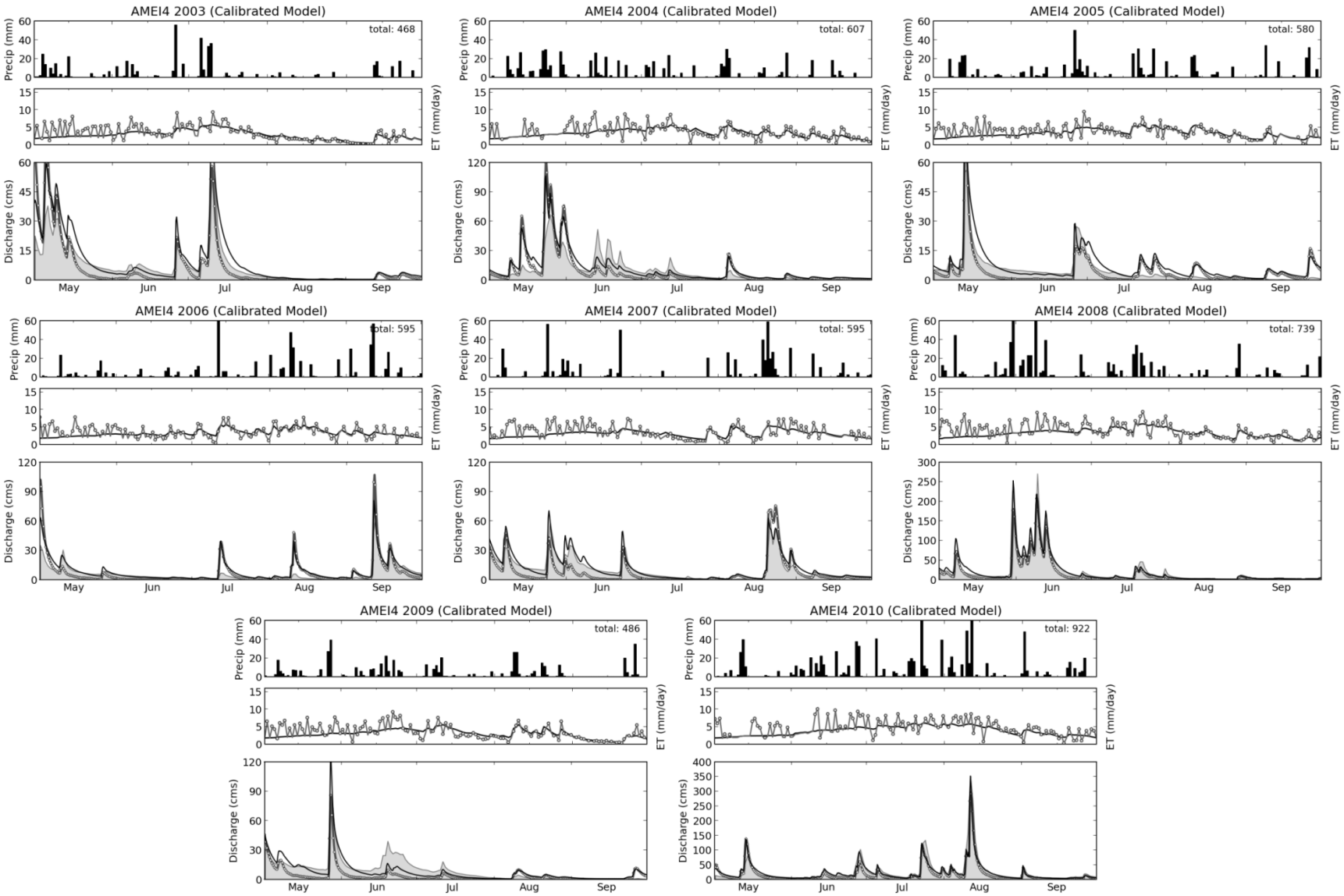
AMEI4 2003 (Calibrated Model)
total: 468
AMEI4 2004 (Calibrated Model)
total: 607
AMEI4 2005 (Calibrated Model)
total: 580
AMEI4 2006 (Calibrated Model)
total: 595
AMEI4 2007 (Calibrated Model)
total: 595
AMEI4 2008 (Calibrated Model)
total: 739
AMEI4 2009 (Calibrated Model)
total: 486
AMEI4 2010 (Calibrated Model)
total: 922
Precip (mm)
ET (mm/day)
Discharge (cms)
May
Jun
Jul
Aug
Sep

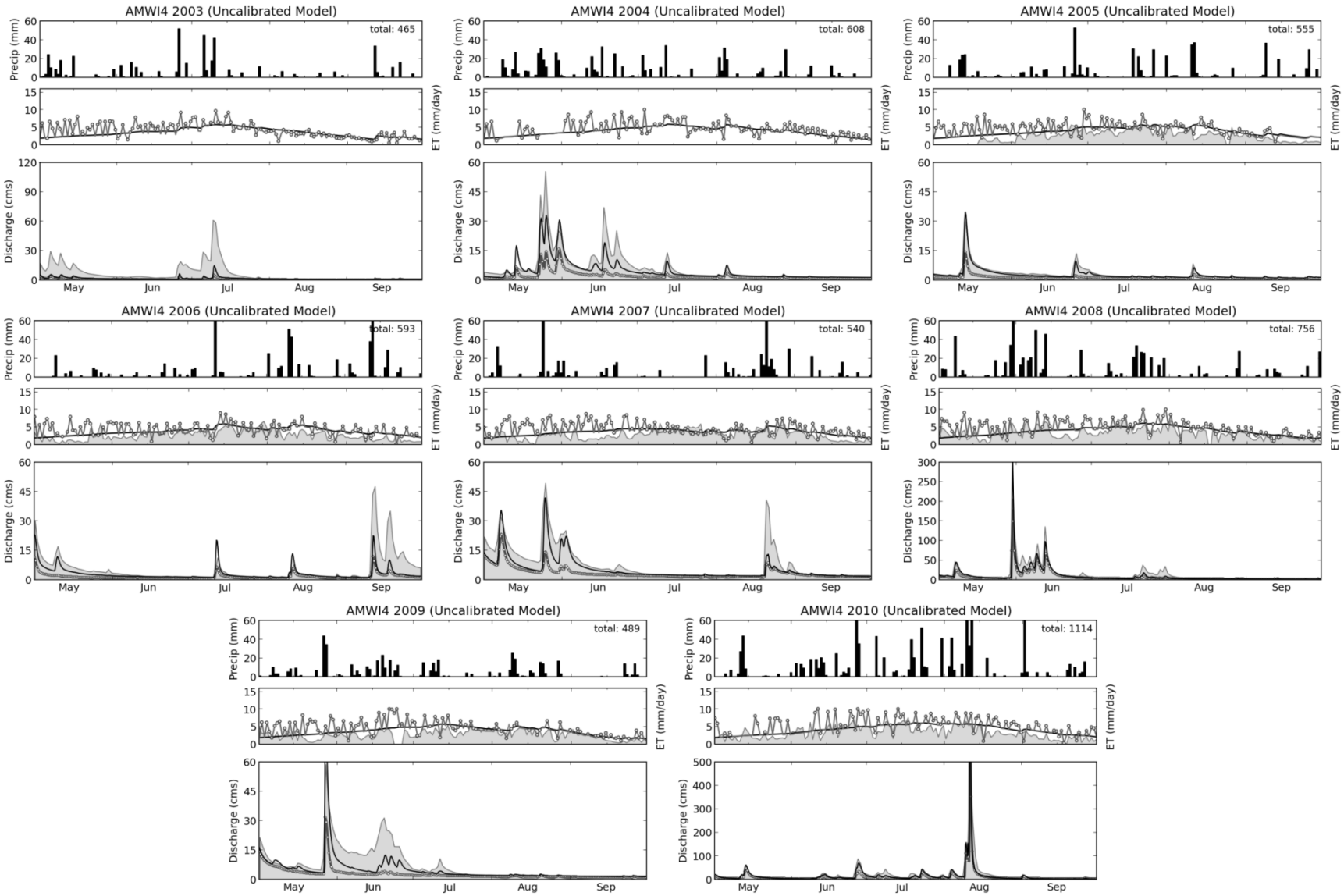
AMWI4 2003 (Uncalibrated Model)
total: 465
AMWI4 2004 (Uncalibrated Model)
total: 608
AMWI4 2005 (Uncalibrated Model)
total: 555
AMWI4 2006 (Uncalibrated Model)
total: 593
AMWI4 2007 (Uncalibrated Model)
total: 540
AMWI4 2008 (Uncalibrated Model)
total: 756
AMWI4 2009 (Uncalibrated Model)
total: 489
AMWI4 2010 (Uncalibrated Model)
total: 1114
Precip (mm)
ET (mm/day)
Discharge (cms)
May
Jun
Jul
Aug
Sep

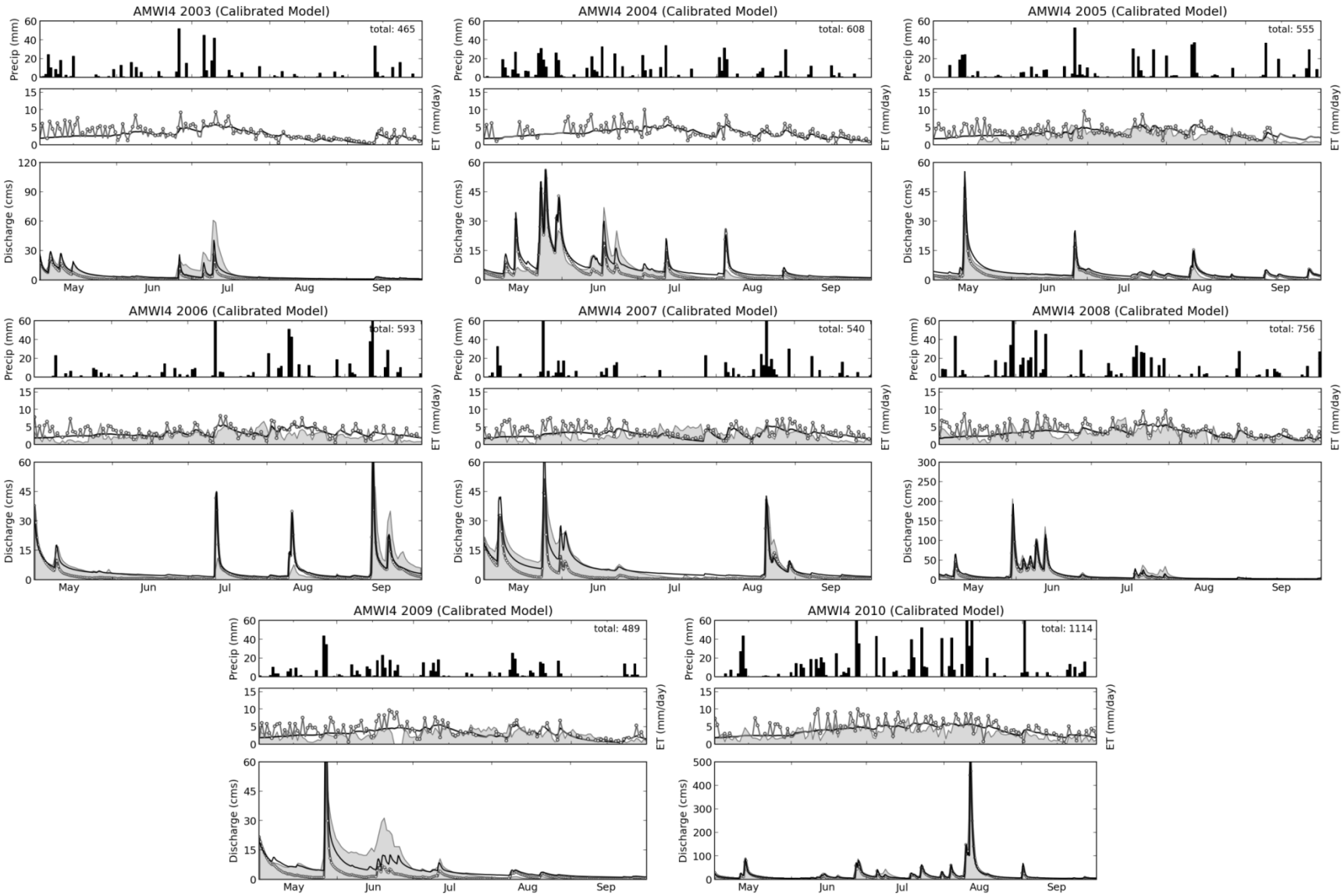
AMWI4 2003 (Calibrated Model)
total: 465
AMWI4 2004 (Calibrated Model)
total: 608
AMWI4 2005 (Calibrated Model)
total: 555
AMWI4 2006 (Calibrated Model)
total: 593
AMWI4 2007 (Calibrated Model)
total: 540
AMWI4 2008 (Calibrated Model)
total: 756
AMWI4 2009 (Calibrated Model)
total: 489
AMWI4 2010 (Calibrated Model)
total: 1114
Precip (mm)
ET (mm/day)
Discharge (cms)
May
Jun
Jul
Aug
Sep

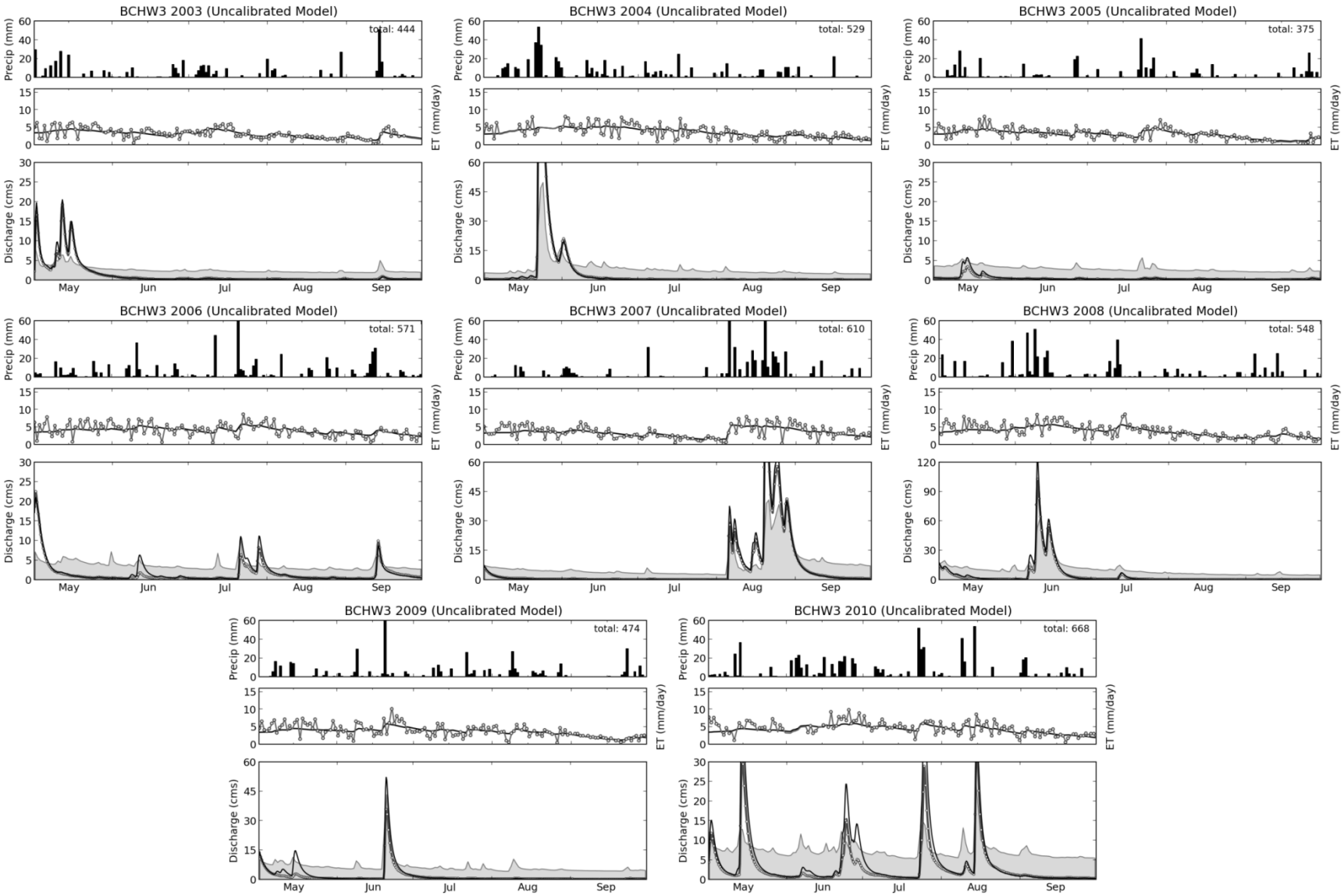
BCHW3 2003 (Uncalibrated Model)
total: 444
BCHW3 2004 (Uncalibrated Model)
total: 529
BCHW3 2005 (Uncalibrated Model)
total: 375
BCHW3 2006 (Uncalibrated Model)
total: 571
BCHW3 2007 (Uncalibrated Model)
total: 610
BCHW3 2008 (Uncalibrated Model)
total: 548
BCHW3 2009 (Uncalibrated Model)
total: 474
BCHW3 2010 (Uncalibrated Model)
total: 668
Precip (mm)
ET (mm/day)
Discharge (cms)
May
Jun
Jul
Aug
Sep

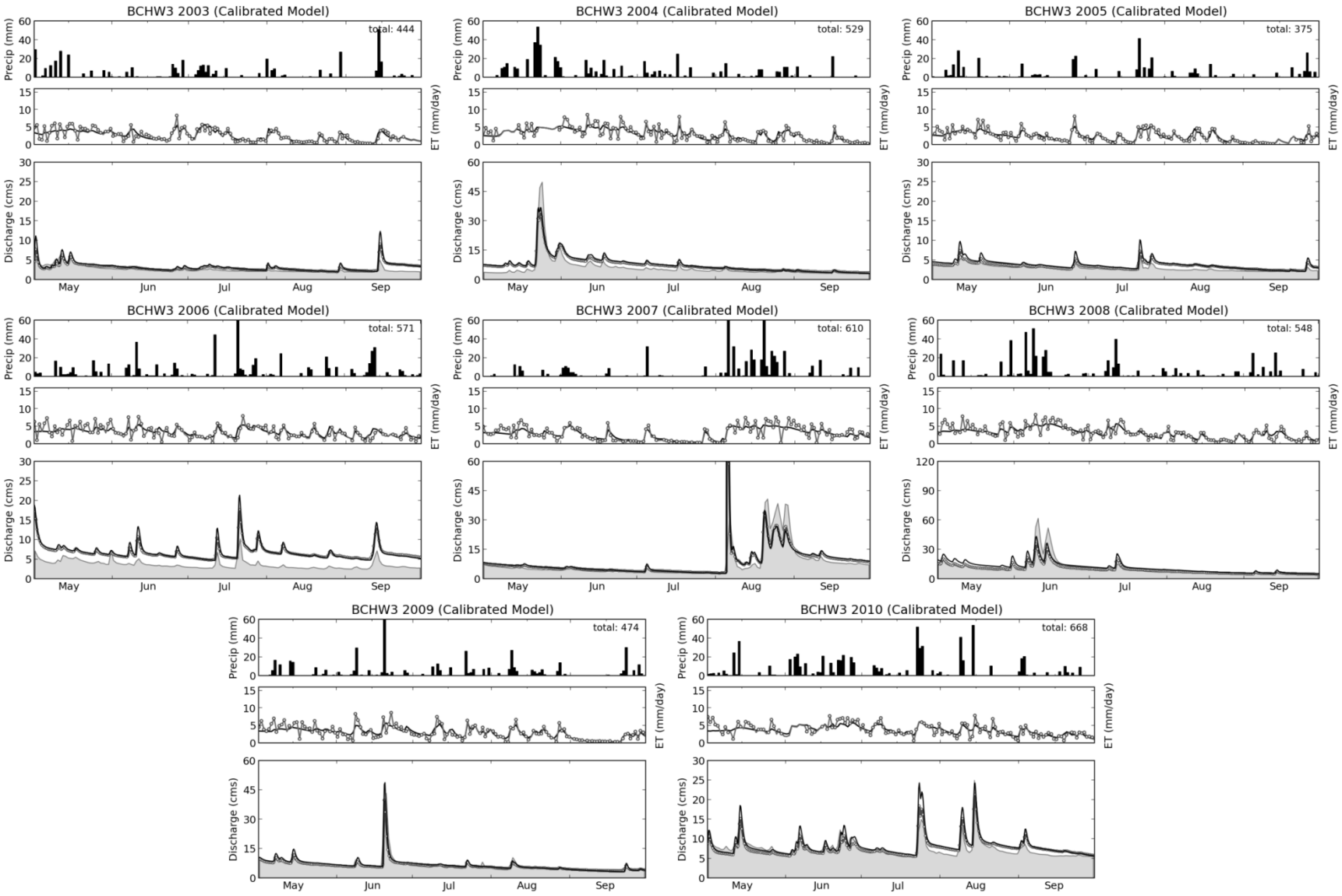
BCHW3 2003 (Calibrated Model)
total: 444
BCHW3 2004 (Calibrated Model)
total: 529
BCHW3 2005 (Calibrated Model)
total: 375
BCHW3 2006 (Calibrated Model)
total: 571
BCHW3 2007 (Calibrated Model)
total: 610
BCHW3 2008 (Calibrated Model)
total: 548
BCHW3 2009 (Calibrated Model)
total: 474
BCHW3 2010 (Calibrated Model)
total: 668
Precip (mm)
ET (mm/day)
Discharge (cms)
May
Jun
Jul
Aug
Sep

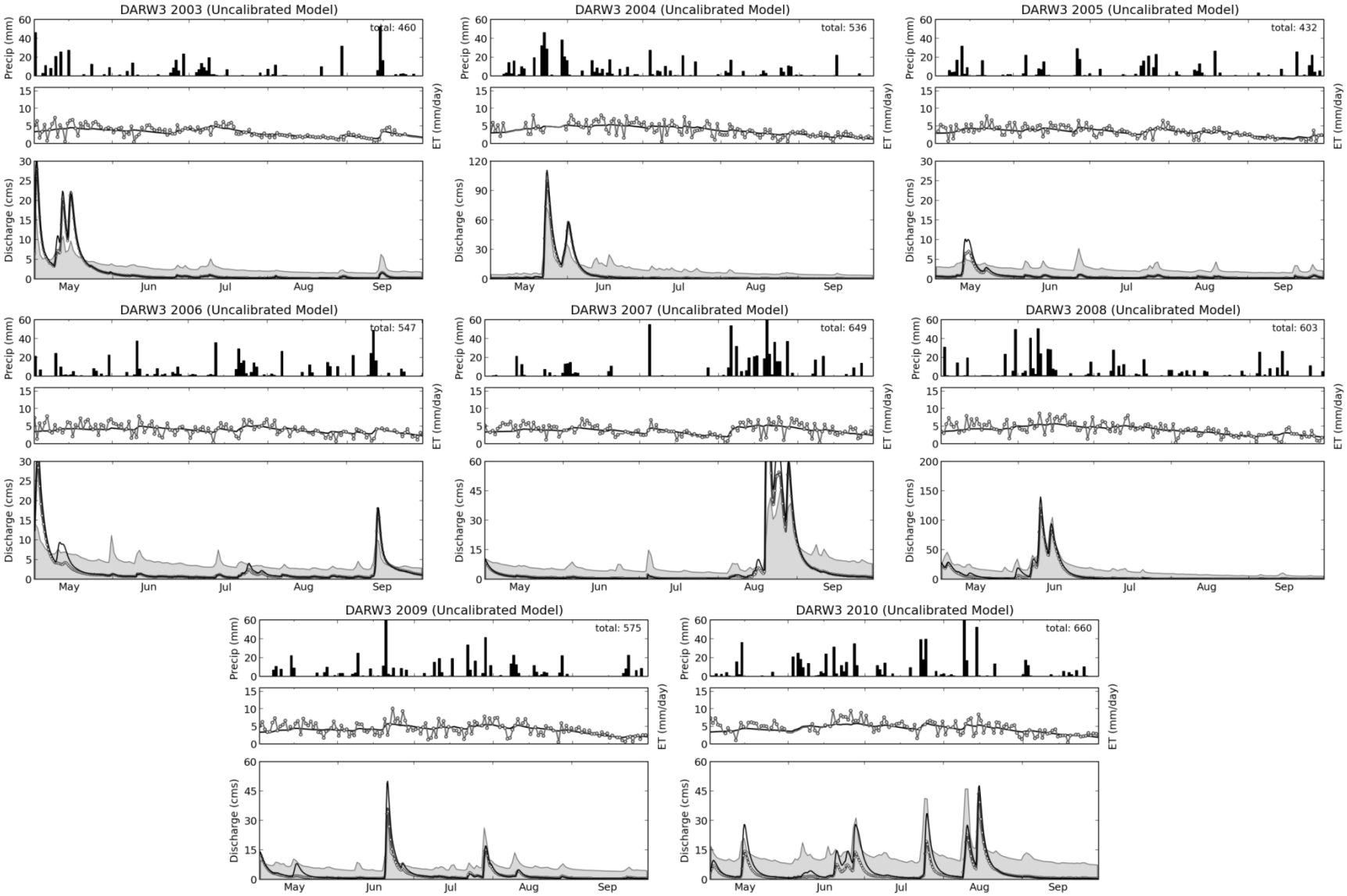
DARW3 2003 (Uncalibrated Model)
total: 460
DARW3 2004 (Uncalibrated Model)
total: 536
DARW3 2005 (Uncalibrated Model)
total: 432
DARW3 2006 (Uncalibrated Model)
total: 547
DARW3 2007 (Uncalibrated Model)
total: 649
DARW3 2008 (Uncalibrated Model)
total: 603
DARW3 2009 (Uncalibrated Model)
total: 575
DARW3 2010 (Uncalibrated Model)
total: 660
Precip (mm)
ET (mm/day)
Discharge (cms)
May
Jun
Jul
Aug
Sep

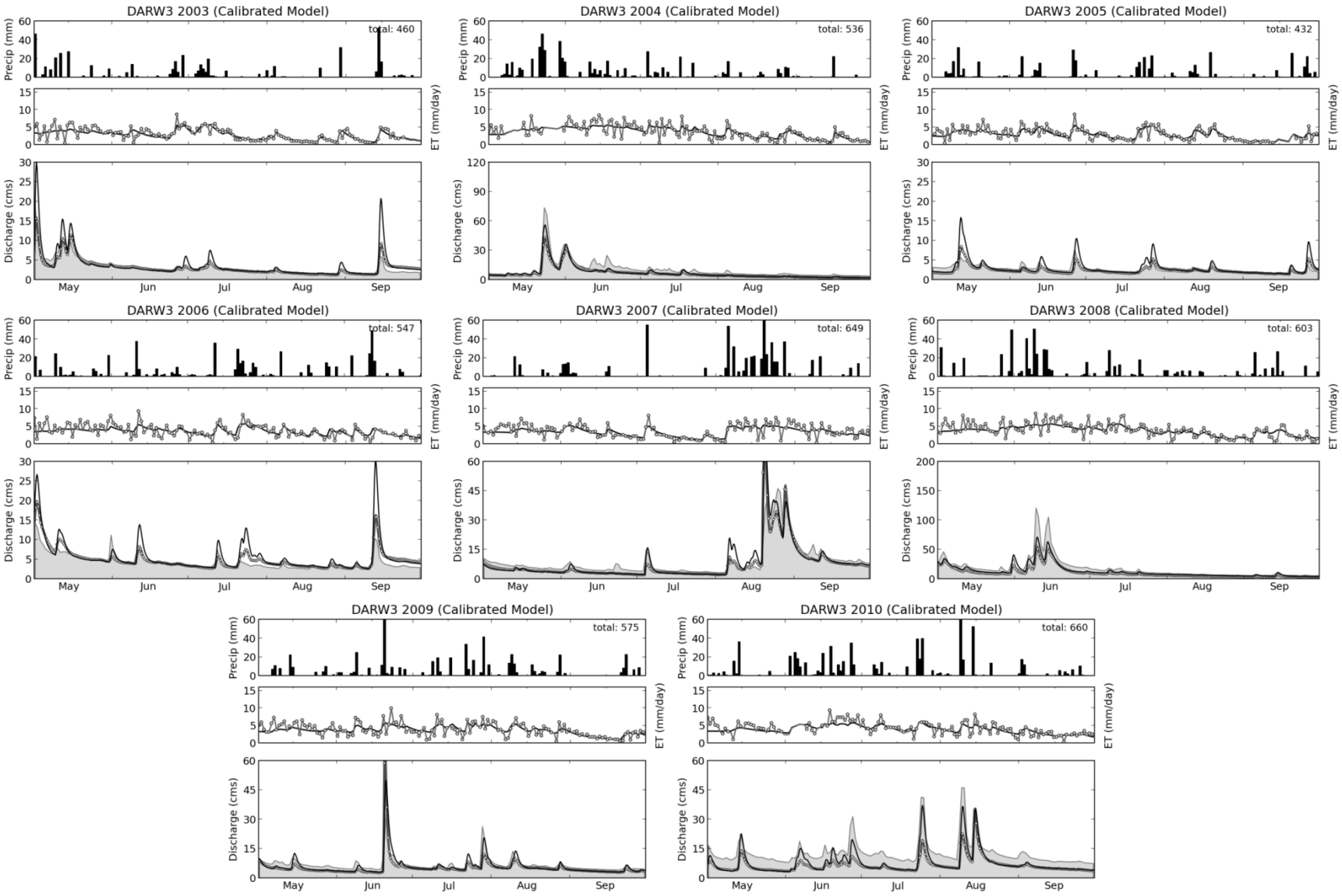
DARW3 2003 (Calibrated Model)
total: 460
DARW3 2004 (Calibrated Model)
total: 536
DARW3 2005 (Calibrated Model)
total: 432
DARW3 2006 (Calibrated Model)
total: 547
DARW3 2007 (Calibrated Model)
total: 649
DARW3 2008 (Calibrated Model)
total: 603
DARW3 2009 (Calibrated Model)
total: 575
DARW3 2010 (Calibrated Model)
total: 660
Precip (mm)
ET (mm/day)
Discharge (cms)
May
Jun
Jul
Aug
Sep

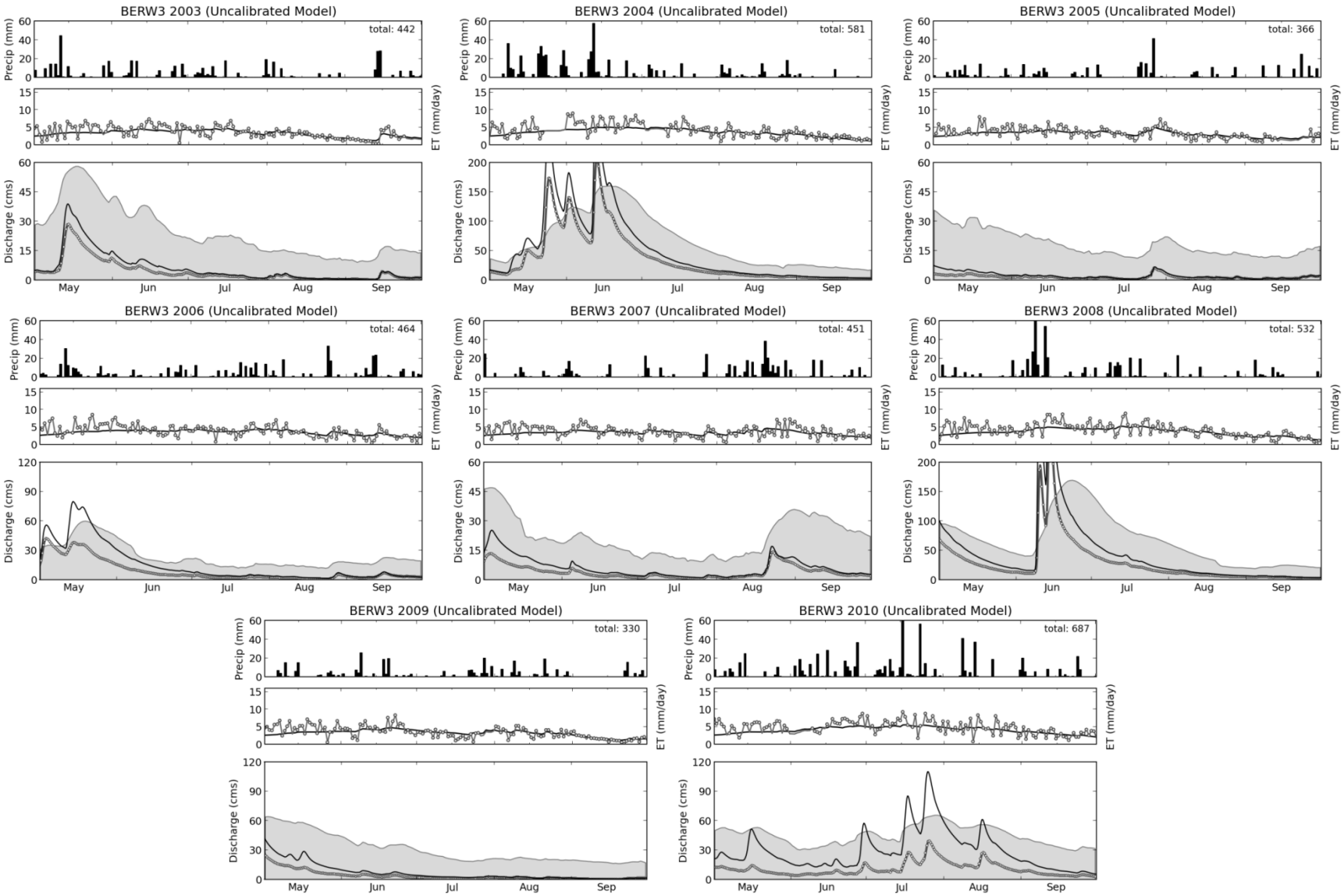
BERW3 2003 (Uncalibrated Model)
total: 442
BERW3 2004 (Uncalibrated Model)
total: 581
BERW3 2005 (Uncalibrated Model)
total: 366
BERW3 2006 (Uncalibrated Model)
total: 464
BERW3 2007 (Uncalibrated Model)
total: 451
BERW3 2008 (Uncalibrated Model)
total: 532
BERW3 2009 (Uncalibrated Model)
total: 330
BERW3 2010 (Uncalibrated Model)
total: 687
Precip (mm)
ET (mm/day)
Discharge (cms)
May
Jun
Jul
Aug
Sep

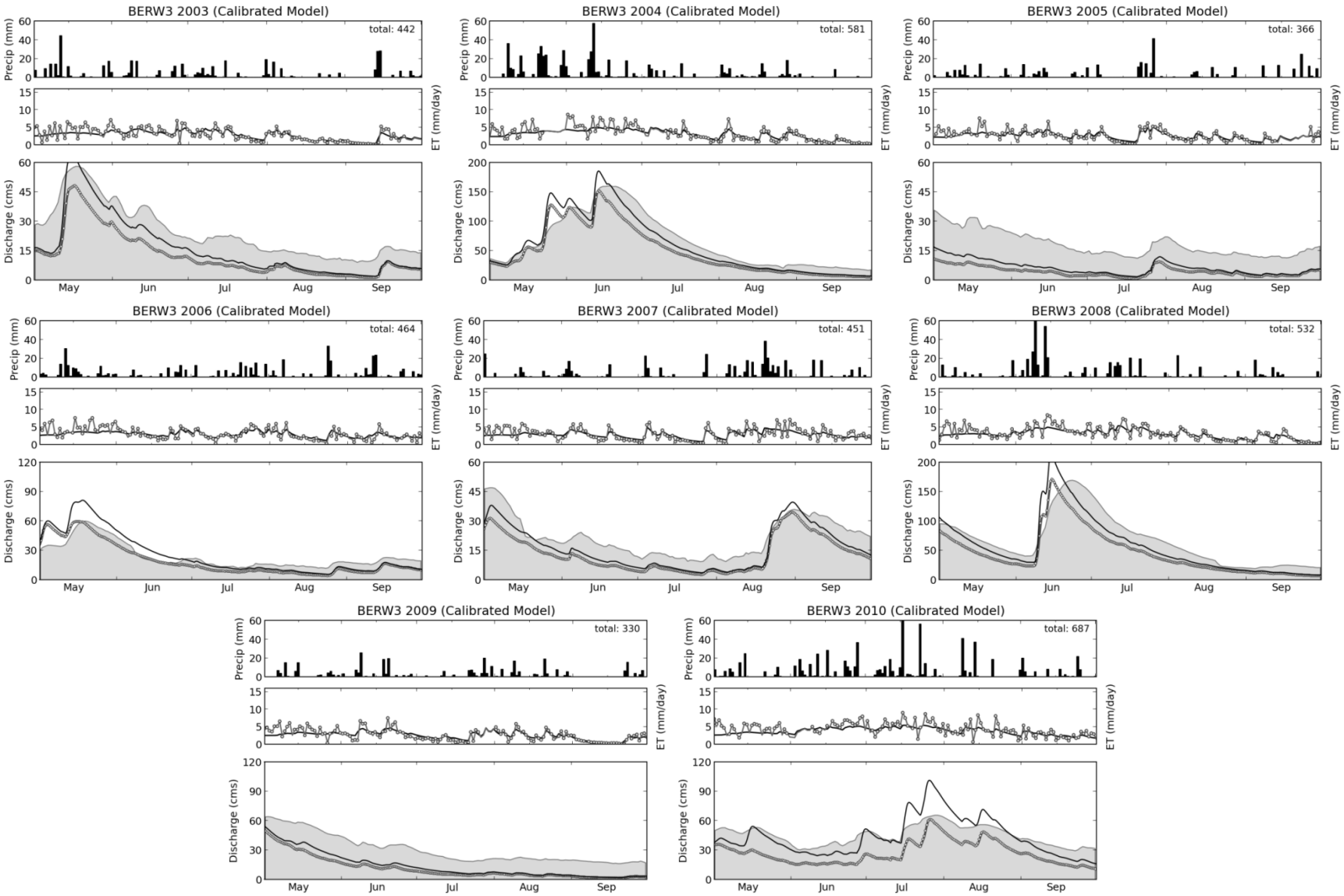
BERW3 2003 (Calibrated Model)
total: 442
BERW3 2004 (Calibrated Model)
total: 581
BERW3 2005 (Calibrated Model)
total: 366
BERW3 2006 (Calibrated Model)
total: 464
BERW3 2007 (Calibrated Model)
total: 451
BERW3 2008 (Calibrated Model)
total: 532
BERW3 2009 (Calibrated Model)
total: 330
BERW3 2010 (Calibrated Model)
total: 687
Precip (mm)
ET (mm/day)
Discharge (cms)
May
Jun
Jul
Aug
Sep

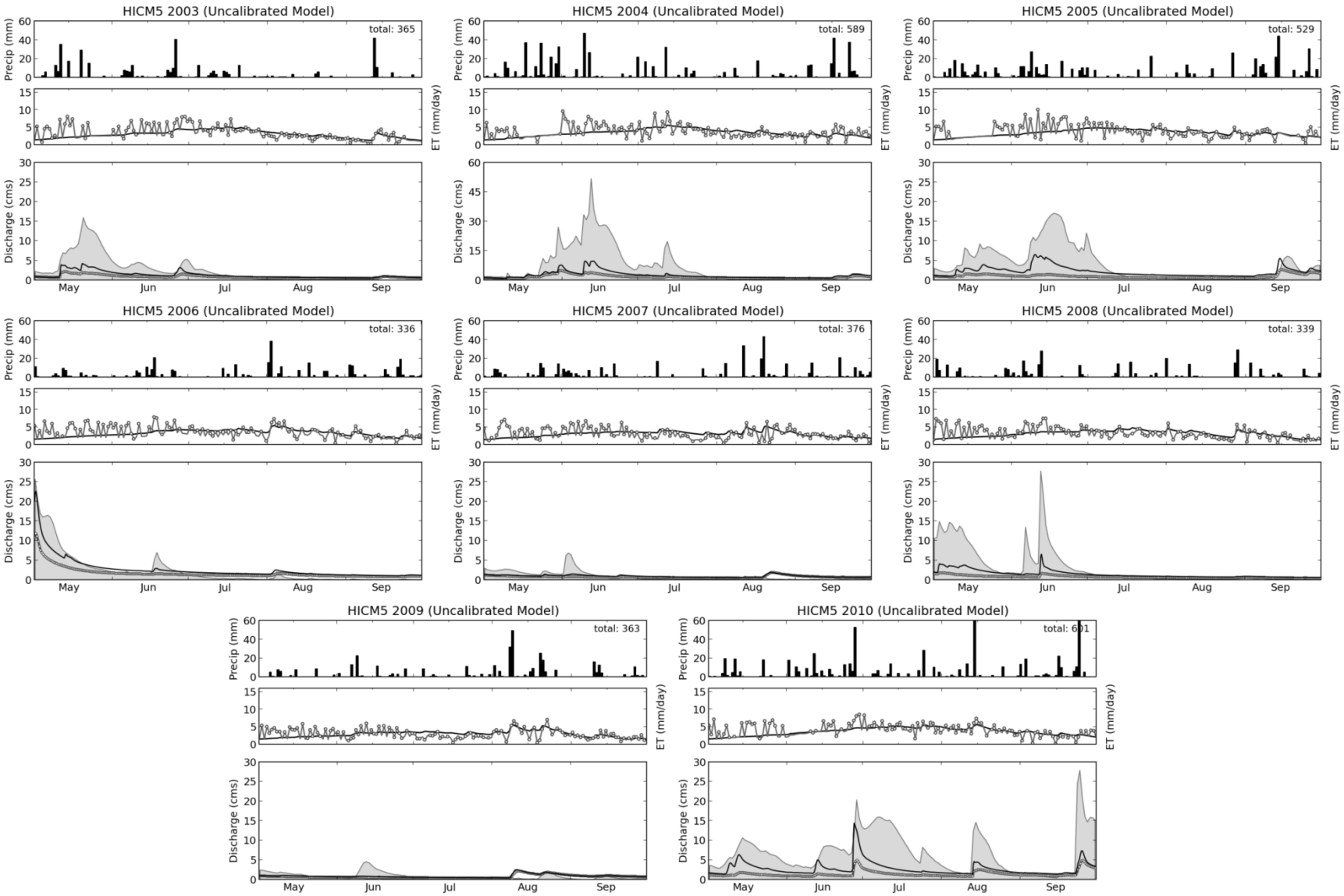
HICM5 2003 (Uncalibrated Model)
total: 365
HICM5 2004 (Uncalibrated Model)
total: 589
HICM5 2005 (Uncalibrated Model)
total: 529
HICM5 2006 (Uncalibrated Model)
total: 336
HICM5 2007 (Uncalibrated Model)
total: 376
HICM5 2008 (Uncalibrated Model)
total: 339
HICM5 2009 (Uncalibrated Model)
total: 363
HICM5 2010 (Uncalibrated Model)
total: 601
Precip (mm)
ET (mm/day)
Discharge (cms)
May
Jun
Jul
Aug
Sep

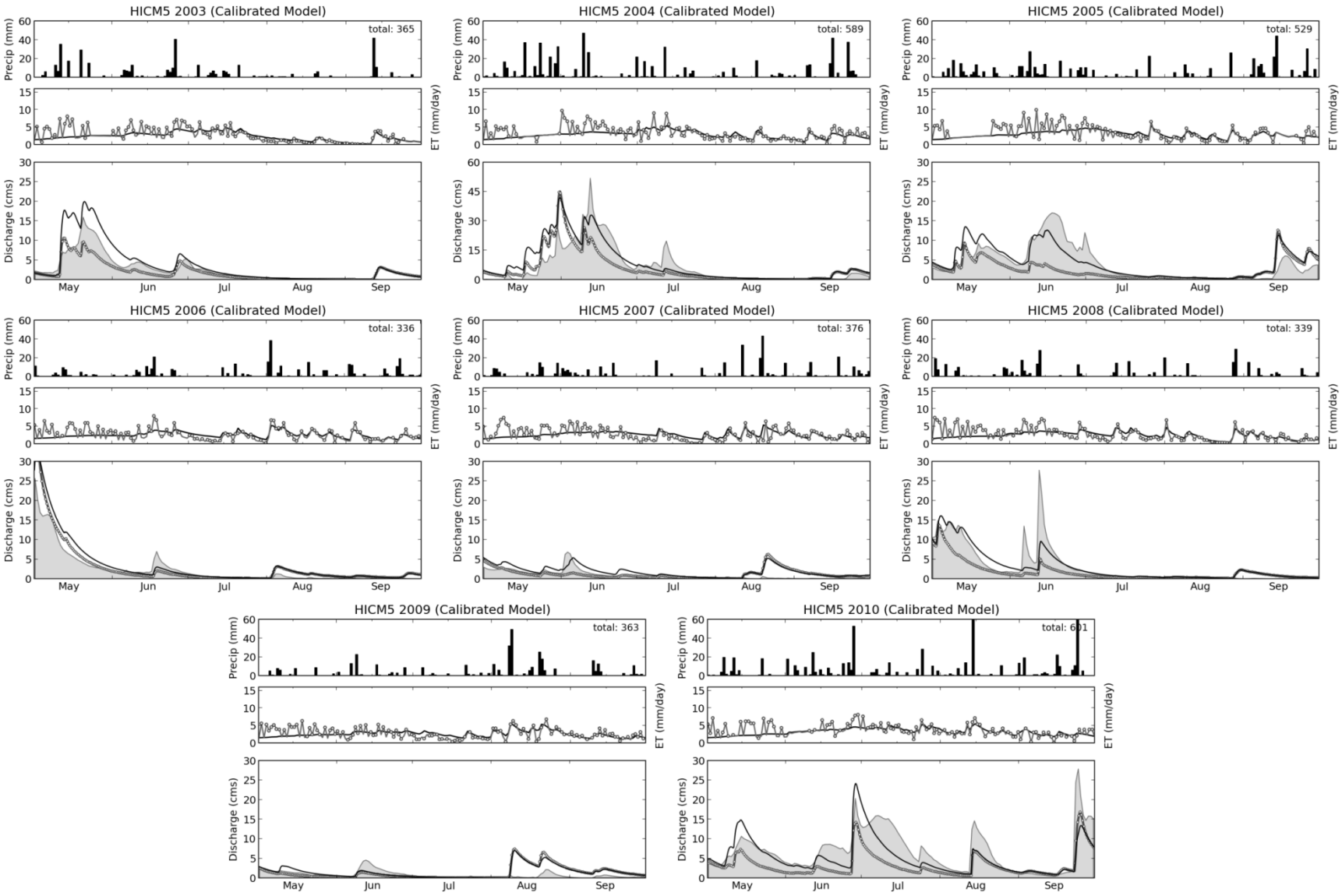
HICM5 2003 (Calibrated Model)
total: 365
HICM5 2004 (Calibrated Model)
total: 589
HICM5 2005 (Calibrated Model)
total: 529
HICM5 2006 (Calibrated Model)
total: 336
HICM5 2007 (Calibrated Model)
total: 376
HICM5 2008 (Calibrated Model)
total: 339
HICM5 2009 (Calibrated Model)
total: 363
HICM5 2010 (Calibrated Model)
total: 601
Precip (mm)
ET (mm/day)
Discharge (cms)
May
Jun
Jul
Aug
Sep

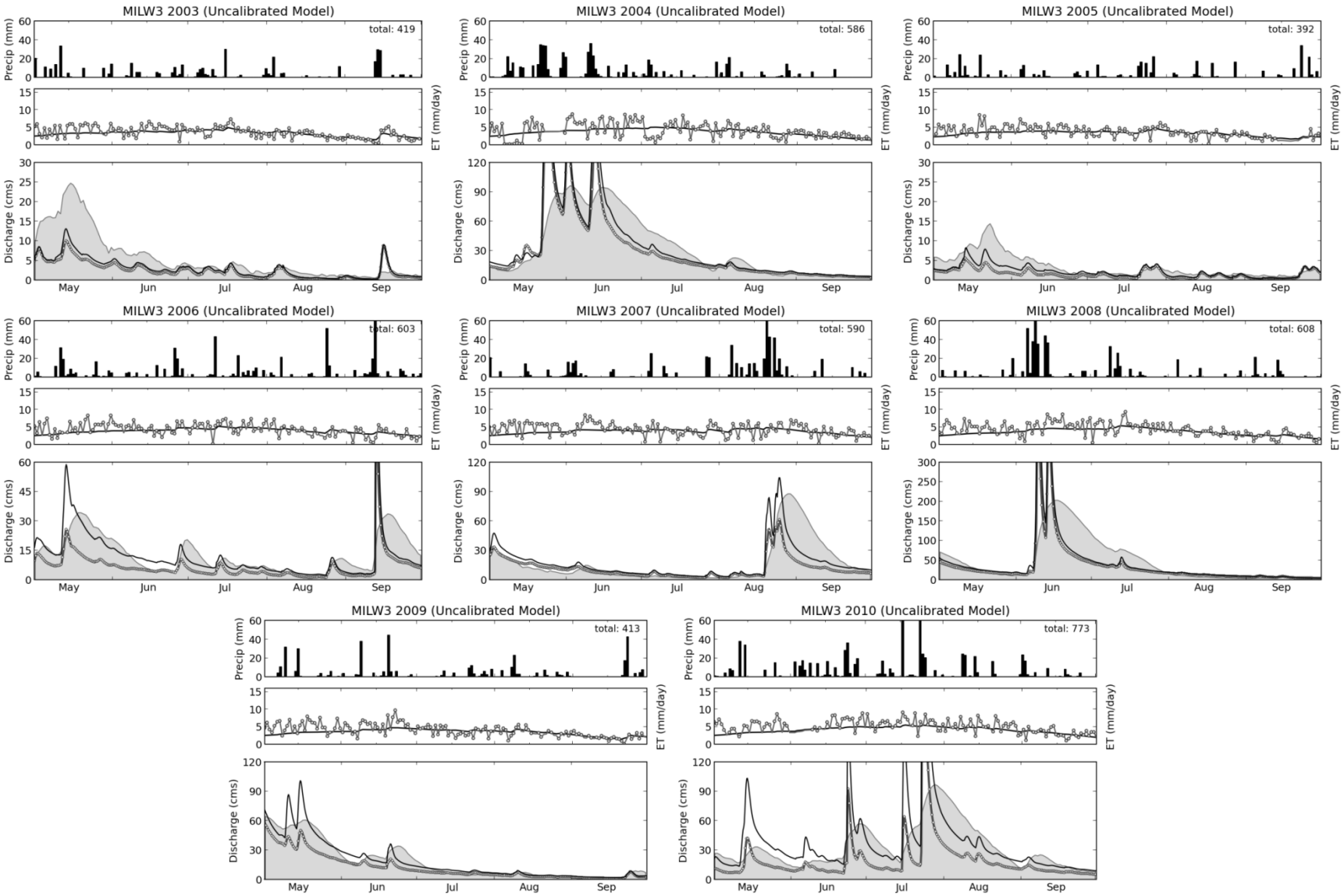
MILW3 2003 (Uncalibrated Model)
total: 419
MILW3 2004 (Uncalibrated Model)
total: 586
MILW3 2005 (Uncalibrated Model)
total: 392
MILW3 2006 (Uncalibrated Model)
total: 603
MILW3 2007 (Uncalibrated Model)
total: 590
MILW3 2008 (Uncalibrated Model)
total: 608
MILW3 2009 (Uncalibrated Model)
total: 413
MILW3 2010 (Uncalibrated Model)
total: 773
Precip (mm)
ET (mm/day)
Discharge (cms)
May
Jun
Jul
Aug
Sep

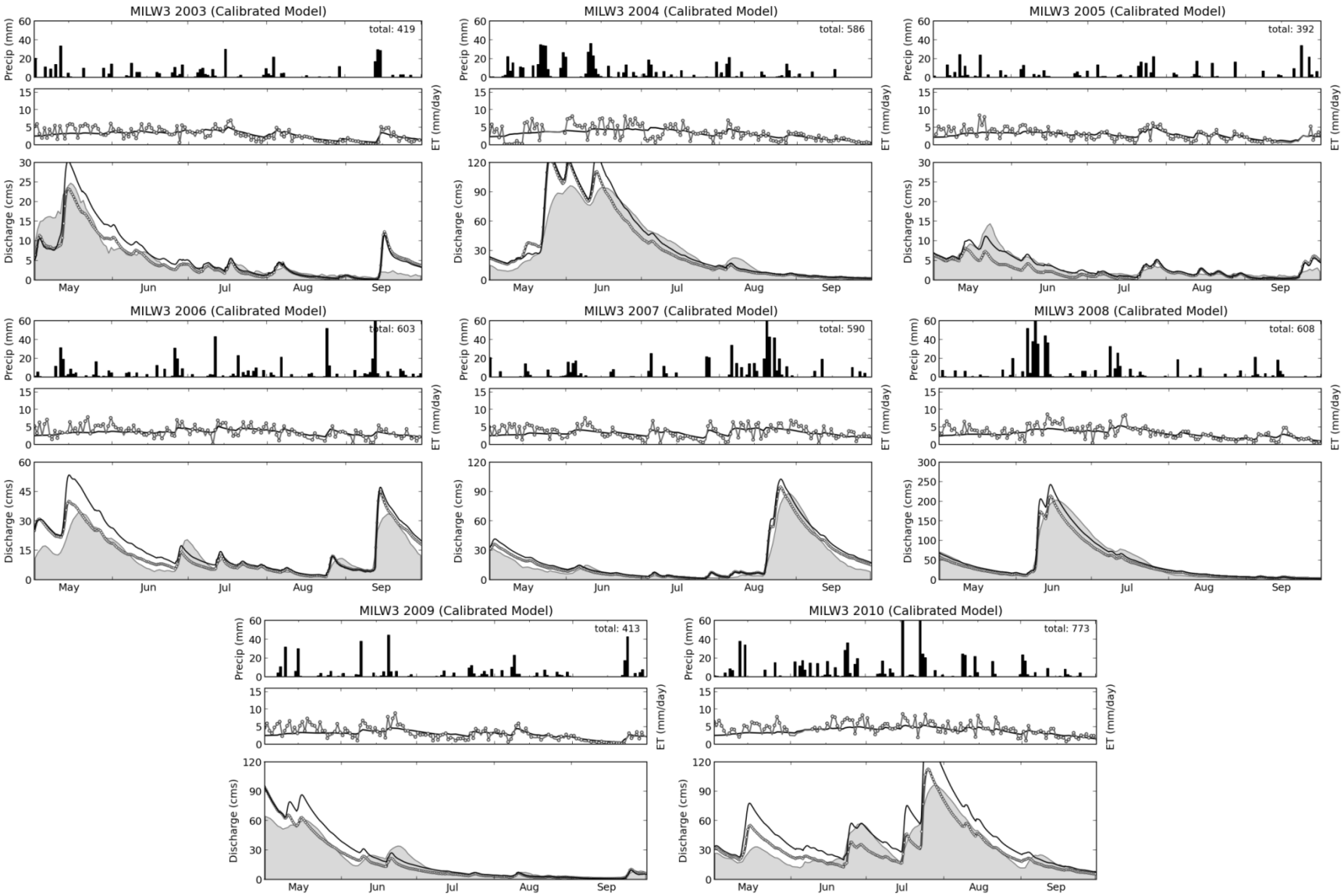
MILW3 2003 (Calibrated Model)
total: 419
MILW3 2004 (Calibrated Model)
total: 586
MILW3 2005 (Calibrated Model)
total: 392
MILW3 2006 (Calibrated Model)
total: 603
MILW3 2007 (Calibrated Model)
total: 590
MILW3 2008 (Calibrated Model)
total: 608
MILW3 2009 (Calibrated Model)
total: 413
MILW3 2010 (Calibrated Model)
total: 773
Precip (mm)
ET (mm/day)
Discharge (cms)
May
Jun
Jul
Aug
Sep

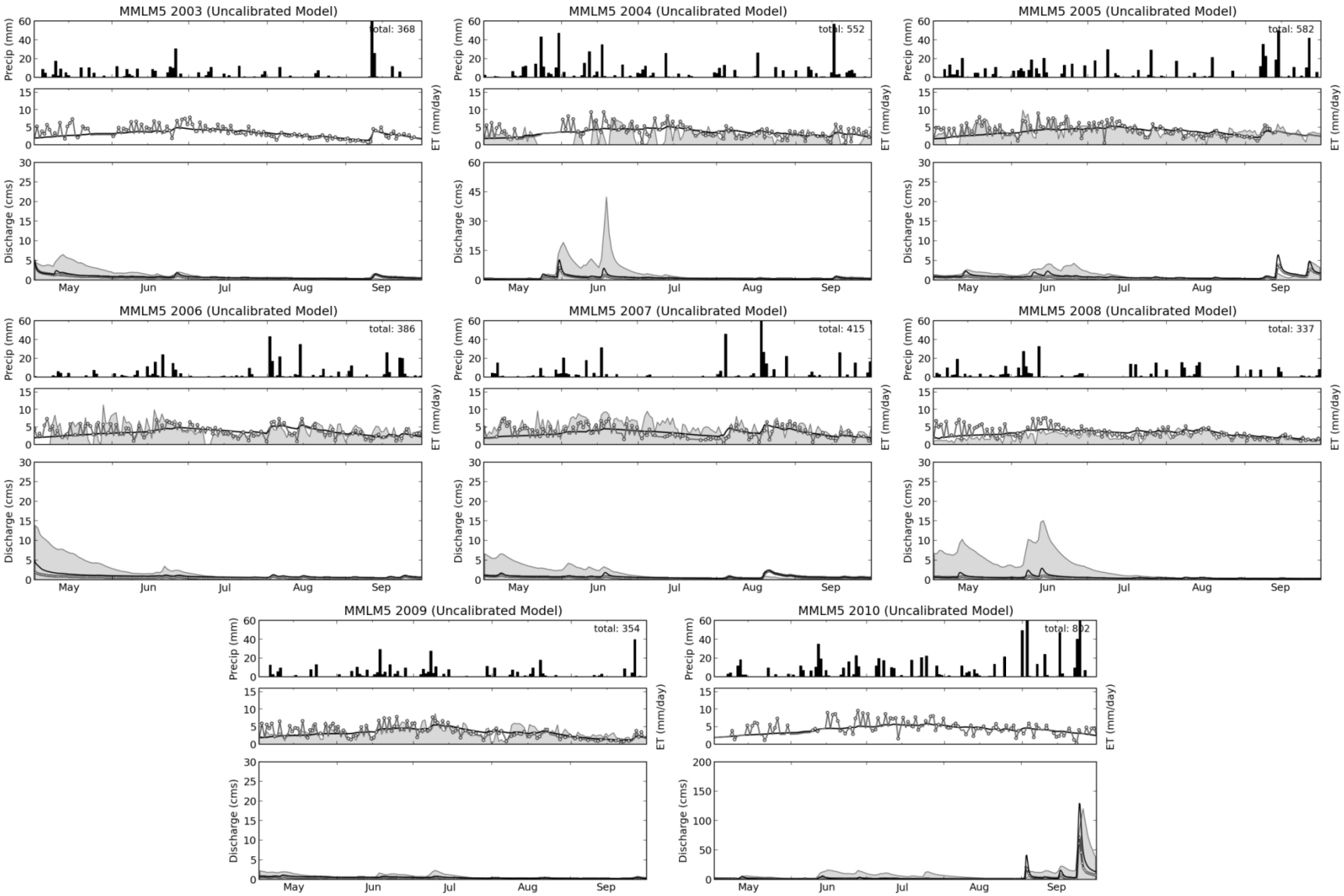
MMLM5 2003 (Uncalibrated Model)
total: 368
MMLM5 2004 (Uncalibrated Model)
total: 552
MMLM5 2005 (Uncalibrated Model)
total: 582
MMLM5 2006 (Uncalibrated Model)
total: 386
MMLM5 2007 (Uncalibrated Model)
total: 415
MMLM5 2008 (Uncalibrated Model)
total: 337
MMLM5 2009 (Uncalibrated Model)
total: 354
MMLM5 2010 (Uncalibrated Model)
total: 802
Precip (mm)
ET (mm/day)
Discharge (cms)
May
Jun
Jul
Aug
Sep

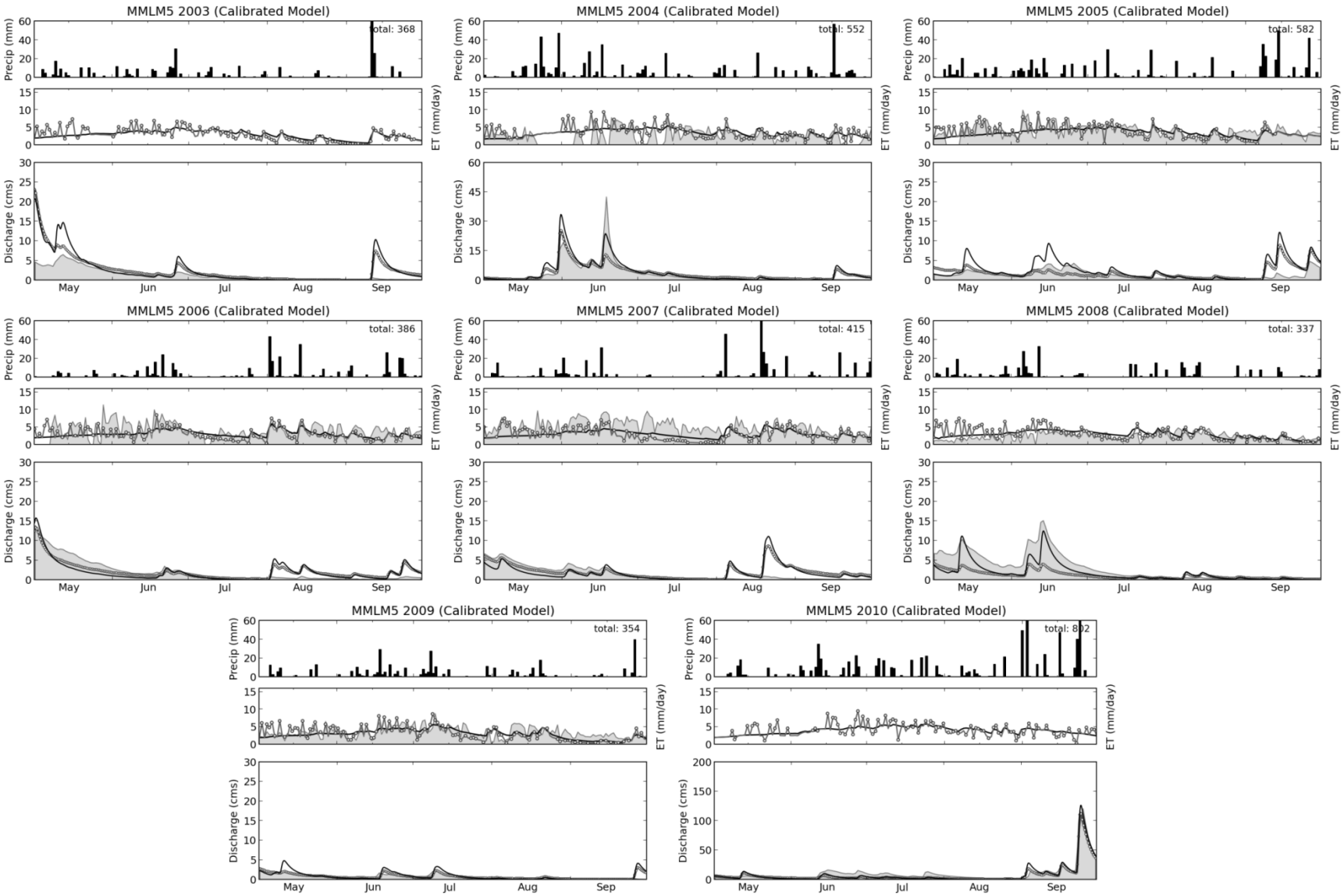
MMLM5 2003 (Calibrated Model)
total: 368
MMLM5 2004 (Calibrated Model)
total: 552
MMLM5 2005 (Calibrated Model)
total: 582
MMLM5 2006 (Calibrated Model)
total: 386
MMLM5 2007 (Calibrated Model)
total: 415
MMLM5 2008 (Calibrated Model)
total: 337
MMLM5 2009 (Calibrated Model)
total: 354
MMLM5 2010 (Calibrated Model)
total: 802
Precip (mm)
ET (mm/day)
Discharge (cms)
May
Jun
Jul
Aug
Sep

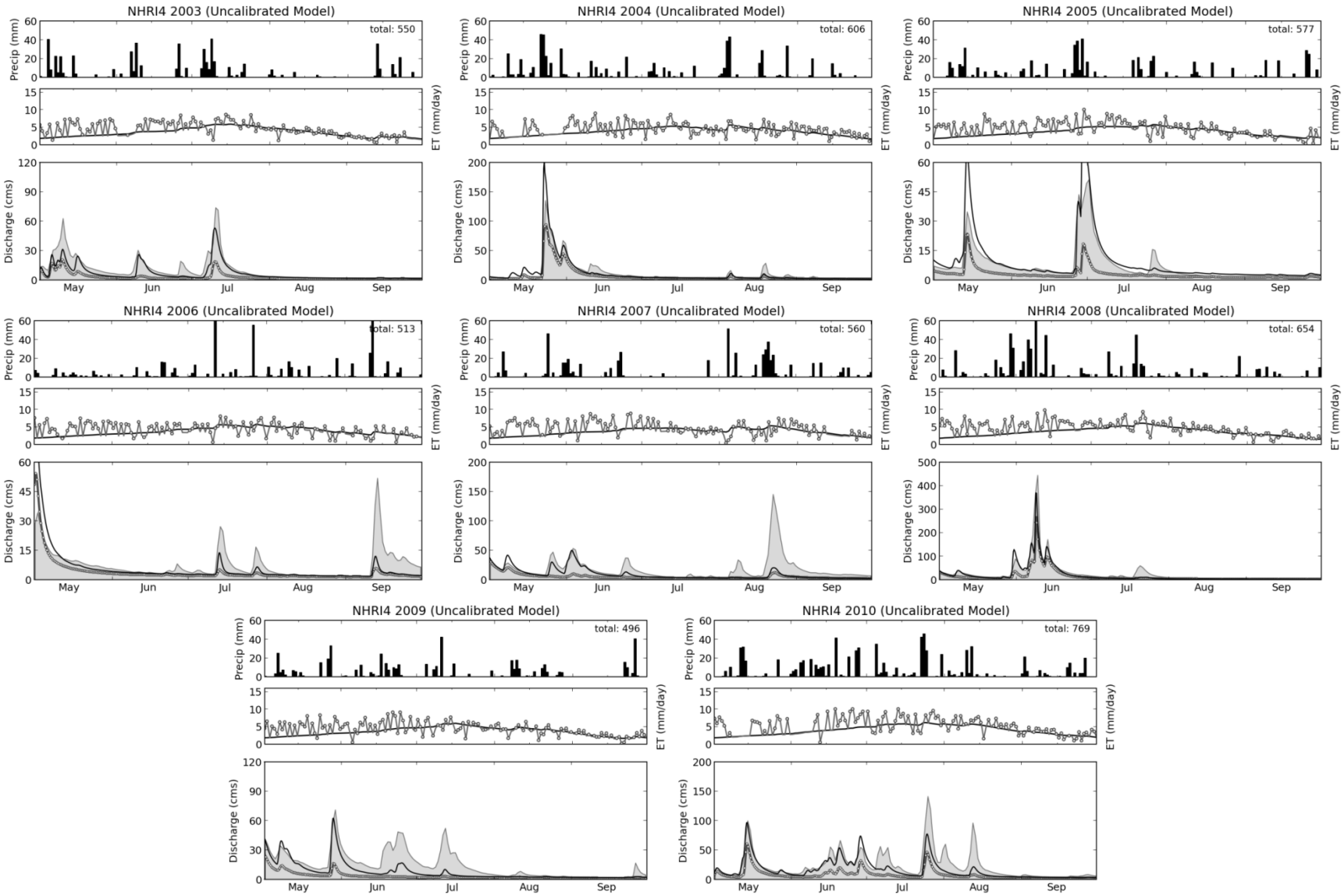
NHRI4 2003 (Uncalibrated Model)
total: 550
NHRI4 2004 (Uncalibrated Model)
total: 606
NHRI4 2005 (Uncalibrated Model)
total: 577
NHRI4 2006 (Uncalibrated Model)
total: 513
NHRI4 2007 (Uncalibrated Model)
total: 560
NHRI4 2008 (Uncalibrated Model)
total: 654
NHRI4 2009 (Uncalibrated Model)
total: 496
NHRI4 2010 (Uncalibrated Model)
total: 769
Precip (mm)
ET (mm/day)
Discharge (cms)
May
Jun
Jul
Aug
Sep

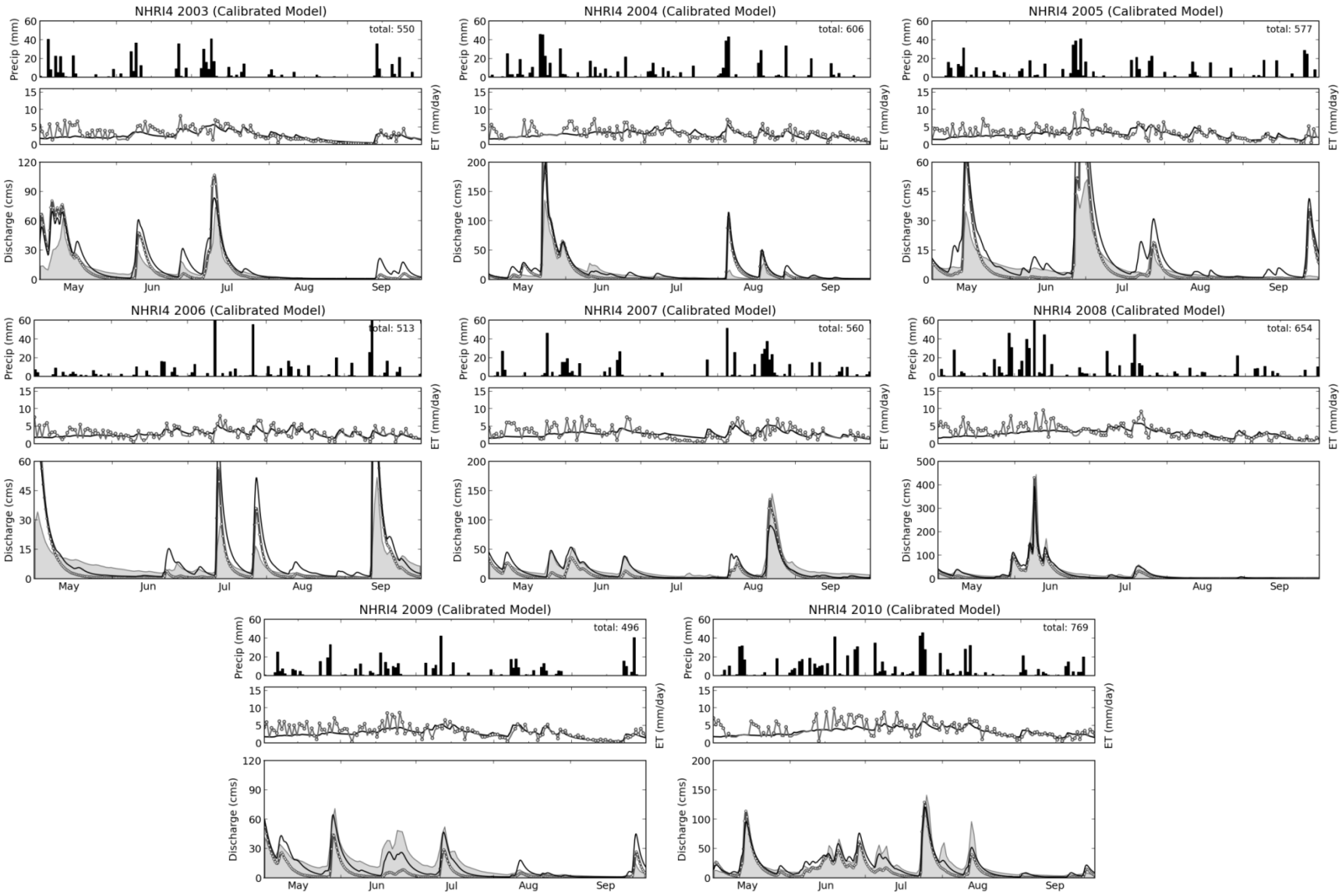
NHRI4 2003 (Calibrated Model)
total: 550
NHRI4 2004 (Calibrated Model)
total: 606
NHRI4 2005 (Calibrated Model)
total: 577
NHRI4 2006 (Calibrated Model)
total: 513
NHRI4 2007 (Calibrated Model)
total: 560
NHRI4 2008 (Calibrated Model)
total: 654
NHRI4 2009 (Calibrated Model)
total: 496
NHRI4 2010 (Calibrated Model)
total: 769
Precip (mm)
ET (mm/day)
Discharge (cms)
May
Jun
Jul
Aug
Sep

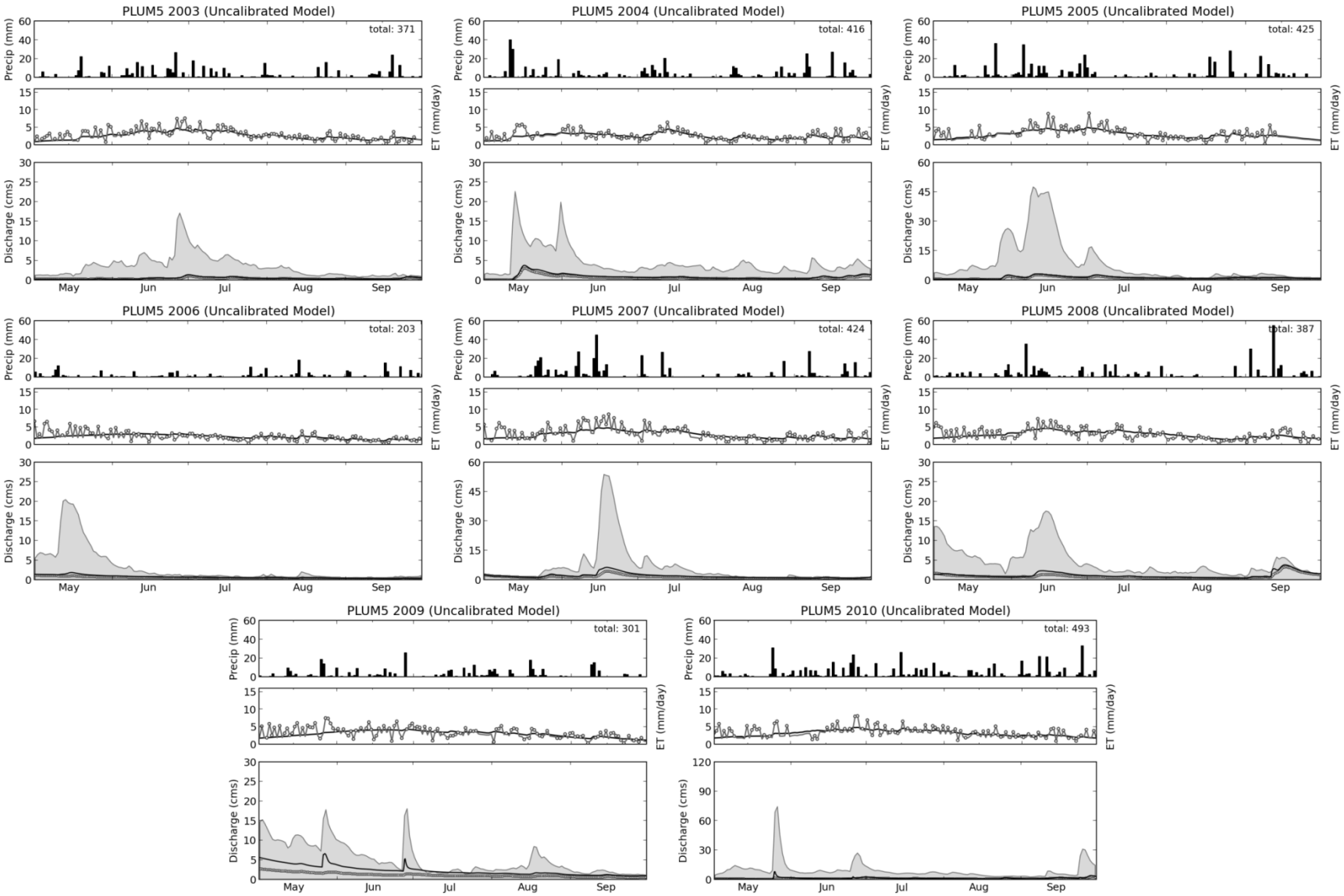
PLUM5 2003 (Uncalibrated Model)
total: 371
PLUM5 2004 (Uncalibrated Model)
total: 416
PLUM5 2005 (Uncalibrated Model)
total: 425
PLUM5 2006 (Uncalibrated Model)
total: 203
PLUM5 2007 (Uncalibrated Model)
total: 424
PLUM5 2008 (Uncalibrated Model)
total: 387
PLUM5 2009 (Uncalibrated Model)
total: 301
PLUM5 2010 (Uncalibrated Model)
total: 493
Precip (mm)
ET (mm/day)
Discharge (cms)
May
Jun
Jul
Aug
Sep

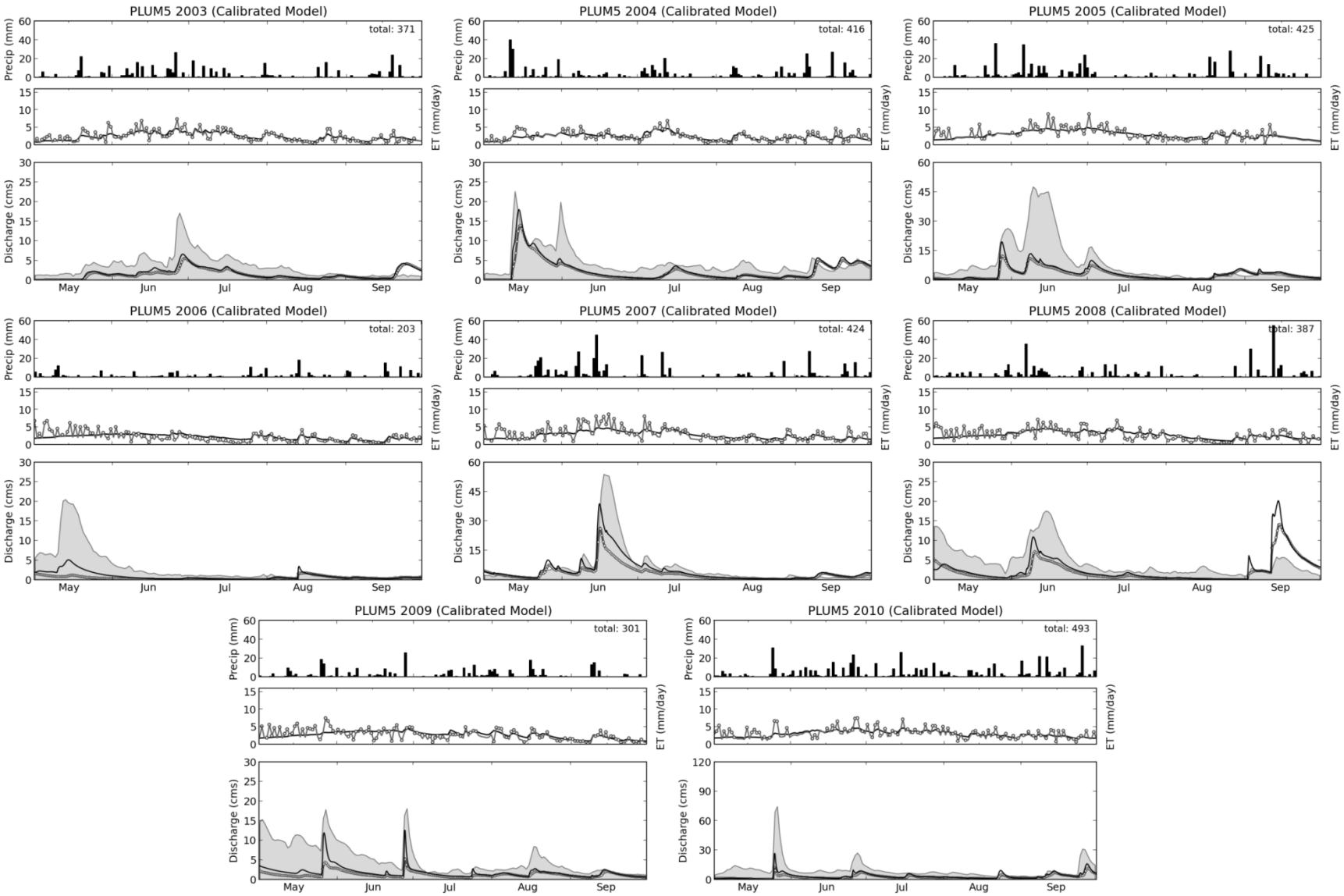
PLUM5 2003 (Calibrated Model)
total: 371
PLUM5 2004 (Calibrated Model)
total: 416
PLUM5 2005 (Calibrated Model)
total: 425
PLUM5 2006 (Calibrated Model)
total: 203
PLUM5 2007 (Calibrated Model)
total: 424
PLUM5 2008 (Calibrated Model)
total: 387
PLUM5 2009 (Calibrated Model)
total: 301
PLUM5 2010 (Calibrated Model)
total: 493
Precip (mm)
ET (mm/day)
Discharge (cms)
May
Jun
Jul
Aug
Sep

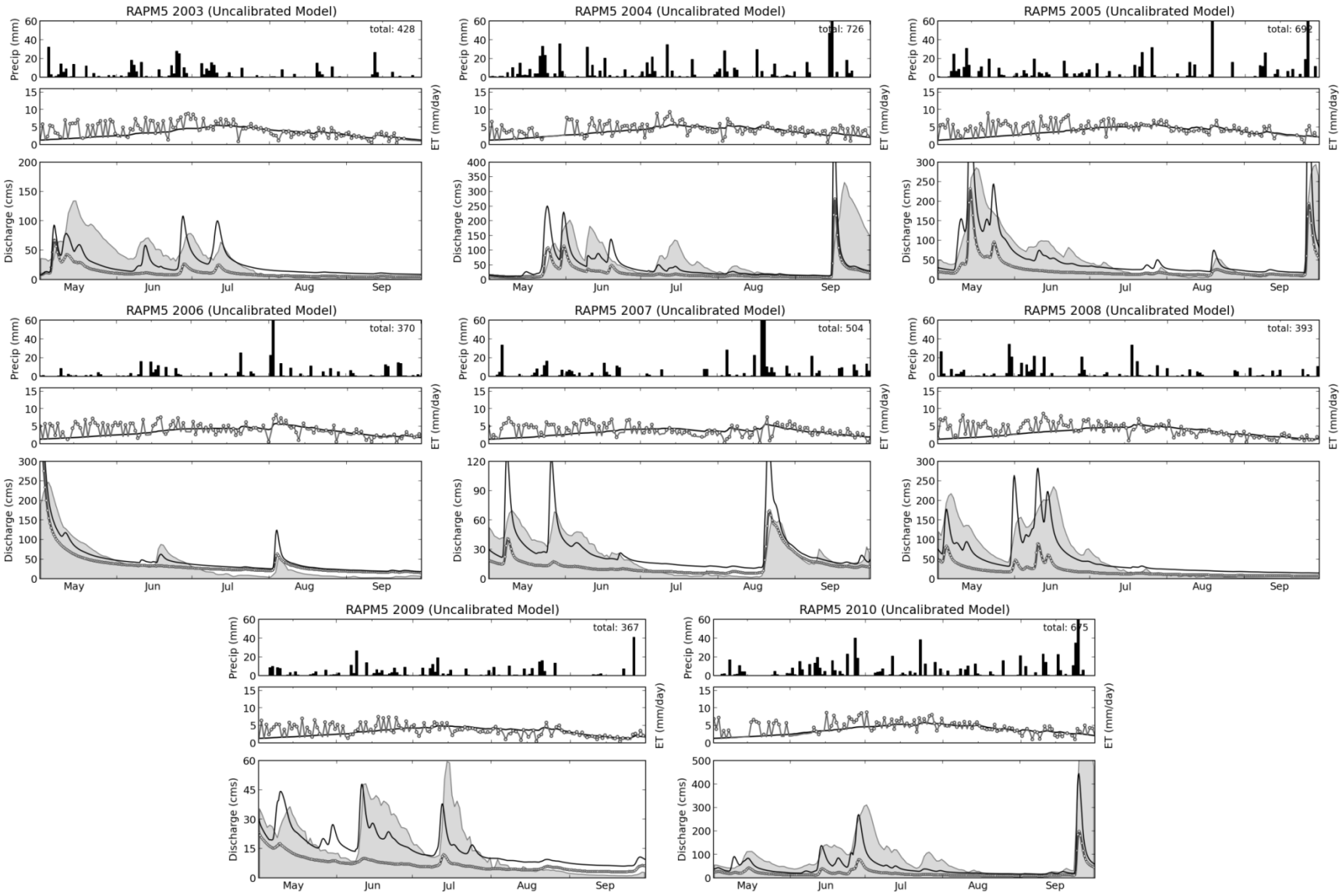
RAPM5 2003 (Uncalibrated Model)
total: 428
RAPM5 2004 (Uncalibrated Model)
total: 726
RAPM5 2005 (Uncalibrated Model)
RAPM5 2006 (Uncalibrated Model)
total: 370
RAPM5 2007 (Uncalibrated Model)
total: 504
RAPM5 2008 (Uncalibrated Model)
total: 393
RAPM5 2009 (Uncalibrated Model)
total: 367
RAPM5 2010 (Uncalibrated Model)
Precip (mm)
ET (mm/day)
Discharge (cms)
May
Jun
Jul
Aug
Sep

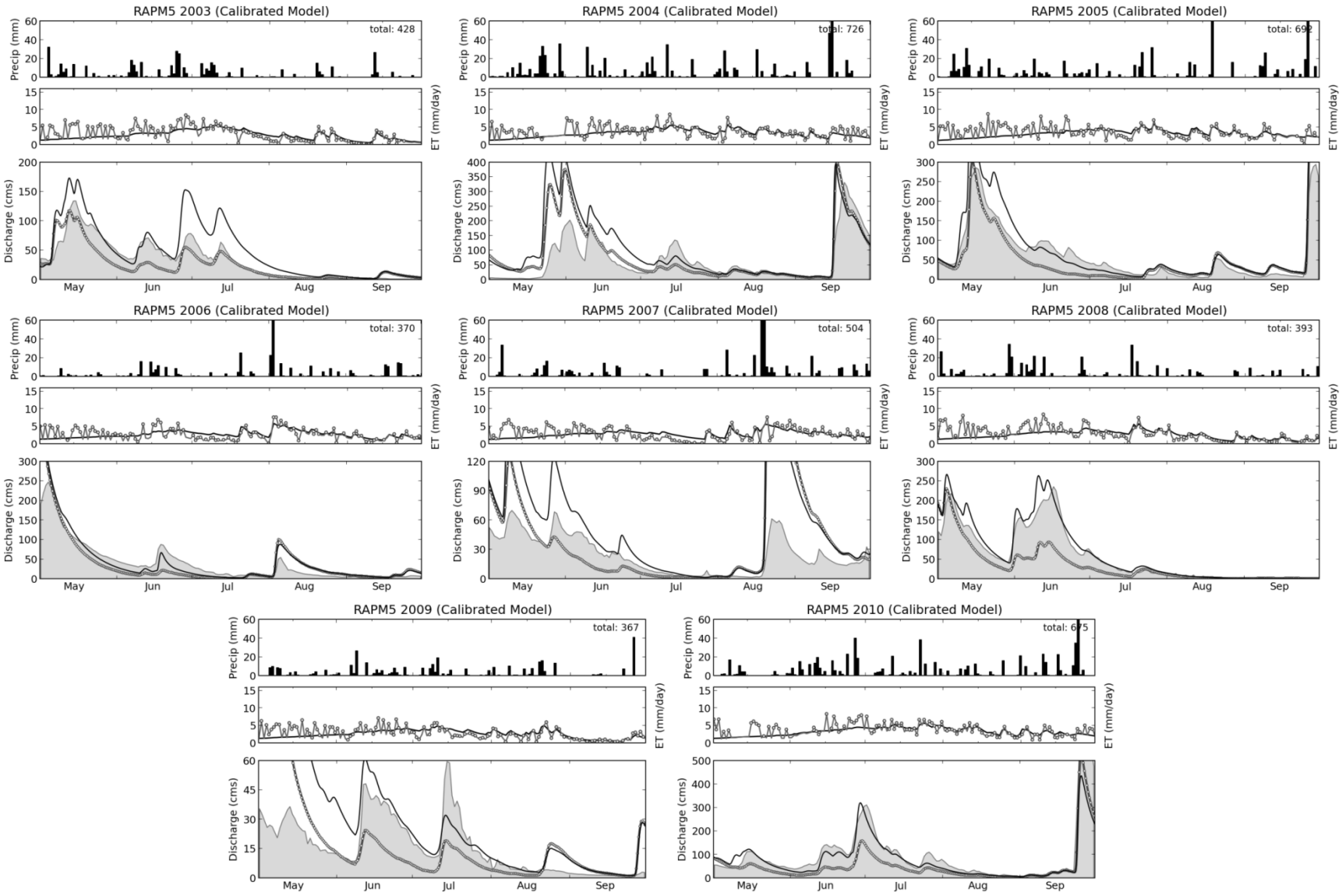
RAPM5 2003 (Calibrated Model)
total: 428
RAPM5 2004 (Calibrated Model)
total: 726
RAPM5 2005 (Calibrated Model)
total: 692
RAPM5 2006 (Calibrated Model)
total: 370
RAPM5 2007 (Calibrated Model)
total: 504
RAPM5 2008 (Calibrated Model)
total: 393
RAPM5 2009 (Calibrated Model)
total: 367
RAPM5 2010 (Calibrated Model)
total: 675
Precip (mm)
ET (mm/day)
Discharge (cms)
May
Jun
Jul
Aug
Sep

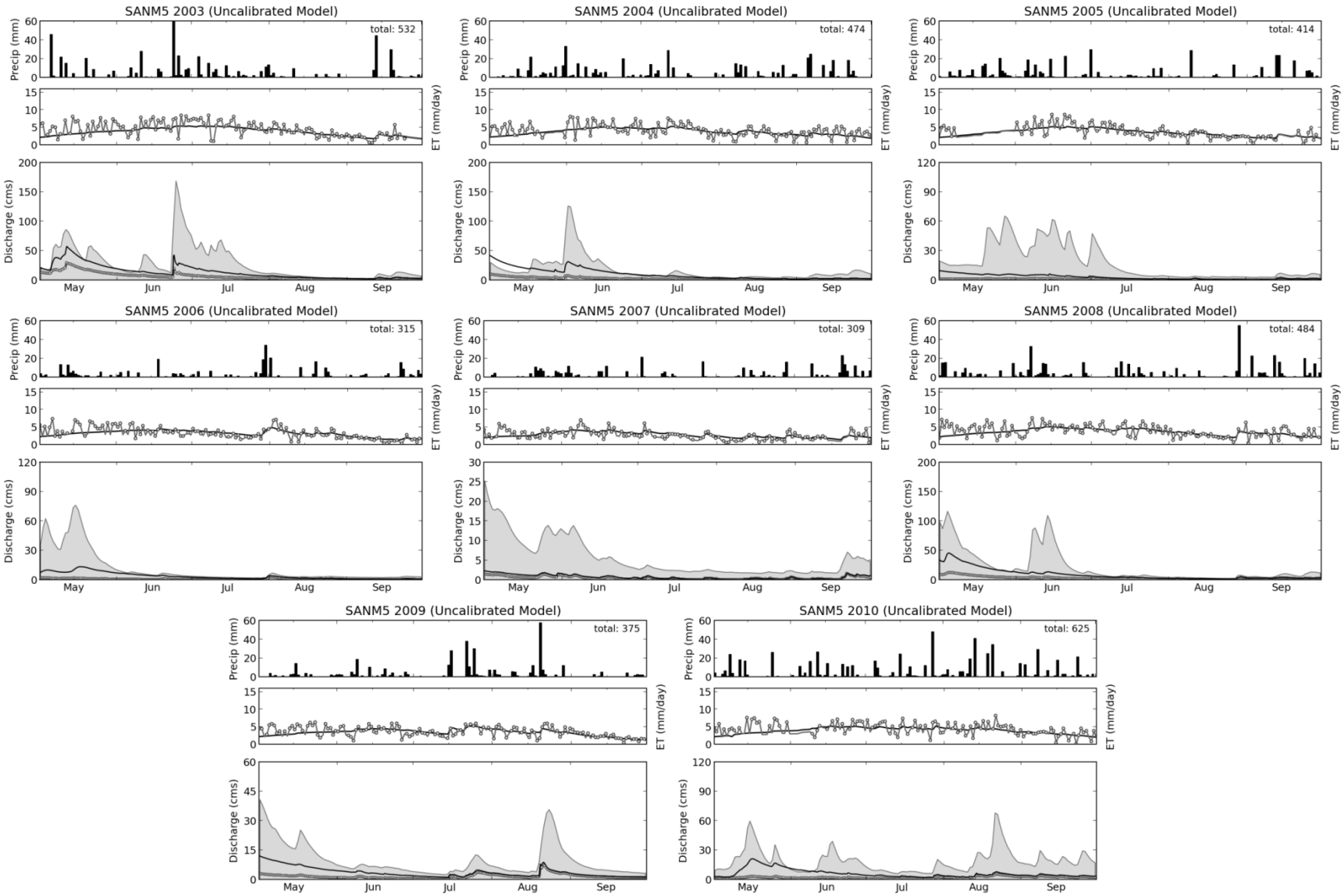
SANM5 2003 (Uncalibrated Model)
total: 532
SANM5 2004 (Uncalibrated Model)
total: 474
SANM5 2005 (Uncalibrated Model)
total: 414
SANM5 2006 (Uncalibrated Model)
total: 315
SANM5 2007 (Uncalibrated Model)
total: 309
SANM5 2008 (Uncalibrated Model)
total: 484
SANM5 2009 (Uncalibrated Model)
total: 375
SANM5 2010 (Uncalibrated Model)
total: 625
Precip (mm)
ET (mm/day)
Discharge (cms)
May
Jun
Jul
Aug
Sep

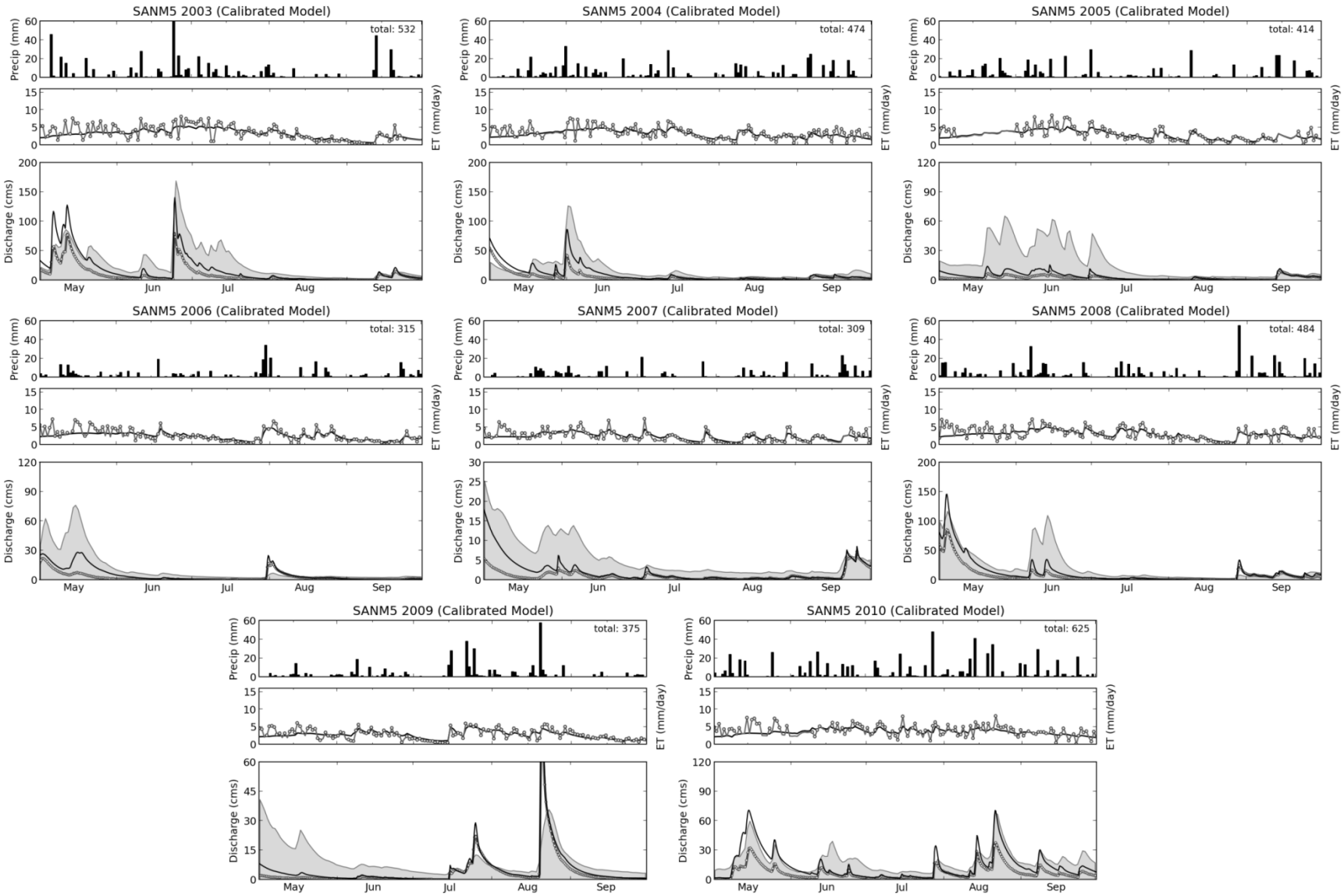
SANM5 2003 (Calibrated Model)
total: 532
SANM5 2004 (Calibrated Model)
total: 474
SANM5 2005 (Calibrated Model)
total: 414
SANM5 2006 (Calibrated Model)
total: 315
SANM5 2007 (Calibrated Model)
total: 309
SANM5 2008 (Calibrated Model)
total: 484
SANM5 2009 (Calibrated Model)
total: 375
SANM5 2010 (Calibrated Model)
total: 625
Precip (mm)
ET (mm/day)
Discharge (cms)
May
Jun
Jul
Aug
Sep

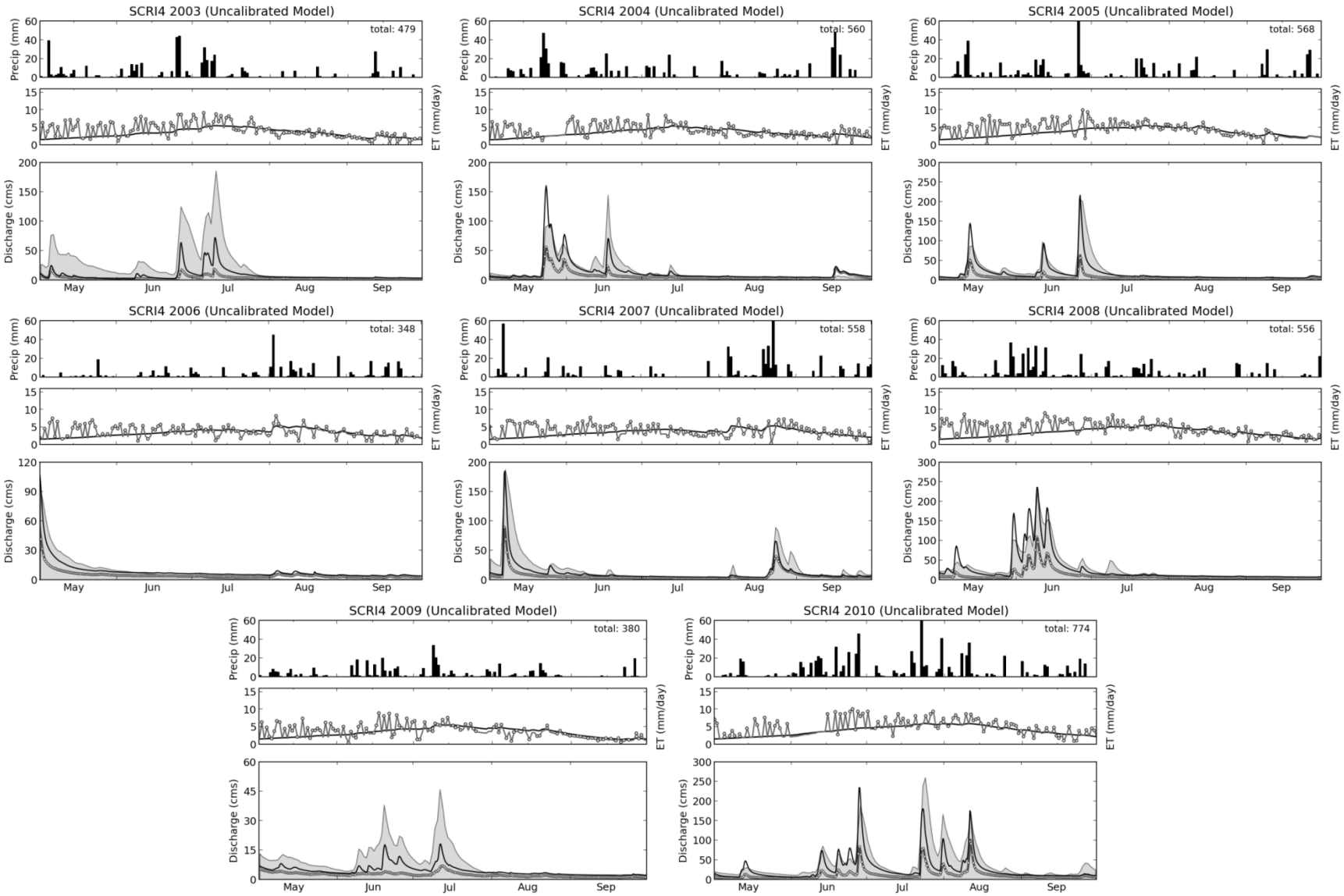
SCRI4 2003 (Uncalibrated Model)
total: 479
SCRI4 2004 (Uncalibrated Model)
total: 560
SCRI4 2005 (Uncalibrated Model)
total: 568
SCRI4 2006 (Uncalibrated Model)
total: 348
SCRI4 2007 (Uncalibrated Model)
total: 558
SCRI4 2008 (Uncalibrated Model)
total: 556
SCRI4 2009 (Uncalibrated Model)
total: 380
SCRI4 2010 (Uncalibrated Model)
total: 774
Precip (mm)
ET (mm/day)
Discharge (cms)
May
Jun
Jul
Aug
Sep

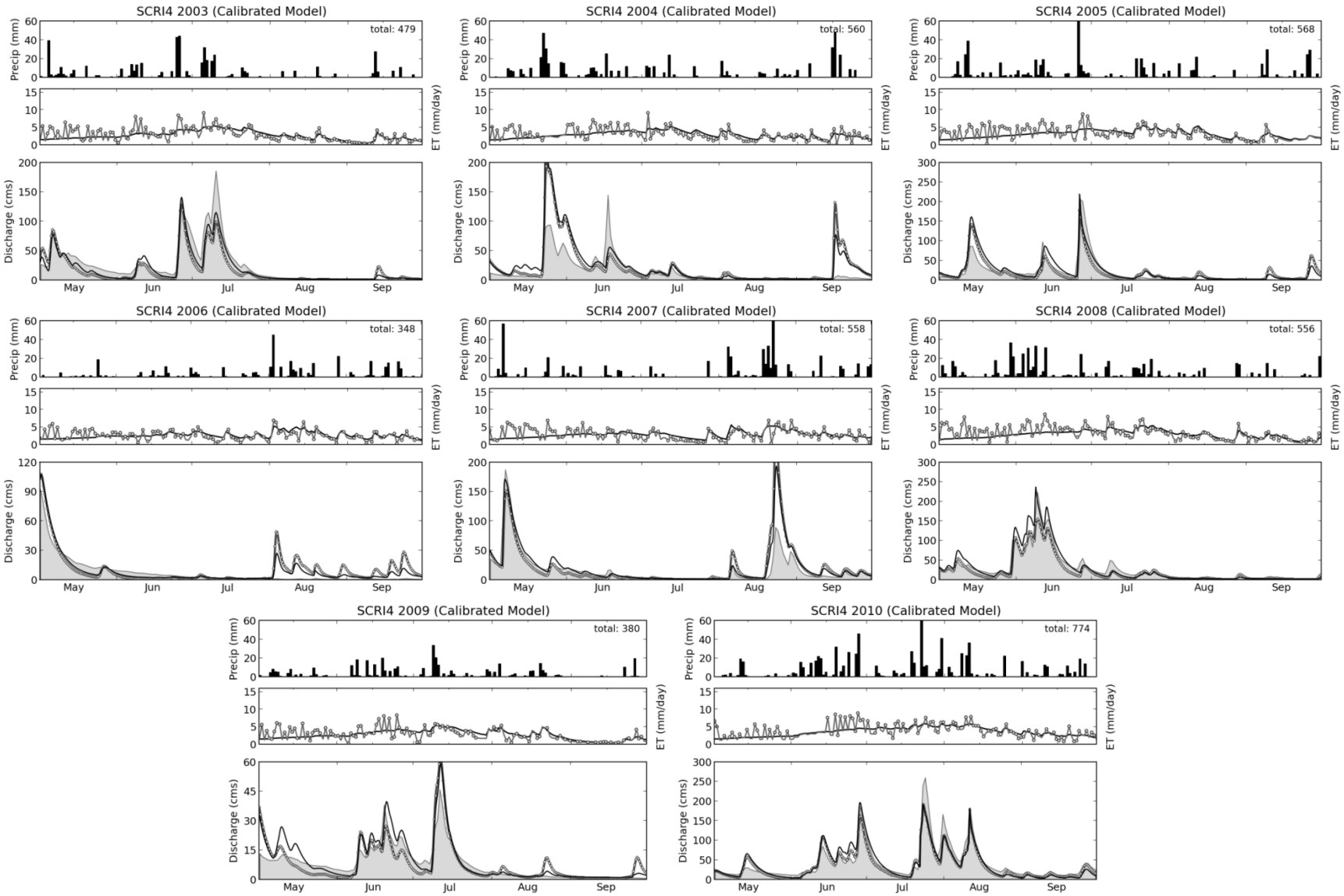
SCRI4 2003 (Calibrated Model)
total: 479
SCRI4 2004 (Calibrated Model)
total: 560
SCRI4 2005 (Calibrated Model)
total: 568
SCRI4 2006 (Calibrated Model)
total: 348
SCRI4 2007 (Calibrated Model)
total: 558
SCRI4 2008 (Calibrated Model)
total: 556
SCRI4 2009 (Calibrated Model)
total: 380
SCRI4 2010 (Calibrated Model)
total: 774
Precip (mm)
ET (mm/day)
Discharge (cms)
May
Jun
Jul
Aug
Sep

A.12 Discharge Error Statistics

Correlation Coefficient (R)

	Default (a priori)		MODIS (a priori)		Default (Calibrated)		MODIS (Calibrated)		
Basin	Ver	Cal	Ver	Cal	Ver	Cal	Ver	Cal	Annual Precip
BCHW3	0.89	0.84	0.91	0.84	0.87	0.71	0.86	0.72	937
BERW3	0.87	0.78	0.87	0.81	0.96	0.94	0.96	0.95	809
DARW3	0.88	0.84	0.87	0.85	0.89	0.90	0.92	0.88	939
MILW3	0.84	0.70	0.84	0.75	0.95	0.97	0.95	0.96	939
AMEI4	0.89	0.91	0.87	0.88	0.91	0.92	0.83	0.87	1008
AMWI4	0.77	0.87	0.74	0.83	0.85	0.93	0.76	0.88	1032
NHRI4	0.89	0.83	0.88	0.83	0.88	0.85	0.87	0.83	970
SCRI4	0.79	0.84	0.71	0.79	0.86	0.89	0.80	0.81	809
HICM5	0.88	0.78	0.79	0.67	0.87	0.85	0.77	0.74	680
MMLM5	0.73	0.69	0.67	0.61	0.80	0.79	0.74	0.74	725
PLUM5	0.66	0.66	0.64	0.66	0.74	0.73	0.69	0.70	545
RAPM5	0.59	0.68	0.64	0.65	0.83	0.84	0.85	0.78	798
SANM5	0.69	0.71	0.59	0.61	0.77	0.77	0.72	0.69	694
Mean	0.80	0.78	0.77	0.75	0.86	0.85	0.82	0.81	837

Table A.16. Stream discharge correlation coefficient (dimensionless) values for each basin and mean of all basins. Light shaded bars indicate large R values (good performance).

Normalized Root Mean Squared Error (normalized to mean)

	Default (a priori)		MODIS (a priori)		Default (Calibrated)		MODIS (Calibrated)		
Basin	Ver	Cal	Ver	Cal	Ver	Cal	Ver	Cal	Annual Precip
BCHW3	1.66	1.28	1.46	1.16	0.51	0.86	0.45	0.78	937
BERW3	0.76	0.84	0.79	0.83	0.35	0.38	0.46	0.47	809
DARW3	0.96	1.00	0.91	0.94	0.55	0.56	0.53	0.69	939
MILW3	1.03	1.44	0.94	1.08	0.51	0.48	0.49	0.44	939
AMEI4	0.79	0.80	1.26	1.23	0.94	0.77	1.11	0.96	1008
AMWI4	1.31	0.99	1.59	1.33	0.87	0.72	1.13	0.96	1032
NHRI4	0.76	0.97	1.03	1.24	1.25	0.98	1.36	1.09	970
SCRI4	1.14	0.96	1.56	1.49	0.88	0.87	1.00	1.01	809
HICM5	1.32	1.41	1.55	1.67	0.98	1.01	1.00	1.19	680
MMLM5	1.46	1.54	1.58	1.72	1.55	1.13	1.48	1.13	725
PLUM5	1.34	1.49	1.38	1.56	0.98	1.12	1.06	1.26	545
RAPM5	0.99	1.00	1.11	1.16	1.08	1.05	0.75	0.96	798
SANM5	1.02	1.16	1.30	1.45	0.84	0.96	1.09	1.21	694
Mean	1.12	1.14	1.27	1.30	0.87	0.84	0.92	0.93	837

Table A.17. Stream discharge NRMSE (dimensionless) values for each basin and mean of all basins. Light shaded bars indicate large NRMSE values (poor performance).

Mean Absolute Error ($m^3 s^{-1}$)

	Default (a priori)		MODIS (a priori)		Default (Calibrated)		MODIS (Calibrated)	
Basin	Ver	Cal	Ver	Cal	Ver	Cal	Ver	Cal
AMEI4	3.3	3.7	4.8	5.5	3.9	4.0	4.3	5.3
AMWI4	3.6	3.1	4.4	4.4	2.5	2.5	3.3	3.5
BCHW3	3.3	4.3	3.2	4.2	1.3	2.0	1.1	1.6
BERW3	20.9	21.2	22.8	24.0	10.2	10.8	13.7	13.9
DARW3	3.6	4.9	3.5	5.0	1.5	2.2	1.4	2.4
HICM5	2.7	2.3	3.1	2.6	2.0	1.7	2.1	1.9
MILW3	5.8	9.1	6.1	9.2	3.4	5.0	3.6	4.6
MMLM5	1.2	1.5	1.3	1.7	1.4	1.4	1.2	1.3
NHRI4	3.5	5.3	5.6	7.8	6.5	6.4	6.4	7.7
PLUM5	3.7	4.0	3.9	4.4	2.7	3.1	3.0	3.5
RAPM5	26.9	24.0	32.0	29.9	28.9	25.8	21.7	25.1
SANM5	12.7	10.2	18.4	14.0	12.7	9.6	16.0	12.1
SCRI4	12.8	9.2	16.3	13.3	8.7	7.6	10.9	9.5
Mean	8.0	7.9	9.6	9.7	6.6	6.3	6.8	7.1

Root Mean Squared Error ($m^3 s^{-1}$)

	Default (a priori)		MODIS (a priori)		Default (Calibrated)		MODIS (Calibrated)	
Basin	Ver	Cal	Ver	Cal	Ver	Cal	Ver	Cal
AMEI4	5.56	7.84	8.89	12.02	6.62	7.46	7.85	9.28
AMWI4	7.2	6.82	8.69	9.14	4.78	4.95	6.21	6.57
BCHW3	6.39	7.03	5.62	6.36	1.94	4.69	1.73	4.29
BERW3	26.11	29.6	26.76	29.17	11.89	13.36	15.76	16.6
DARW3	4.83	7.32	4.58	6.91	2.72	4.19	2.79	5.14
HICM5	5.1	4.48	5.97	5.32	3.71	3.22	3.94	3.78
MILW3	14.08	27.68	12.2	20.41	6.67	8.87	6.33	8.14
MMLM5	2.83	3.47	3.07	3.91	2.8	2.47	2.69	2.48
NHRI4	7.35	12.68	10.03	16.39	12.11	12.79	13.17	14.26
PLUM5	6.09	7.75	6.27	8.11	4.5	5.81	4.89	6.55
RAPM5	47.06	46.17	52	53.74	51.23	48.43	36.15	44.04
SANM5	22.83	18.82	29.08	23.64	18.67	15.6	24.32	19.81
SCRI4	22.65	17.17	30.72	26.6	16.76	15.41	19.3	17.91
Mean	13.70	15.14	15.68	17.06	11.11	11.33	11.16	12.22